

# **Anorganisch-geochemische Untersuchung quartärer Sedimente des Arktischen Ozeans**

An der Fakultät für Mathematik und Naturwissenschaften der  
Carl von Ossietzky Universität Oldenburg  
zur Erlangung des Grades und Titels einer

Doktorin der Naturwissenschaften

– Dr. rer. nat. –

angenommene Dissertation

von Frau Ann-Katrin Meinhardt  
geboren am 27.07.1985 in Cuxhaven

Erstgutachter: Prof. Dr. Hans-Jürgen Brumsack  
Zweitgutachterin: Dr. Katharina Pahnke

Tag der Disputation: 03.11.2015

## Kurzfassung

Der Arktische Ozean ist eine der klimasensitivsten Regionen der Erde und reagiert stark auf den globalen Wandel. Um die Auswirkungen von aktuellen und zukünftigen Klimaschwankungen vorherzusagen, ist ein Verständnis des Systems Arktischer Ozean im Hinblick auf vergangene Klimaänderungen unerlässlich. In dieser Arbeit wurden Sedimente des zentralen Arktischen Ozeans untersucht, um diagnostische geochemische Parameter für Materialeintrag, Strömungssysteme, diagenetische Milieus und die Variabilität dieser Parameter auf Glazial-/Interglazialzeitskalen zu entwickeln.

Die Sedimente sind allgemein durch alternierende dunkelbraune und olivbraune Lagen gekennzeichnet. Die dunkelbraunen Lagen weisen erhöhte Gehalte an Mn, Fe, und assoziierten Spurenmetallen (As, Co, Cu, Mo, Ni, V) auf, welche durch Adsorption („scavenging“) aus der Wassersäule angereichert wurden. Diese Lagen entstehen hauptsächlich durch erhöhten Materialeintrag (Flusseintrag und Küstenerosion) während Interglazialen und werden aufgrund ihrer visuellen Auffälligkeit als vielversprechende Alternative zur stratigraphischen Kernkorrelation angesehen. In Oberflächensedimenten sind diese Lagen primären Ursprungs und somit diagnostisch für Interglaziale. Sediment- und Porenwasseruntersuchungen von tieferen Sedimentkernen ergaben, dass die Kerne durch  $\text{NO}_3^-$ - und Mn-Reduktion beeinflusst sind und diagenetische Prozesse die Sedimentgeochemie beeinflussen. Das Verhältnis der an Mn-Lagen gebundenen Überschussgehalte von Co und Mo ( $\text{Co}_{\text{xs}}/\text{Mo}_{\text{xs}}$ ) kann als diagnostischer Anzeiger dafür verwendet werden, ob die dunkelbraunen Lagen durch diagenetische Auflösung oder Zufuhr aus dem Porenwasser beeinflusst wurden. Das diagenetische Milieu variiert stark. Daher ist grundsätzlich eine detaillierte Porenwasser-Untersuchung an jeder einzelnen Kernlokation notwendig, um primäre von diagenetisch beeinflussten Lagen unterscheiden zu können. Erst dann kommt eine stratigraphische Nutzung dieser Lagen in Betracht.

Die synchrone Anreicherung von Fe in den Mn-reichen Lagen lässt sich durch die große Ähnlichkeit des Verhaltens von beiden Elementen im marinen Bereich erklären. Daher lag es nahe, über das Verhältnis stabiler Fe-Isotope (bezeichnet als  $\delta^{56}\text{Fe}$ ) zu versuchen, die Transportwege zu entschlüsseln. Mit zunehmender

Fe-Anreicherung im Sediment werden die  $\delta^{56}\text{Fe}$ -Werte negativer, was die Annahme erhärtet, dass isotopisch leichtes Fe von den Schelfgebieten zu den tiefen Becken transportiert wurde. Dieser Mechanismus ist in Analogie vermutlich auch für die Mn-Anreicherungen verantwortlich.

Die Signaturen von Ca/Al, Mg/Al und TIC sind in Sedimenten der amerasischen Seite diagnostisch für Dolomit und dokumentieren den Eintrag vom Arktischen Archipel. Si/Al und K/Al Profile zeigen eine basaltische Komponente an, vermutlich vom sibirischen Hinterland. Die Parameter  $\text{Ca}_{\text{bio}}$  und  $\text{Sr}_{\text{xs}}$  können als Anzeiger für erhöhten Eintrag einer biogenen Komponente verwendet werden.

Die Bestimmung der Nd-Isotopenverhältnisse (bezeichnet als  $\epsilon_{\text{Nd}}$ ) an der authigenen Sedimentfraktion ermöglichte Aussagen über die Tiefenwasserzirkulation. Im modernen Arktischen Ozean ist ein deutlicher Einfluss von Wassermassen des Nordatlantiks erkennbar. Die Oberflächensedimente weisen homogene, gut durchmischte Signaturen auf. Im Vergleich dazu sind die Signaturen während des letzten Glazialen Maximums (LGM) weniger homogen und durch lokale Einflüsse, wie das Absinken von sehr salzhaltigem Wasser („brine“) bei der Meereisbildung in den Schelfgebieten, gekennzeichnet. Die generelle Tiefenwasserzirkulation mit nordatlantischem Ursprung scheint sich jedoch nicht geändert zu haben.

An der lithogenen Sedimentfraktion wurden  $\epsilon_{\text{Nd}}$  und Sr-Isotopenverhältnisse ( $^{87}\text{Sr}/^{86}\text{Sr}$ ) verwendet, um Aussagen über die Sedimentherkunft zu treffen. Die Proben können keiner eindeutigen Quelle zugeordnet werden und weisen ein Mischsignal auf. Proben im amerasischen Teil des Arktischen Ozeans zeigen jedoch eine stärkere Beeinflussung durch nordamerikanische Quellen und Proben des eurasischen Teils durch eurasische Quellen. Während des LGM weisen die Proben ein ähnliches Verteilungsmuster der Isotopensignaturen auf, streuen aber mehr. Ursache sind die spezifischen Umweltbedingungen während des LGM: eine größere Eisbedeckung und ein verringerter Meeresspiegel ließen die Küstenlinie näher an den Arktischen Ozean reichen und verkürzten somit die Sediment-Transportwege.

## Abstract

The Arctic Ocean is one of the most climate-sensitive regions of the world and strongly reacts to global change. In order to predict the impact of current and future climate variability, the understanding of the Arctic Ocean system with regard to past climate change is essential. In this study, sediments of the central Arctic Ocean have been investigated in order to identify geochemical parameters diagnostic for material input, current systems, diagenetic regimes and the variability of these parameters on glacial/interglacial timescales.

The sediments are generally characterized by alternating dark brown and olive-brown layers. The dark brown layers have increased contents of Mn, Fe, and associated trace metals (As, Co, Cu, Mo, Ni, V), which were removed from the water column by scavenging. These layers are mainly formed by increased material input (riverine and coastal erosion) during interglacials and are therefore a promising tool for potential stratigraphic core correlation. In surface sediments these layers are of primary origin and therefore diagnostic for interglacials. Sediment and porewater analyses of deeper sediment cores show that the sediments are influenced by  $\text{NO}_3^-$  and Mn-reduction and that sediment geochemistry is affected by diagenetic processes. The ratio of the Mn-bound excess contents of Co and Mo ( $\text{Co}_{\text{xs}}/\text{Mo}_{\text{xs}}$ ) can be used as a diagnostic parameter for assessing whether the dark brown layers are affected by diagenetically-induced dissolution resp. removal or addition resp. adsorption of components from the pore water pool. The diagenetic regime varies strongly. Therefore in principle a detailed porewater study is necessary at each core location to be able to distinguish between primary and diagenetically influenced layers. Only then these layers may be considered as stratigraphic markers.

The synchronous enrichment of Fe in Mn-rich layers may be explained by the close similarity of the behavior of these elements in the marine environment. Therefore it seems justified using stable Fe isotope ratios (expressed as  $\delta^{56}\text{Fe}$ ) to decipher possible transport ways. With increasing Fe enrichment in the sediment  $\delta^{56}\text{Fe}$  values are decreasing, which led to the assumption that isotopically light Fe from the shelf areas is exported to the deep basins. In analogy this transport mechanism is likely responsible for the observed Mn enrichments.

The signatures of Ca/Al, Mg/Al and TIC are diagnostic for dolomite in sediments from the Amerasian side and document input from the Arctic archipelago. Si/Al and K/Al profiles indicate a basaltic component, presumably from the Siberian hinterland. The parameters  $Ca_{bio}$  and  $Sr_{xs}$  can be used as indicators for the increased input of a biogenic component.

The determination of Nd isotope ratios (expressed as  $\epsilon_{Nd}$ ) in the authigenic sediment fraction provides information about deep water circulation. In the modern Arctic Ocean a distinct signal for the influence of water masses from the North Atlantic can be detected. The surface sediments show homogeneous, well-mixed signatures. During the Last Glacial Maximum (LGM) the signatures are less homogeneous and the sediments are locally influenced by brine rejection during sea ice formation in shelf areas. However, the general deep water circulation with water masses of North Atlantic origin does not seem to have changed.

Neodymium ( $\epsilon_{Nd}$ ) and Sr isotope ratios ( $^{87}Sr/^{86}Sr$ ) in the lithogenic sediment fractions were used to investigate sediment provenance. The samples cannot be assigned to distinct sediment sources but show a mixed signal. However, samples from the Amerasian section of the Arctic Ocean have a stronger influence from North American sources whereas samples from the Eurasian section are more related to Eurasian sources. During the LGM, the samples show a similar isotopic distribution pattern with slightly less homogenous signatures. This was most probably caused by the specific environmental conditions during the LGM: Due to a larger ice cover and a lower sea level the coastline reached further into the basins and sediment transport pathways were shorter.

# Inhaltsverzeichnis

Abstract .....	III
Abbildungsverzeichnis .....	IX
Tabellenverzeichnis .....	XIV
1. Einleitung und Zielsetzung .....	1
1.1 Der Arktische Ozean .....	2
1.2 Die geochemische Zusammensetzung arktischer Sedimente: Diagnostische Elemente als Anzeiger für terrigenes, biogenes und redox- reaktives Material .....	4
1.3 Datierung im Arktischen Ozean: Auf der Suche nach Alternativen .....	7
1.4 Diagenetische Prozesse im Sediment und mögliche Beeinflussung Mn- reicher Sedimentlagen.....	9
1.5 Nd-Isotope als Indikator für Tiefenwasserzirkulation und Sedimentherkunft .....	12
1.6 Fe-Isotope als Indikator für Redoxbedingungen und Transportprozesse.....	14
1.7 Fragestellungen dieser Arbeit.....	15
2. Autorenanteil an den hier vorgestellten Publikationen .....	16
3. Regional variations in sediment geochemistry on a transect across the Mendeleev Ridge (Arctic Ocean).....	19
3.1 Abstract .....	19
3.2 Introduction.....	20
3.3 Material and methods .....	22
3.4 Results.....	25
3.4.1 General geochemical characteristics and terrigenous elements .....	25
3.4.2 Elements related to organic matter and carbonate.....	27
3.4.3 Elements related to Mn and Fe (oxyhydr)oxides .....	29

3.4.4 Geochemical trends along the transect.....	31
3.5 Discussion .....	32
3.5.1 Preliminary age model.....	32
3.5.2 Input of terrigenous material and IRD.....	35
3.5.3 Biogenic material .....	36
3.5.4 Elements related to Mn and Fe oxyhydroxides: Temporal and spatial trends.....	39
3.6 Conclusions .....	41
3.7 Acknowledgments .....	42
4. Climate change and response in bottom water circulation and sediment provenance in the Central Arctic Ocean since the Last Glacial Maximum .....	43
4.1 Abstract .....	43
4.2 Introduction.....	44
4.3 Material and methods .....	46
4.3.1 Major and trace elements .....	46
4.3.2 Nd and Sr isotopes .....	49
4.3.3 Sampling strategy for recent Holocene and LGM sediment samples.....	51
4.4 Results.....	52
4.4.1 Geochemical characteristics of the sediment cores .....	52
4.4.2 Nd isotope ratios of authigenic Fe-Mn oxides (leachable fraction).....	53
4.4.3 Nd and Sr isotopes of the terrigenous fraction .....	55
4.5 Discussion .....	58
4.5.1 Bulk sediment characteristics .....	58
4.5.2 Nd isotope ratios of authigenic Fe-Mn oxides .....	60
4.5.2.1 Modern situation .....	60
4.5.2.2: LGM.....	61



4.5.3 Lithogenic material .....	62
4.5.3.1 Modern situation .....	62
4.5.3.2. LGM.....	63
4.6 Conclusions .....	64
4.7 Acknowledgements .....	66
5. Diagenetic regimes in Arctic Ocean sediments: Implications for sediment geochemistry and core correlation .....	67
5.1 Abstract .....	67
5.1 Introduction.....	68
5.2 Material and methods .....	70
5.3 Results and Discussion .....	74
5.3.1 Preliminary stratigraphy.....	74
5.3.2. Sedimentary characteristics and potential origin of the Mn enrichment in core 248-6.....	76
5.3.3 Pore water characteristics and diagenetic trace metal cycling in core 248-6 .....	79
5.3.4 Pore water flux calculation and Mn <sub>diss</sub> reduction rate for core 248-6 .....	85
5.3.5 Diagenetic conditions and their diagnostic parameters in sediment cores from different parts of the central Arctic Ocean .....	88
5.3.6 Sedimentary Fe enrichments.....	94
5.3.6.1 Iron budget .....	94
5.3.6.2 Iron isotope ratios and the Arctic Fe shuttle .....	97
5.4 Conclusions .....	102
5.5 Acknowledgements .....	103
6. Manganese-rich brown layers in Arctic Ocean sediments: Composition, formation mechanisms, and diagenetic overprint .....	104
7. Silica diagenesis and benthic fluxes in the Arctic Ocean .....	106

8. Zusammenfassung und Ausblick.....	108
9. Literatur .....	112
10. Appendix.....	136
Danksagung .....	139
Lebenslauf .....	141
Erklärung .....	142

## Abbildungsverzeichnis

Abb. 1: a) Bathymetrische Karte des Arktischen Ozeans mit Flüssen (schwarz) und Teilmeeren (weiß, nach Jakobsson et al., 2003). b) Vergrößerter Ausschnitt mit Bezeichnung der Ozeanrücken und -becken. ....	2
Abb. 2: Schema der Stratifizierung der arktischen Wassermassen (Stein 2008). ....	4
Abb. 3: Anreicherungsfaktoren der verschiedenen Sedimentintervalle gegenüber mittlerem Tonschiefer. ....	6
Abb. 4: Schematische Tiefenverteilung der gängigen Elektronenakzeptoren in der Natur. Die wirkliche Lage im Sediment sowie die Ausprägung können variieren und die Zonen können überlappen (verändert nach Canfield und Thamdrup, 2009). ....	10
Abb. 5: Map of the Arctic Ocean with investigated core sites 408, 410 and 422, and coring site HLY0503-8JPC from Polyak et al. (2009, based on IBCAO 2.0; Jakobsson et al., 2008). ....	23
Abb. 6: Ternary plot of major components in samples from cores 408 (black symbols), 410 (red symbols), and 422 (blue symbols) in comparison with average shale (AS) (modified after Brumsack, 1989). ....	25
Abb. 7: Element/Al ratios of Si, Zr, Ti, K, Ca, Mg and element contents of Al and TIC for cores 408 (A), 410 (B) and 422 (C) (dashed line: AS; horizontal brown bars: brown layers). ....	26
Abb. 8: TOC, S, $Ca_{bio}$ and $Sr_{xs}$ contents, and Ca/Mg ratios for cores 408 (A), 410 (B) and 422 (C) (solid line: molar Ca/Mg ratio in dolomite: 1.65; horizontal brown bars: brown layers). ....	28
Abb. 9: Element/Al ratios of Mn, Fe, As, Co, Cu, Mo and Ni and excess contents of Mn and Fe for cores 408 (A), 410 (B) and 422 (C) (filled squares: ICP-MS results; dashed line: AS; AS for As/Al and Co/Al ( $1.13 \cdot 10^4$ and $2.15 \cdot 10^4$ ) not shown; horizontal brown bars: brown layers). ....	30

Abb. 10: Enrichment factors of Mo, Mn, Co, As, Ni, Cu and Fe in selected Mn-rich layers of the three cores.....	31
Abb. 11: Photographs of giant box corer (GKG) cores PS72/408-3, PS72/410-1, and PS72/422-3, recovered at the same locations than the corresponding multicorer cores. Dark brown layers B1 and B2 and the dolomite-rich “white layer” W3 are indicated (Figure from Stein et al. 2010b; age of W3 according to Polyak et al., 2004, 2009).....	33
Abb. 12: (A) XRF calcium (green) and manganese (blue) contents, sand content (>63 $\mu\text{m}$ ; black), planktonic foraminifers (>150 $\mu\text{m/g}$ ; red), $^{14}\text{C}$ ages (red) and AAR ages (purple) of sediment core HLY0503-8JPC (Polyak et al., 2009). (B) XRF Mn (blue) and Ca (green) contents of cores 408, 410 and 422. Yellow shading: interglacial/interstadial units, light gray: interval with clastic IRD, dark gray: fine grained LGM sediment. Ages for core 410 from Jang et al. (2013).....	33
Abb. 13: Linear correlations of $\text{Sr}_{\text{xs}}$ and $\text{Ca}_{\text{bio}}$ for cores (A) 408, (B) 410 and (C) 422. Gray dots were omitted for calculating the correlation factor. ....	37
Abb. 14: (based on IBCAO, Jakobsson et al., 2008) a) Map of the Arctic Ocean with core locations and major rivers. Black numbers: 1: Chukchi Peninsula 2: Okhotsk-Chukotka volcanic belt 3: Arctic Archipelago; 4: Svalbard. b) Recent deep water currents (adapted from Rudels et al., 2012), literature values for deep water $\epsilon_{\text{Nd}}$ and river water $\epsilon_{\text{Nd}}$ . Black circles and arrows: possible sites of slope convection from cold, brine enriched shelf waters to the deep waters (Nansen, 1906; Rudels et al., 2012). Black numbers: Atlantic inflow from the Greenland Sea deep water (Piepgras and Wasserburg, 1987) and Pacific inflow (Dahlgvist et al., 2004). ....	48
Abb. 15: Mn/Al ratios of the studied multicorer cores. Open circles mark samples for isotope measurements. Dashed line marks average shale (Wedepohl, 1971, 1991).....	51

Abb. 16: Sedimentary Ca/Al (black), Mg/Al (blue), and TIC (red) data for cores 231 and 237 from the Canada Basin. Dashed lines: average shale. Gray bars indicate sediment layers with supposed occurrence of dolomite.....	53
Abb. 17: (based on IBCAO, Jakobsson et al., 2008) $\epsilon_{Nd}$ values of the leachates from a) surface sediments, b) sediments from the Last Glacial Maximum. Additional literature values of sediment leachates are given. Modern deep water circulation in white (adapted from Rudels et al., 2012). .....	54
Abb. 18: $\epsilon_{Nd}$ versus $^{87}Sr/^{86}Sr$ diagram for the lithogenic fraction of a) surface sediments, b) sediments from the Last Glacial Maximum. Reference data for potential source areas: Siberian Putorana basalts: Lightfoot et al., 1993; Wooden et al., 1993. Chukchi peninsula: Ledneva et al., 2011 (from Georoc database); Akinin et al., 2013. Okhotsk-Chukotka volcanic belt: Tikhomirov et al., 2008. Alaska peninsula: Andronikov and Mukasa, 2010; Akinin et al., 2013. Mackenzie particles: Goldstein et al., 1984; Millot et al., 2003. Mackenzie LIP: Dupuy et al., 1992. Svalbard: Johansson et al., 1995; 1999. Canadian Shield: McCulloch and Wasserburg, 1978. North Greenland: Kalsbeek and Jepsen, 1983; 1984; Estrada et al., 2001; Upton et al., 2005; Kalsbeek and Frei, 2006; Thorarinsson et al., 2011. Arctic Archipelago: Patchett et al., 2004 (only $\epsilon_{Nd}$ values). Khatanga/Lena/Yana suspended particulate matter (SPM): Eisenhauer et al., 1999 (only $^{87}Sr/^{86}Sr$ values). .....	56
Abb. 19: (based on IBCAO, Jakobsson et al., 2008) $\epsilon_{Nd}$ values of the lithogenic fraction from a) surface sediments, b) sediments from the Last Glacial Maximum. Modern surface water circulations (BG Beaufort Gyre and TPD Transpolar Drift) are shown schematically. ....	57
Abb. 20: Enlarged section of Abb. 18 with arrows pointing from the LGM values towards the modern values for each core. Red: modern samples, black: LGM samples.....	58
Abb. 21: Map of the core locations. ....	70

Abb. 22: Stratigraphic correlation of core 248-6 to three sediment cores (LRG09-GC03; 96/12-1PC; ACEX core) from the central Lomonosov Ridge (from Löwemark et al., 2014). Horizontal gray bars: gray sediment layers in core 248-6. Gray patterned intervals mark coarse-grained diamicts. Stippled vertical gray bar: zone of low Mn abundance in the diamicts. ....	75
Abb. 23: Sedimentary Mn/Al, Fe/Al, Co/Al, Mo/Al, and Ni/Al values (black) and pore water Mn <sup>2+</sup> , Co <sup>2+</sup> , Mo <sup>6+</sup> (all red), NO <sub>3</sub> <sup>-</sup> (blue), SO <sub>4</sub> <sup>2-</sup> (green) and NH <sub>4</sub> <sup>+</sup> (orange) concentrations in core 248-6. Dashed black line represents average shale (Wedepohl 1971, 1991), dashed red line represents mean Arctic seawater Mo value (Tovar-Sánchez et al., 2010), gray bars represent gray sediment layers, brown bars represent dark brown sediment layers. ....	76
Abb. 24: X-ray radiographs, Mn <sub>xs</sub> contents, and core photos of core 248-6 (x-ray radiographs and photos: Matthiessen, 2011). Thin white bands in the x-ray radiographs correspond to higher Mn <sub>xs</sub> contents and dark brown sediment color. ....	81
Abb. 25: Co <sub>xs</sub> versus Mo <sub>xs</sub> relationship of different dark brown sediment layers. a) core 248-6, b) core 206-3, c) core 220-7, d) core 237-3. Layers with diagenetic addition of Mn from the pore water have lower Co <sub>xs</sub> /Mo <sub>xs</sub> . Layers that were subjected to Mn reduction have higher ratios. ....	84
Abb. 26: Net Mn <sup>2+</sup> rate of core 248-6 from the REC model (Lettmann et al., 2012). Positive values indicate Mn <sup>2+</sup> production and negative values indicate Mn <sup>2+</sup> consumption. ....	87
Abb. 27: Sedimentary Mn/Al, Fe/Al, Co/Al, Mo/Al, and Ni/Al values (black) and pore water Mn <sup>2+</sup> , Co <sup>2+</sup> , Mo <sup>6+</sup> (all red), NO <sub>3</sub> <sup>-</sup> (blue), SO <sub>4</sub> <sup>2-</sup> (green) and NH <sub>4</sub> <sup>+</sup> (orange) concentrations in core 206-3. For additional information see Abb. 23. ....	89

Abb. 28: Sedimentary Mn/Al, Fe/Al, Co/Al, Mo/Al, and Ni/Al values (black) and pore water Mn <sup>2+</sup> , Co <sup>2+</sup> , Mo <sup>6+</sup> (all red), NO <sub>3</sub> <sup>-</sup> (blue), SO <sub>4</sub> <sup>2-</sup> (green) and NH <sub>4</sub> <sup>+</sup> (orange) concentrations in core 220-7. For additional information see Abb. 23 .....	91
Abb. 29: Sedimentary Mn/Al, Fe/Al, Co/Al, Mo/Al, and Ni/Al values (black) and pore water Mn <sup>2+</sup> , Co <sup>2+</sup> , Mo <sup>6+</sup> (all red), NO <sub>3</sub> <sup>-</sup> (blue), SO <sub>4</sub> <sup>2-</sup> (green) and NH <sub>4</sub> <sup>+</sup> (orange) concentrations in core 237-3. For additional information see Abb. 23 .....	92
Abb. 30: Pore water SO <sub>4</sub> <sup>2-</sup> , Mn <sup>2+</sup> , Mo <sup>6+</sup> , and Co <sup>2+</sup> concentrations in core 343-1 (from März et al., 2011). Gray bars represent dark brown sediment layers.....	93
Abb. 31: Fe/Al (black) and δ <sup>56</sup> Fe values (blue) of sediment cores 206, 237, 248, 410 (gravity corer and multicorer), 275, 277, 280, and 285 (multicorer). See also Tab. 5. Dashed black line represents average shale (Wedepohl 1971, 1991), blue line represents δ <sup>56</sup> Fe = 0, gray bars represent gray sediment layers, brown bars represent dark brown sediment layers. ....	98
Abb. 32: Fe/Al relative to δ <sup>56</sup> Fe values. Residual Fe in the gray layers is isotopically heavier, indicating the lithogenic background. Fe-rich samples and surface samples are isotopically lighter, indicating a mobile Fe fraction. ....	99

## Tabellenverzeichnis

Tab. 1: Berechnete Gibbs-Energie für die prinzipiellen Atmungswege bei der Mineralisierung von organischem Material in der Natur mit Azetat als Elektronendonator (aus Canfield und Thamdrup, 2009). .....	10
Tab. 2: Core locations. ....	24
Tab. 3: Estimated sedimentation rates of the 3 cores by means of an age model determined by Polyak et al. (2009). Values in parentheses are from Stein et al., 2010b for corresponding longer cores 408-5, 410-3 and 422-5, respectively. ....	34
Tab. 4: Core locations, bulk element contents and Nd and Sr isotopic composition of the leachable and lithogenic fractions of modern and LGM (bold) samples. ....	47
Tab. 5: Core locations, $\delta^{56}\text{Fe}$ values, Fe/Al, and ratios of lithogenic and non-lithogenic Fe. Stars mark cores without $\delta^{56}\text{Fe}$ measurement. ....	71
Tab. 6: Sedimentary $\text{Mn}_{\text{xs}}$ and $\text{Fe}_{\text{xs}}$ calculations for five different sediment cores. ....	78
Tab. 7: Boundary parameters used for the calculation of diffusive fluxes of cores 248-6, 206-3, and 220-7. $D_{\text{sw}}$ for Mn and Co from Boudreau (1997). $D_{\text{sw}}$ for Mo estimated from Li and Gregory (1974). See chapter 5.3.4 and Appendix for details. ....	86
Tab. 8: Parameters and references for the Fe budget. <sup>a</sup> Wagemann et al., 1977; Gaillardet et al., 1999. <sup>b</sup> Reeder et al. 1972. <sup>c</sup> Nolting et al., 1996; Rachold et al., 1996; Gordeev et al., 2004; Hölemann et al., 2005. <sup>d</sup> Martin et al., 1993; Hölemann et al., 1995; 1999; 2005; Pokrovsky et al., 2010. <sup>e</sup> Average b and d. <sup>f</sup> 3% of the global estimate from Duce and Tindale, 1991, and Zhuang et al., 1995. <sup>g</sup> Aguilar-Islas et al., 2007; Kuma et al., 2013. <sup>h</sup> Klunder et al., 2012. <sup>i</sup> Turekian and Wedepohl, 1961. <sup>j</sup> See chapter 3.7.1. <sup>k</sup> Strekopytov 2003. <sup>l</sup> Data from cores 206-3, 220-7, 237-3, and 248-6. ....	95



## 1. Einleitung und Zielsetzung

Der Arktische Ozean spielt eine enorm wichtige Rolle für das globale Klima. Durch das Aufeinandertreffen von arktischem Wasser, welches geringe Temperaturen und eine geringe Salinität aufweist, und atlantischem Wasser, welches höhere Temperaturen und eine höhere Salinität aufweist, wird Nordatlantisches Tiefenwasser gebildet (Aagaard et al., 1985). Dieses treibt die globale thermohaline Zirkulation an. Durch die vorherrschenden Temperaturen um den Gefrierpunkt von Wasser haben selbst geringe Temperaturschwankungen potentiell große Auswirkungen auf die Tiefenwasserbildung. Abschmelzende Eismassen sorgen für einen erhöhten Eintrag von Frischwasser und verringern den Albedo-Effekt, was zu weiterer Erwärmung führt. Änderungen der thermohalinen Zirkulation können allerdings auch ausschlaggebend für Vereisungen der Nordhemisphäre sein (Driscoll und Haug, 1998). In der Vergangenheit wurden diverse Glazial-/Interglazialzyklen durchlaufen, die die Umweltbedingungen in der Arktis drastisch verändert haben. Sedimente sind wertvolle Klimaarchive, aus denen Informationen über Glazial- und Interglazialereignisse gewonnen werden können. Kenntnisse über vergangene Umweltbedingungen und die Reaktion des Arktischen Ozeans auf klimatische Veränderungen können dabei helfen, zukünftige Klimaentwicklungen vorherzusagen (Anisimov et al., 2007).

Ziel dieser Arbeit ist die Entwicklung diagnostischer geochemischer Parameter, um das Klimageschehen im Arktischen Ozean rekonstruieren zu können. Dazu müssen bisher hauptsächlich geophysikalisch, mineralogisch und paläontologisch untersuchte Sedimente umfassend geochemisch charakterisiert werden, um geochemische Parameter zu identifizieren, die diagnostisch für bestimmte Ereignisse oder Zeitintervalle sind. Hierbei ist eine kritische Betrachtung der möglichen frühdiagenetischen Überprägung wichtig. Durch diagenetische Prozesse nach der Ablagerung können primäre Signaturen verfälscht werden. Deshalb sind Porenwasseruntersuchungen unerlässlich, da nur durch die kombinierte Betrachtung von Sediment- und Porenwasserdaten eine eindeutige Erfassung dieser Prozesse möglich ist. Es existieren bisher wenige Studien, die sich mit diagenetischen Prozessen im zentralen Arktischen Ozean befassen.

Somit soll diese Arbeit ein weitreichenderes Verständnis für die Anwendbarkeit und Beschränkungen von Klimarekonstruktionen dieser spezifischen Region ermöglichen.

## 1.1 Der Arktische Ozean

Der Arktische Ozean hat eine Fläche von ca.  $9.5 \cdot 10^6 \text{ km}^2$  und ein Volumen von ca.  $13 \cdot 10^6 \text{ km}^3$ , dies sind etwa 2.6% der globalen Ozeanfläche und weniger als 1% des globalen Ozeanvolumens (Jakobsson 2002; Jakobsson et al., 2003). Grund für das relativ geringe Volumen sind die großen Schelfgebiete, die ca. 53% der Gesamtfläche des Arktischen Ozeans einnehmen und mittlere Wassertiefen von 50 bis 200 m aufweisen (Jakobsson et al., 2003). Während einer Eiszeit mit entsprechend geringerem Meeresspiegel können große Teile der Schelfgebiete zu Landfläche werden.

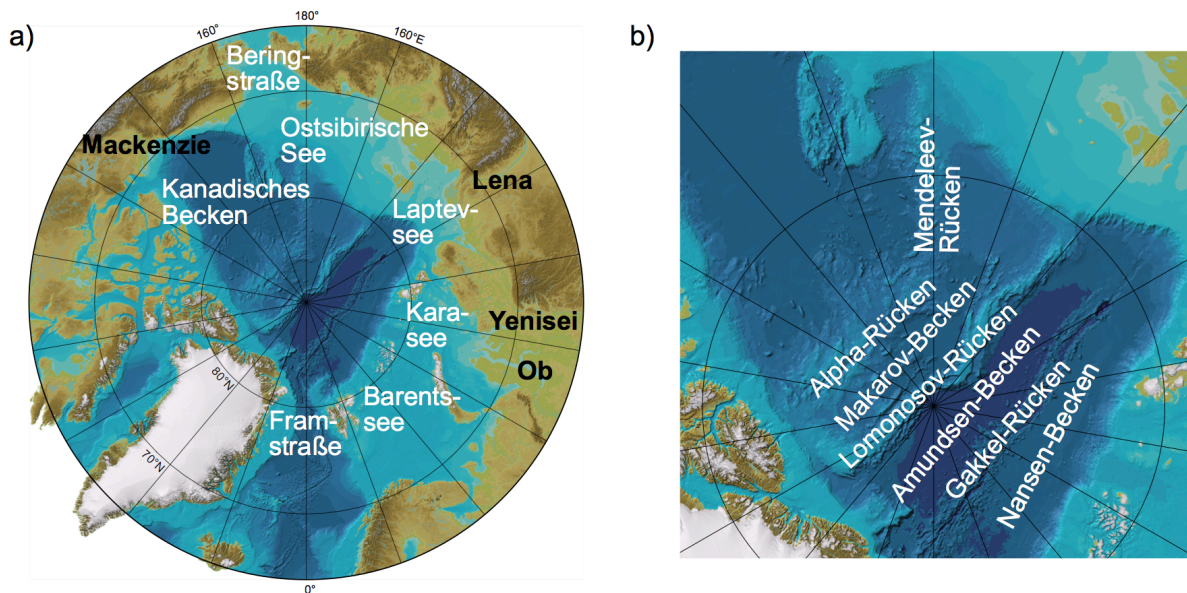


Abb. 1: a) Bathymetrische Karte des Arktischen Ozeans mit Flüssen (schwarz) und Teilmeeren (weiß, nach Jakobsson et al., 2003). b) Vergrößerter Ausschnitt mit Bezeichnung der Ozeanrücken und -becken.

Es existieren mehrere submarine Ozeanrücken, die den Arktischen Ozean in verschiedene Becken unterteilen (Abb. 1). Übergeordnet trennt der Lomonosovrücken das amerasische vom eurasischen Becken. Im amerasischen Becken werden das Kanadische und Makarov-Becken durch den Alpha-

Mendeleev-Rücken getrennt. Das eurasische Becken wird durch den Gakkel-Rücken in zwei Subbecken unterteilt, das Amundsen- und das Nansen-Becken. Der Gakkel-Rücken stellt die Verlängerung des mittelatlantischen Rückens dar. Entlang des Gakkel-Rückens wurde hydrothermale Aktivität festgestellt (Edmonds et al., 2003).

Charakteristisch für den Arktischen Ozean ist eine weitgehende Meereisbedeckung, die in den nördlichsten Gebieten und vor Grönland aus mehrjährigem Eis besteht (Stein, 2008). An der Eiskante kommt es saisonal zur Bildung von einjährigem Eis. Bei der Eisbildung in den Schelfgebieten wird partikuläres Material im Eis eingeschlossen und kann durch die vorherrschenden Strömungssysteme im zentralen Arktischen Ozean verteilt werden. Hierbei dominiert im arktischen Becken als Oberflächenströmung der antizyklonisch verlaufende Beaufort-Wirbel. Die zweite Haupt-Oberflächenströmung ist die Transpolar drift, die von den sibirischen Schelfgebieten über den Nordpol bis zur Framstraße verläuft.

Die Verbindung zum Nordpazifischen Ozean über die Beringstraße weist nur eine mittlere Tiefe von 80 m auf (Jakobsson, 2002), sodass Tiefenwasseraustausch nur über die Framstraße mit dem Nordatlantischen Ozean erfolgen kann. Diese Verbindung ist somit essentiell für die thermohaline Zirkulation und das globale Klima. Der Flusseintrag durch die nordamerikanischen und sibirischen Flüsse, darunter Yenisei, Ob, Lena und Mackenzie, ist sehr groß und mit ca.  $3.3 \cdot 10^3 \text{ km}^3 \text{ a}^{-1}$  äquivalent zu 10% des globalen Flusseintrags von ca.  $33 \cdot 10^3 \text{ km}^3 \text{ a}^{-1}$  (Milliman und Meade, 1983; Gordeev et al., 1996; Holmes et al., 2002). Durch den großen Frischwassereintrag und den alleinigen Tiefenwasseraustausch mit dem Nordatlantik kommt es zu einer Schichtung des Arktischen Ozeans in drei Hauptwassermassen: Oberflächen-, Zwischen- und Tiefenwasser (Abb. 2; Aagaard et al., 1985; Macdonald und Bowers, 1996).

Das Oberflächenwasser weist Temperaturen um den Gefrierpunkt auf und besteht aus einer polaren Misch-Schicht mit sehr niedrigen Salinitäten und der Arktischen Halokline. Die Bildung von Meereis im Winter sorgt für die Entstehung von salzhaltigerem, dichterem Wasser („brine“), welches durch Absinken für eine Stratifizierung des Oberflächenwassers sorgt. Das Zwischenwasser ist wärmer, salzhaltiger und wird aufgrund des atlantischen Ursprungs auch Atlantische

Schicht genannt. Tiefenwasser weist die höchsten Salinitäten und höchsten Verweilzeiten von ca. 300 Jahren auf.

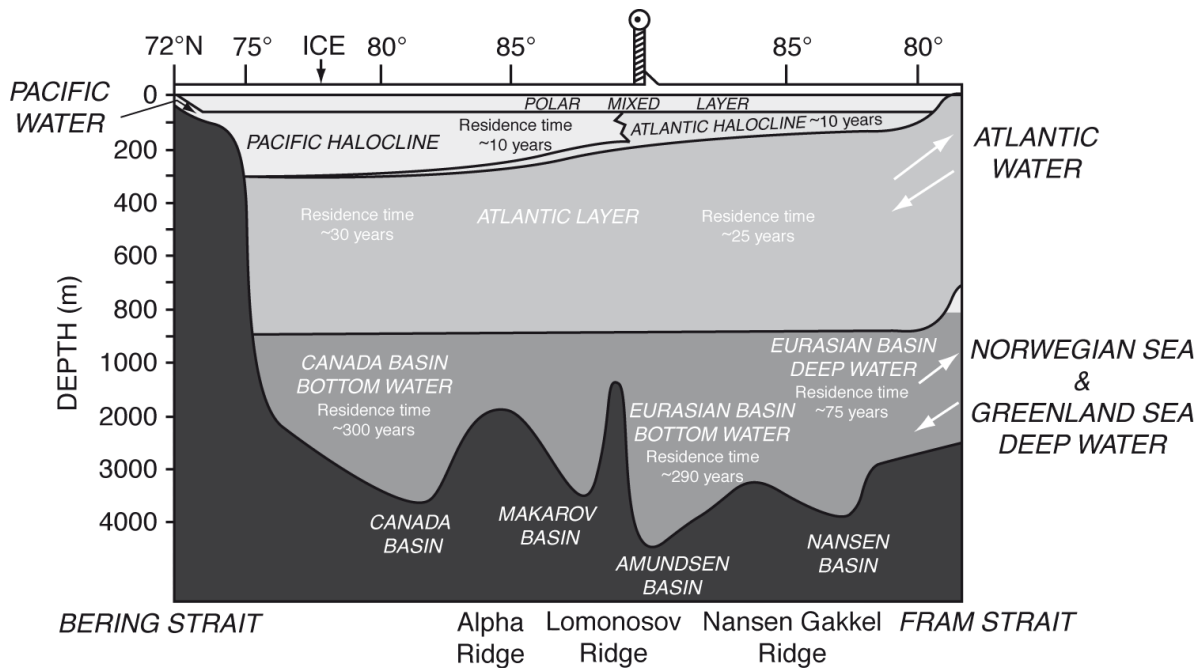


Abb. 2: Schema der Stratifizierung der arktischen Wassermassen (Stein 2008).

## 1.2 Die geochemische Zusammensetzung arktischer Sedimente: Diagnostische Elemente als Anzeiger für terrigenes, biogenes und redox-reaktives Material

Anorganisch-geochemische Untersuchungen an Sedimenten werden häufig in den Geowissenschaften angewendet, da mit Hilfe der chemischen Zusammensetzung des Sediments Aussagen über Materialherkunft, Paläoumweltbedingungen sowie die zeitliche Variabilität dieser Parameter getroffen werden können. Die Verwendung von Analysemethoden wie Röntgenfluoreszenzanalyse ermöglichen die schnelle, simultane, qualitative und quantitative Bestimmung einer Vielzahl von Elementen.

Um die ermittelten Elementgehalte in einen Zusammenhang zu stellen, werden sie mit einem Referenzmaterial verglichen; hierbei wird häufig der mittlere Tonschiefer verwendet (Wedepohl, 1971, 1991). Dieser repräsentiert die mittlere Zusammensetzung der Verwitterungsprodukte der oberen kontinentalen Erdkruste.

Hauptbestandteile sind  $\text{SiO}_2$  und  $\text{Al}_2\text{O}_3$  mit Anteilen von jeweils 59% und 17% vom Gesamtsediment. Um An- oder Abreicherungen zu quantifizieren, werden Anreicherungsfaktoren benutzt (engl. enrichment factor, EF; Brumsack, 2006):

$$\text{EF} = (\text{Element/Al})_{\text{Probe}} / (\text{Element/Al})_{\text{Tonschiefer}} \quad (1)$$

Hierbei zeigen Werte größer 1 eine Anreicherung und Werte kleiner 1 eine Abreicherung. Anstelle des Tonschiefers können je nach geologischem Umfeld weitere Referenzmaterialien verwendet werden oder auch das niedrigste Element/Al-Verhältnis eines Sedimentkerns, welches dann den lokalen Hintergrund darstellt.

Die Elemente Al, Cr, K, Mg, Rb, Ti und Zr dienen als Anzeiger für terrigenen Sedimenteintrag. Sie kommen in Tonmineralen vor und werden durch Verwitterung in marine Sedimente eingetragen.

Biogener Sedimenteintrag wird durch Ba, Ca, P, Sr und organischen Kohlenstoff (engl. total organic carbon, TOC) charakterisiert. Die Schalen von Foraminiferen bestehen aus  $\text{CaCO}_3$ , in dessen Gerüst, je nach Modifikation (Calcit oder Aragonit), auch unterschiedliche Anteile von Sr eingebaut werden können (Rickaby et al., 2002). Ca kommt weiterhin in Dolomit vor ( $\text{CaMg}(\text{CO}_3)_2$ ) und ist dann Bestandteil der terrigenen Sedimentkomponente. Einige Übergangsmetalle können mit organischen Sedimentbestandteilen assoziiert sein (Cd, Cu, Ni, V, Zn; Tribovillard et al., 2006). Silizium kann einerseits in Alumosilikaten und Quarz vorkommen und somit zur terrigenen Gruppe zählen, andererseits als biogene Kieselsäure (Opal) ein Anzeiger für biogenes Material sein.

Zu den authigenen Elementen, deren Verhalten sich je nach vorherrschenden Umweltbedingungen ändert, zählen Cd, Cr, Cu, Fe, Mn, Mo, Ni, Re, U, V und Zn (Calvert und Pedersen, 1993). Unter oxischen Bedingungen liegen z.B. Fe und Mn als feste  $\text{Fe}^{\text{III}}$ - und  $\text{Mn}^{\text{IV}}$ -Verbindungen vor. Diese können unter sub- bzw. anoxischen Bedingungen zu löslichen  $\text{Fe}^{\text{II}}$ - und  $\text{Mn}^{\text{II}}$ -Spezies reduziert werden. Das Vorhandensein von gelösten Fe- und Mn-Verbindungen im Porenwasser zeigt somit reduzierende Bedingungen an.

Die meisten der untersuchten arktischen Sedimente weisen in den obersten Zentimetern eine dunkelbraune Farbe auf. Es folgen Sedimentschichten von

beige-olivbrauner Farbe, die sich mit weiteren dunkelbraunen Schichten abwechseln. Teilweise sind dunkelgraue Schichten oder rosa-weiße grobkörnige Lagen vorhanden. Die unterschiedlich farbigen Intervalle weisen auch unterschiedliche chemische Charakteristika auf. Für die Zusammenstellung in Abb. 3 wurden Mittelwerte von 232 Proben aus braunen, 197 aus hellen, 9 aus rosa, 34 aus grauen und 12 aus weißen Lagen gebildet.

Dunkelbraune Sedimentintervalle sind durch sehr große Anreicherungen von Mn, As, Co und Mo gekennzeichnet. Dies lässt auf das Vorhandensein von Mn-oxiden oder -hydroxiden schließen, die diese Spurenmetalle aus der Wassersäule adsorbieren können („scavenging“; Goldberg, 1954). Auch andere typische Spurenmetalle, die an solche Oberflächen adsorbieren (Cu, Ni, V, Zn), sind angereichert.

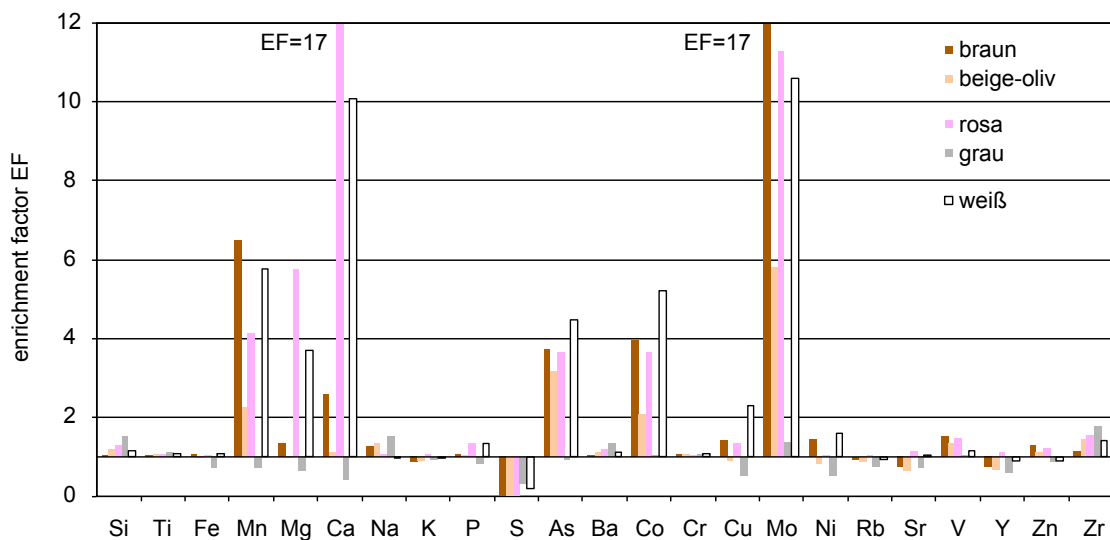


Abb. 3: Anreicherungsfaktoren der verschiedenen Sedimentintervalle gegenüber mittlerem Tonschiefer.

In der gewählten Darstellungsweise scheint Fe nicht signifikant angereichert zu sein. Dies liegt an den relativ hohen Gehalten von Fe im Hintergrundsediment. Normiert auf den lokalen Hintergrund zeigen Fe und Mn vergleichbare absolute Anreicherungen (Meinhardt, 2009). Schwefel ist in allen Sedimentlagen nicht angereichert, was das Vorhandensein von signifikanten Anteilen sulfidischer Verbindungen (vor allem Pyrit) ausschließt.

Helle Lagen sind auch an redox-sensitiven Elementen wie Mn, As, Co und Mo angereichert, jedoch sind die Anreicherungen geringer ausgeprägt als in den dunkelbraunen Lagen.

Rosa Lagen treten in Sedimenten der arktischen Seite des Arktischen Ozeans auf (Stein et al., 2010). Sie sind stark an Mg und Ca angereichert und weisen außerdem erhöhte Gehalte an karbonatischem Kohlenstoff auf (nicht gezeigt). Dies ist charakteristisch für Dolomit. Mögliche Quellen sind die Gebiete des arktischen Archipels, vor allem die Banks- und Victoria-Inseln (Bischof et al., 1996; Bischof und Darby, 1997). Mit dem Beaufort-Wirbel kann dieses Material im arktischen Becken verteilt werden. Weiterhin sind Si, Ti, und Zr angereichert, was den Eintrag einer terrigenen Sedimentkomponente impliziert. Mn, As, Co und Mo sind auch in den rosa Lagen angereichert. Weiße Sedimentlagen sind chemisch ähnlich zu den rosa Lagen. Das Vorhandensein von Dolomit ist auch hier wahrscheinlich.

Die grauen Lagen unterscheiden sich am stärksten von den anderen Sedimentintervallen, da viele Elemente abgereichert sind. Deutlich angereichert sind nur Si und Zr. Dies lässt darauf schließen, dass das Material als repräsentativ für das terrigene Hintergrundgestein angesehen werden kann und keine zusätzlichen biogenen oder authigenen Anteile enthält.

### 1.3 Datierung im Arktischen Ozean: Auf der Suche nach Alternativen

Basis jeglicher Paläoumweltrekonstruktionen ist ein verlässliches Altersmodell. Für Sedimente existieren eine Vielzahl von Datierungsmethoden, von denen im Folgenden die Radiokarbon ( $^{14}\text{C}$ )-Datierung und die  $\delta^{18}\text{O}$ -Stratigraphie exemplarisch im Hinblick auf ihre Nutzbarkeit in der spezifischen Umgebung des Arktischen Ozeans diskutiert werden.

Radiokarbon ( $^{14}\text{C}$ )-Datierung ist die am häufigsten benutzte Methode zur Altersbestimmung von organischem Material (z.B. Oswald et al., 2005). In großen Teilen des Arktischen Ozeans ist die Produktion sehr gering, was zu geringen Gehalten von organischem Material im Sediment führt. Deswegen werden oft Fossilien datiert, vor allem Weichtiere und Walknochen. Ein Problem bei der Datierung mariner Fossilien ist die unsichere Abschätzung des marinen

Reservoiralters, welches für viele Küstengebiete bestimmt wurde, jedoch nicht direkt auf Tiefsee-Fossilien angewendet werden kann (Alexanderson et al., 2014). Weiterhin ist das Vorkommen dieser Fossilien in arktischen Sedimenten begrenzt (Backman et al., 2004; Stein, 2008).

$\delta^{18}\text{O}$ -Stratigraphie an Foraminiferen ist eine Standardmethode zur Datierung mariner Sedimente. Variationen in den  $\delta^{18}\text{O}$ -Signalen repräsentieren das globale Eisvolumen und sind somit diagnostisch für Wechsel von Glazialen und Interglazialen. Im Arktischen Ozean weisen diese Variationen größere Amplituden im Vergleich zu anderen Ozeanen auf (Polyak et al., 2004; Spielhagen et al., 2004). Problematisch sind spezifische Gegebenheiten wie Meereisbildung, Bildung von „brines“ und starker Frischwassereintrag durch die Flüsse (Polyak et al., 2003; Brennan et al., 2013). Diese Parameter variieren saisonal wie auch auf größeren Zeitskalen stark. Die Größe der Foraminiferen spielt eine Rolle, und zusätzlich treten diese Mikrofossilien nicht während glazialer Maxima auf (Hillaire-Marcel et al., 2004). Aus diesen Gründen ist die Nutzung der  $\delta^{18}\text{O}$ -Stratigraphie für arktische Sedimente stark eingeschränkt.

Essentiell für ein Verständnis von Paläoumweltbedingungen ist die Verknüpfung von terrestrischen und marinen Sedimentarchiven durch Korrelation. Erschwerend ist hierbei die unterschiedliche Natur der beiden Sedimentationsräume. Provenanzstudien wirken hierbei unterstützend, um spezifische Sedimentintervalle eindeutigen terrestrischen Herkunftsgebieten zuzuordnen (siehe Kapitel 4). Hierbei müssen die verschiedenen Strömungssysteme des Arktischen Ozeans berücksichtigt werden, durch die das Material nicht gleichflächig verteilt wird.

Auf der Suche nach alternativen, robusten Datierungsmöglichkeiten wurde ein Zusammenhang von dunkelbrauner Sedimentfarbe, erhöhten Mn-Gehalten und potentieller Anwendung als Altersmarkierung in Arktischen Sedimenten zuerst von Jakobsson et al. (2000) für einen Sedimentkern des zentralen Lomonosovrücken entdeckt. Die Autoren entwickelten ein auf Mn-Zyklen basierendes Altersmodell und korrelierten dieses erfolgreich mit einem existierenden auf  $\delta^{18}\text{O}$  Messungen basierenden Altersmodell niedriger Breitengrade. Es wurden zwei mögliche Mechanismen für die Entstehung der Mn-Lagen erörtert. Zum einen können variierende Mn-Gehalte im Sediment durch klimatisch bedingten externen



Materialeintrag aus Nordsibirien erklärt werden. Die sibirischen Flüsse drainieren Torfgebiete, in denen eher saure Bedingungen herrschen und die als Mn-Quelle dienen. Dieses System wäre in Glazialen inaktiv und würde so die Mn-Zyklizität erklären. Zum anderen könnte die Durchlüftung der Wassersäule Einfluss haben. Es werden höhere Sauerstoff-Konzentrationen des Bodenwassers während Interglazialen postuliert, die das Ausfallen von festen Mn-Verbindungen begünstigen. Niedrigere Sauerstoff-Konzentrationen im Bodenwasser während Glazialen würden zu einer Stratifizierung der Wassersäule, reduzierenden Bedingungen und geringeren Anteilen fester Mn-Verbindungen führen. Eine eingeschränkte Bodenwasserdurchlüftung während der Glazialzeiten wird mittlerweile als nicht wahrscheinlich angesehen (März et al., 2010, 2011; Cronin et al., 2012). Die Mn-Lagen haben demnach ein vielversprechendes Potential als alternative Datierungsmöglichkeit, da sie in weiten Teilen des zentralen Arktische Ozeans vorkommen (Löwemark et al., 2014). Einschränkungen treten jedoch auch hier auf, da diagenetische Prozesse in arktischen Sedimenten Mn-Lagen auslöschen oder neu entstehen lassen können (Li et al., 1969; Katsev et al., 2006; Magen et al., 2011). Diese Prozesse werden im folgenden Kapitel näher erläutert.

### 1.4 Diagenetische Prozesse im Sediment und mögliche Beeinflussung Mn-reicher Sedimentlagen

Die mögliche Umverteilung von Mn nach der Ablagerung wurde bereits in frühen Arbeiten von Murray und Irvine (1895) erwähnt. Im Arktischen Ozean erklärten Li et al. (1969) Profile von festem und gelöstem Mn in einem Sedimentkern des Kanadischen Beckens durch Reduktion von Mn nach der Ablagerung, Diffusion Richtung Oberfläche und erneutem Ausfallen an der oxidierenden Oberfläche. Grundlage dieser diagenetischen Prozesse ist die Oxidation von organischem Material durch Mikroorganismen. Die Sedimentzusammensetzung kann nach der Ablagerung durch mikrobiell induzierte Redoxreaktionen verändert werden, die der katabolischen Sequenz von Elektronenakzeptoren während des Abbaus von organischem Material folgen (Tab. 1, Abb. 4; Froelich et al., 1979; Canfield und Thamdrup, 2009). Hierbei spielen die Verfügbarkeit der einzelnen Elektronenakzeptoren, der Energiegewinn der

Reaktion (Gibbs Energie) sowie die vorherrschende mikrobielle Gemeinschaft eine Rolle. Die metabolischen Edukte (z.B.  $\text{NO}_3^-$ ,  $\text{SO}_4^{2-}$ ) sowie Produkte (z.B.  $\text{Mn}^{2+}$ ,  $\text{Fe}^{2+}$ ) der einzelnen Reaktionen können im Porenwasser nachgewiesen werden.

Tab. 1: Berechnete Gibbs-Energie für die prinzipiellen Atmungswege bei der Mineralisierung von organischem Material in der Natur mit Azetat als Elektronendonator (aus Canfield und Thamdrup, 2009).

		kJ pro Reaktion $\Delta G$ (Azetat)*
Oxische Atmung	$\text{O}_2 + 1/2\text{C}_2\text{H}_3\text{O}_2^- \rightarrow \text{HCO}_3^- + 1/2\text{H}^+$	-402
Denitrifikation	$4/5\text{NO}_3^- + 3/5\text{H}^+ + 1/2\text{C}_2\text{H}_3\text{O}_2^- \rightarrow 2/5\text{N}_2 + \text{HCO}_3^- + 1/5\text{H}_2\text{O}$	-359
Mn-Reduktion (von $\text{MnO}_2$ )	$7/2\text{H}^+ + 2\text{MnO}_2 + 1/2\text{C}_2\text{H}_3\text{O}_2^- \rightarrow 2\text{Mn}^{2+} + \text{HCO}_3^- + 2\text{H}_2\text{O}$	-285
Fe-Reduktion ( <i>frisch ausgefallenes amorphes FeOOH</i> )	$15/2\text{H}^+ + 4\text{FeOOH} + 1/2\text{C}_2\text{H}_3\text{O}_2^- \rightarrow 4\text{Fe}^{2+} + \text{HCO}_3^- + 6\text{H}_2\text{O}$	-241
Sulfat-Reduktion	$1/2\text{H}^+ + 1/2\text{SO}_4^{2-} + 1/2\text{C}_2\text{H}_3\text{O}_2^- \rightarrow 1/2\text{H}_2\text{S} + \text{HCO}_3^-$	-43.8
Methanogenese	$1/2\text{H}_2\text{O} + 1/2\text{C}_2\text{H}_3\text{O}_2^- \rightarrow 1/2\text{CH}_4 + 1/2\text{HCO}_3^-$	-19.9

\*Normiert auf einen  $4e^-$  Transfer äquivalent zu der Oxidation von 1 Mol organischen Kohlenstoff mit Oxidationsstufe 0, wie in Kohlenhydraten. Rechnungsbedingungen: 25 °C, einheitliche Aktivität aller Edukte und Produkte, pH = 7.

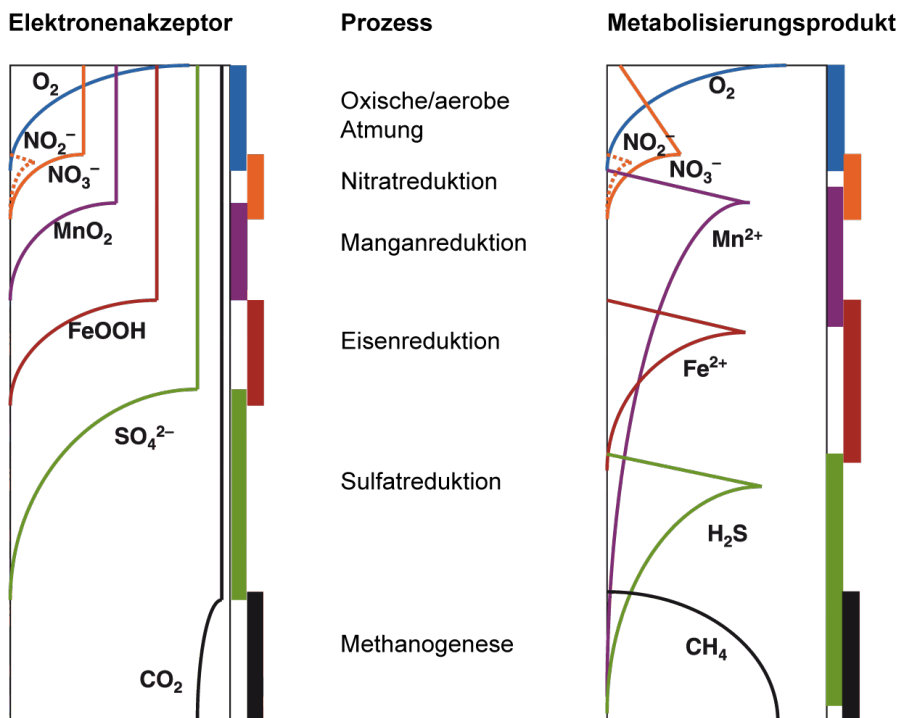


Abb. 4: Schematische Tiefenverteilung der gängigen Elektronenakzeptoren in der Natur. Die wirkliche Lage im Sediment sowie die Ausprägung können variieren und die Zonen können überlappen (verändert nach Canfield und Thamdrup, 2009).

Nach Tab. 1 ist die Nutzung von Sauerstoff demnach die bevorzugte Reaktion. Je nach Umweltbedingungen kann sich die Zone der Sauerstoff-Reduktion auf wenige Zentimeter an der Sedimentoberfläche beschränken oder sich mehrere Meter tief ausdehnen.

Im Arktischen Ozean gibt es zwei unterscheidbare Milieus: Sedimente in Küsten- bzw. Schelfgebieten und Tiefseesedimente des zentralen Arktischen Ozeans. In Küsten- und Schelfgebieten wird durch Flüsse und Küstenerosion organisches Material eingetragen, welches nach obigen Reaktionen abgebaut wird. Es erfolgt ein intensives Recycling der beteiligten Spezies, bei dem z.B. Mn, Fe und assoziierte Metalle reduziert werden, diffundieren, und bei Kontakt mit Sauerstoff wieder ausfallen. Die Zone der Mn-Reduktion befindet sich in den oberen Dezimetern der Schelfsedimente (Gobeil et al., 1997; Macdonald und Gobeil, 2012). Der zentrale Arktische Ozean ist im globalen Vergleich die Region mit der geringsten Produktivität (Stein, 2008). Folglich ist die Intensität der Abbauprozesse in Tiefseesedimenten vermindert und die Mn-Reduktionszone beginnt in einigen Metern Kerntiefe (Backman et al., 2006; März et al., 2011). Die Redoxgrenze im Sediment und somit die Mn-Reduktionszone kann saisonal oder in größeren Zeitskalen aufgrund von variablem Eintrag von organischem Material variieren (Aller, 1994; Gobeil et al. 1997; Katsev et al., 2006).

Der Einfluss diagenetischer Prozesse auf die Sedimentgeochemie von Mn im Arktischen Ozean wurde bisher in wenigen Studien behandelt. März et al. (2011) untersuchten die Sediment- und Porenwassergeochemie eines Sedimentkerns vom Mendeleev-Rücken und konnten feststellen, dass eine dunkelbraune Mn-reiche Sedimentlage durch den Ausfall von gelöstem  $Mn^{2+}$  aus dem Porenwasser nach der Ablagerung wachsen kann und dass sich Mn-Lagen innerhalb der Mn-Reduktionszone teilweise auflösen können. Aufbauend auf dieser Arbeit benutzten Sundby et al. (2015) ein diagenetisches Modell, um der Fragestellung nachzugehen, ob die Mn-Lagen verlässliche Altersmarker darstellen. In ihrem Modell wurde als Bedingung für diagenetische Prozesse das Vorhandensein von partikulärem organischen Material und Gashydraten angenommen. Die Autoren konnten zeigen, dass durch Oxidation von aufwärts diffundierendem  $Mn^{2+}$  aus dem Porenwasser Mn-Anreicherungen im Sediment entstehen können, die nicht von bereits vorhandenen, während Interglazialen entstandenen Mn-Lagen

unterschieden werden können. Folglich ist die Nutzung dieser Lagen als Altersmarker für diese Lokation eingeschränkt. In Umgebungen ohne reaktives organisches Material werden diese Lagen hingegen als diagnostisch für Interglaziale angesehen.

Um diagenetische Prozesse ausschließen zu können, müssen neben der Erfassung der Mn-Gehalte im Sediment demnach auch weitere Parameter erfasst werden, wie organischer Kohlenstoff und gelöstes  $Mn^{2+}$  im Porenwasser. Da nicht zu erwarten ist, dass sich diese Parameter im Arktischen Ozean gleichmäßig verhalten, muss eine Charakterisierung an der jeweiligen Kernlokation erfolgen.

## 1.5 Nd-Isotope als Indikator für Tiefenwasserzirkulation und Sedimentherkunft

Die Zirkulationszeit des globalen Ozeans beträgt etwa 1000 Jahre (Broeker und Peng, 1982). Informationen über die Tiefenwasserzirkulation können aus radiogenen Metallisotopen abgeleitet werden. Radiogene Isotope entstehen durch radioaktiven Zerfall eines Elements. Ist die Verweilzeit eines Spurenmetalls deutlich geringer als die globale Zirkulationszeit, so kann eine Wassermasse keine spezifische Isotopensignatur annehmen, die über längere Distanzen detektiert werden kann. Ist die Verweilzeit hingegen sehr viel größer, wird die Isotopensignatur durch Mischung global einheitlich sein (z.B. Frank 2002). Die Verweilzeit von Nd im Tiefenwasser beträgt etwa 500 Jahre, somit kann es als Indikator für die Tiefenwasserzirkulation benutzt werden (Tachikawa et al., 2003).

Im System Sm/Nd (DePaolo und Wasserburg, 1976; Wilson, 1989) ist Nd das inkompatiblere Element. Bei Schmelzprozessen im Erdmantel werden kompatible Elemente (Sm) bevorzugt in Mantelminerale eingebaut und inkompatible Elemente (Nd) in der Schmelze angereichert. Das Verhältnis von Sm/Nd ist im residualen Erdmantel folglich erhöht.  $^{147}\text{Sm}$  zerfällt im Erdmantel zu  $^{143}\text{Nd}$ . In geologischen Studien wird das  $^{143}\text{Nd}/^{144}\text{Nd}$ -Verhältnis eines Gesteins ermittelt, welches im Erdmantel größer ist als in der Schmelze. Der Unterschied zwischen den  $^{143}\text{Nd}/^{144}\text{Nd}$ -Verhältnissen ist sehr gering, sodass die Isotopenverhältnisse als  $\epsilon_{\text{Nd}}$  ausgedrückt werden (DePaolo und Wasserburg, 1976):

$$\epsilon_{\text{Nd}} = [((^{143}\text{Nd}/^{144}\text{Nd})_{\text{Probe}} - (^{143}\text{Nd}/^{144}\text{Nd})_{\text{CHUR}}) / (^{143}\text{Nd}/^{144}\text{Nd})_{\text{CHUR}}] \cdot 10^4 \quad (2)$$

$(^{143}\text{Nd}/^{144}\text{Nd})_{\text{CHUR}}$  ist das aktuelle Isotopenverhältnis des **Chondritic Uniform Reservoir** von 0,512638, welches die mittlere Zusammensetzung eines primären unfraktionierten Gesteins (wie in Chondriten) widerspiegelt (Jacobsen und Wasserburg, 1980).

Durch Flusseintrag, äolischen Eintrag und Verwitterung gelangt Nd mit unterschiedlicher Isotopenzusammensetzung in die Ozeane. Dabei ist Nd unabhängig von Fraktionierungen durch biologische Prozesse (z.B. Frank, 2002). Nd wird aus der Wassersäule durch Adsorption an Partikel entfernt und weist im Oberflächenwasser geringe Konzentrationen auf. Mit zunehmender Wassertiefe nimmt die Konzentration durch Desorptionsprozesse wieder zu.

Da Sm während der Bildung von kontinentaler Kruste bevorzugt im Erdmantel verbleibt und dort zerfällt, ist  $\epsilon_{\text{Nd}}$  in jungen Mantelgesteinen höher als in älterem, kontinentalem Material. Inselbogengesteine um den Pazifischen Ozean können positive  $\epsilon_{\text{Nd}}$ -Werte bis zu +20 aufweisen, kontinentale Krustengesteine um den Nordatlantik hingegen negative Werte bis -40. Folglich werden die niedrigsten Werte in Wassermassen gefunden, die verwittertes Material von alter kontinentaler Kruste erhalten, wie in der Baffin Bucht zwischen Kanada und Grönland ( $\epsilon_{\text{Nd}}$  von -26; Stordal und Wasserburg, 1986).

Die aktuellen Nd-Isotopenverhältnisse einer Wassermasse können durch direkte Messung bestimmt werden. Jedoch kann auch die Paläosignatur aus Sedimentarchiven extrahiert werden. Mn-Fe-(Oxihydr)oxide adsorbieren Nd aus der Wassersäule. Dabei steht das Nd-Isotopenverhältnis an den Partikeln im Gleichgewicht mit dem der Wassersäule. Frisch abgelagerte Partikel am Meeresboden weisen somit die Isotopenzusammensetzung des Tiefenwassers auf. Durch Sedimentation wird das Signal im Sediment erhalten. Für Paläoumweltstudien können die Mn-Fe-(Oxihydr)oxide aus dem Sediment extrahiert und somit vom lithogenen Material getrennt werden. Die Messung der Nd-Isotopenverhältnisse an dem Extrakt ist somit charakteristisch für die Nd-Isotopenverhältnisse des Tiefenwassers zur Zeit der Ablagerung. Weiterhin kann das Signal aus Foraminiferen, Korallen und Fischzähnen extrahiert werden

(Palmer und Elderfield, 1986; Vance und Burton, 1999; Martin und Haley, 2000). Das Nd-Isotopenverhältnis der lithogenen Sedimentfraktion repräsentiert das Signal des Umgebungsgesteins und wird für Provenanzstudien benutzt.

## 1.6 Fe-Isotope als Indikator für Redoxbedingungen und Transportprozesse

Die Nutzung von Fe-Isotopen wurde in den letzten Jahren intensiviert, da dieses Isotopensystem wertvolle Informationen über Paläo-Umweltbedingungen wie Metallkreisläufe und Redoxzustände liefern kann. Es existieren vier natürlich vorkommende Fe-Isotope:  $^{54}\text{Fe}$ ,  $^{56}\text{Fe}$ ,  $^{57}\text{Fe}$  und  $^{58}\text{Fe}$ . Am häufigsten ist  $^{56}\text{Fe}$  mit ~92% (Anbar und Rouxel, 2007). In geologischen Studien wird das  $^{56}\text{Fe}/^{54}\text{Fe}$ -Verhältnis als  $\delta^{56}\text{Fe}$ -Wert relativ zu einem Standard (häufig der internationale Fe-Isotopie-Standard IRMM-14; Belshaw et al., 2000) angegeben:

$$\delta^{56}\text{Fe} = \left[ \left( \frac{^{56}\text{Fe}/^{54}\text{Fe}}{^{56}\text{Fe}/^{54}\text{Fe}} \right)_{\text{Probe}} / \left( \frac{^{56}\text{Fe}/^{54}\text{Fe}}{^{56}\text{Fe}/^{54}\text{Fe}} \right)_{\text{IRMM-14}} - 1 \right] \cdot 1000 \quad (3)$$

Bei jeglichen chemischen Reaktionen von Fe erfolgt eine massenabhängige Fraktionierung, was bedeutet, dass das leichtere Isotop bevorzugt reagiert (Bigeleisen und Mayer, 1947).

Da die dunkelbraunen Sedimentlagen sowohl erhöhte Mn- als auch Fe-Gehalte aufweisen, kommt Fe eine möglicherweise vergleichbare Bedeutung im Hinblick auf die Nutzung als stratigraphisches Werkzeug zu. Die Untersuchung der  $\delta^{56}\text{Fe}$ -Werte von verschiedenen Sedimentlagen kann Informationen darüber liefern, ob diese Lagen unter sauerstoffreichen Bedingungen abgelagert wurden und primärer Natur sind, was eine Nutzung als Altersmarker ermöglichen würde. Diagenetische Prozesse nach der Ablagerung, die zu einer Isotopenfraktionierung führen, wie z.B. mikrobiell induzierte  $\text{Fe}^{\text{III}}$ -Reduktion, würden zu einer Verringerung der  $\delta^{56}\text{Fe}$ -Werte führen (Beard et al., 1999). Somit ist die Bestimmung der Fe-Isotopenverhältnisse in Arktischen Sedimenten ein potentiell Werkzeug zur Frage der Genese und möglichen Beeinflussung der dunkelbraunen Sedimentlagen.

## 1.7 Fragestellungen dieser Arbeit

Welche anorganisch geochemischen Charakteristika weisen Sedimente des Arktischen Ozeans auf und wie ist ihre räumliche und zeitliche Verteilung?

In diesem Zusammenhang wurde die Haupt- und Spurenmetallverteilung der Sedimente untersucht, um herauszufinden, ob sich spezielle Elemente in verschiedene Sedimentbestandteile gruppieren lassen.

→ Kapitel 3

Welche geochemischen Parameter sind diagnostisch für Materialeintrag und Tiefenwasserströmungen und wie haben sich diese im Verlauf des späten Quartärs verändert? Was sind die Quellen der Sedimentkomponenten?

→ Kapitel 4

Wie sind Mn-reiche Lagen im Sediment zusammengesetzt und wie entstehen sie? Können sie als Altersmarker benutzt werden oder verfälschen interne Umlagerungsprozesse dieses Signal? Gibt es diagnostische Parameter, um diagenetisch veränderte Sedimentlagen zu erkennen? Welche anderen Elemente sind durch Diagenese beeinflusst? Gibt es dabei lokale Unterschiede?

→ Kapitel 5

## 2. Autorenanteil an den hier vorgestellten Publikationen

Die Dissertation basiert auf fünf Manuskripten, in denen Sedimente und Porenwässer des Arktischen Ozeans geochemisch untersucht werden, um Aussagen über Materialeintrag, Strömungssysteme, Sedimentcharakteristika, interne Umwandlungsprozesse und die Auswirkungen von wechselnden klimatischen Bedingungen (Glazial-/Interglazialzyklen) auf diese Parameter zu treffen. Drei Manuskripte werden im Detail vorgestellt (Kapitel 3 bis 6). Weiterhin wurde an zwei bereits publizierten Manuskripten mitgewirkt, deren jeweilige Kurz-Zusammenfassung in den Kapiteln 7 und 8 dargestellt werden. Der Autorenanteil an den Manuskripten wird im Folgenden erläutert.

### **Kapitel 3: Regional variations in sediment geochemistry on a transect across the Mendeleev Ridge (Arctic Ocean)**

In diesem Manuskript wurden terrigene, biogene und redox-sensitive Komponenten in Sedimenten des Mendeleev Rückens anhand von Haupt- und Spurenmetallen charakterisiert. Es basiert in Teilen auf der Diplomarbeit von Ann-Katrin Meinhardt (Meinhardt, 2009), deren Ergebnisse umfassend überarbeitet und durch neue Berechnungen und Interpretationen ergänzt wurden. Die Autorin hat die geochemischen Analysen durchgeführt. Die Sedimentkerne wurden von Dr. Christian März zur Verfügung gestellt. Ann-Katrin Meinhardt hat die Daten ausgewertet, interpretiert und mit allen Koautoren diskutiert. Das Manuskript wurde von Ann-Katrin Meinhardt in Zusammenarbeit mit allen Autoren verfasst und wie folgt publiziert:

Meinhardt, A.-K., März, C., Stein, R., Brumsack, H.-J., 2014. Regional variations in sediment geochemistry on a transect across the Mendeleev Ridge (Arctic Ocean). *Chemical Geology* 369, 1-11.



#### **Kapitel 4: Variations of bottom water circulation and sediment provenance in the Central Arctic Ocean since the Last Glacial Maximum**

Mit Hilfe von Nd- und Sr-Isotopenverhältnissen sowie Elementdaten wurden die Tiefenwasserzirkulation und der lithogene Sedimenteintrag des Arktischen Ozeans im letzten Glazialen Maximum mit der aktuellen Situation verglichen. Ann-Katrin Meinhardt hat die geochemischen Analysen durchgeführt, die Daten ausgewertet, interpretiert und mit allen Koautoren diskutiert. Dr. Philipp Böning hat die Messung der Nd- und Sr-Isotopenverhältnisse durchgeführt. Das Manuskript wurde von Ann-Katrin Meinhardt in Zusammenarbeit mit allen Koautoren verfasst.

Dieses Kapitel wurde eingereicht bei: Chemical Geology.

#### **Kapitel 5: Diagenetic regimes in Arctic Ocean sediments: Implications for sediment geochemistry and core correlation**

In diesem Manuskript wurden mögliche Quellen von Mn- und Fe-Anreicherungen in Sedimenten des Arktischen Ozeans sowie die Auswirkungen diagenetischer Prozesse auf die Sedimentgeochemie untersucht. Ann-Katrin Meinhardt hat die geochemischen Analysen durchgeführt, die Daten ausgewertet, interpretiert und mit allen Koautoren diskutiert. Die Modellrechnung stammt von Dr. Karsten Lettmann. Die Aufbereitung für die Fe-Isotopie Messungen wurden von Ann-Katrin Meinhardt unter Anleitung von Dr. Stephan Schuth durchgeführt, der anschließend die Messung der Fe-Isotopenverhältnisse durchgeführt hat. Das Manuskript wurde von Ann-Katrin Meinhardt in Zusammenarbeit mit allen Koautoren verfasst.

Dieses Kapitel wurde eingereicht bei: Geochimica et Cosmochimica Acta.

## **Kapitel 6: Manganese-rich brown layers in Arctic Ocean sediments: Composition, formation mechanisms, and diagenetic overprint**

In dieser Arbeit wurden Mn-Anreicherungen in Arktischen Sedimenten des Lomonosov-Rückens detailliert geochemisch untersucht, um Aussagen über die Entstehung und Anwendung als stratigraphisches Werkzeug zu machen. Ann-Katrin Meinhardt war an der Diskussion beteiligt. Das Manuskript wurde von Dr. Christian März verfasst und wie folgt publiziert:

März, C., Stratmann, A., Matthiessen, J., Meinhardt, A.-K., Eckert, S., Schnetger, B., Vogt, C., Stein, R., Brumsack, H.-J., 2011. Manganese-rich brown layers in Arctic Ocean sediments: Composition, formation mechanisms, and diagenetic overprint. *Geochimica et Cosmochimica Acta* 75 (23), 7668-7687.

## **Kapitel 7: Silica diagenesis and benthic fluxes in the Arctic Ocean**

Der Kieselsäurekreislauf im Arktischen Ozean wurde mit Hilfe von Porenwasseruntersuchungen und der Berechnung benthischer Flüsse umfassend untersucht. Ann-Katrin Meinhardt und Dr. Christian März haben die Porenwasseruntersuchungen durchgeführt. Ann-Katrin Meinhardt war an der Diskussion und Interpretation beteiligt. Das Manuskript wurde von Dr. Christian März verfasst und wie folgt publiziert:

März, C., Meinhardt, A.-K., Schnetger, B., Brumsack, H.-J., 2015. Silica diagenesis and benthic fluxes in the Arctic Ocean. *Marine Chemistry* 171, 1-9.

### 3. Regional variations in sediment geochemistry on a transect across the Mendeleev Ridge (Arctic Ocean)

Meinhardt, A.-K.<sup>1</sup>, März, C.<sup>1,2</sup>, Stein, R.<sup>3</sup>, Brumsack, H.-J.<sup>1</sup>

<sup>1</sup> Microbiogeochemistry, Institute for Chemistry and Biology of the Marine Environment (ICBM), Carl von Ossietzky University Oldenburg, P.O. Box 2503, 26111 Oldenburg, Germany

<sup>2</sup> Geosciences, School of Civil Engineering and Geosciences, Newcastle University, NE1 7RU Newcastle upon Tyne, United Kingdom

<sup>3</sup> Alfred Wegener Institute for Polar and Marine Research, 27568 Bremerhaven, Germany

Dieses Kapitel wurde publiziert in: *Chemical Geology* 369, 1-11 (2014).

#### 3.1 Abstract

Inorganic geochemical investigations were performed on three Arctic surface sediment cores (PS72/408-4, PS72/ 410-2 and PS72/422-4) recovered during RV Polarstern expedition ARK-XXIII/3 on a transect across the Mendeleev Ridge. Dark brown layers are geochemically characterized by elevated Mn/Al and Fe/Al ratios and trace metal enrichments. Trace metals, such as As, Co, Cu, Mo and Ni, seem to be adsorbed onto Mn/Fe oxyhydroxide surfaces due to scavenging from the water column. Similar enrichment patterns of Mn, Co, Mo and Ni suggest that these trace metals are predominantly bound to Mn, whereas different patterns for Fe, As and Cu reveal that these trace metals are most probably mainly bound to other sediment phases like Fe- oxyhydroxides or clay minerals. Calculating Mn and Fe excess amounts reveals that the dark brown color of the layers, which so far has predominantly been attributed to enhanced Mn oxyhydroxide contents alone, may as well result from a higher Fe-oxyhydroxide contribution. In the investigated surface sediments Mn-rich layers seem to originate primarily from particulates formed within the water column. This implies that the composition of

brown layers may be spatially variable even at short distances. A diagenetic overprint is not necessarily required, putting constraints on the large-scale correlation of brown layers across Arctic Basins. The Mn enrichments are presumably related to both Siberian river discharge and coastal erosion. Material input related to ice rafted debris is documented in Ca/Al, Mg/Al and TIC patterns indicating the occurrence of dolomite from the Canadian Archipelago. This material is transported via the Beaufort Gyre and shows decreasing abundance towards the west along the transect. A more basaltic component, presumably originating from the East Siberian hinterland, is characterized by low Si/Al and K/Al records. Ca<sub>bio</sub> and Sr<sub>xs</sub> patterns may serve as additional indicators for biogenic carbonate input and glacial/interglacial changes.

### 3.2 Introduction

The Arctic Ocean is currently undergoing rapid environmental changes that are in the focus of scientific and public discussions, especially the decrease in sea ice (Anisimov et al., 2007; Polyak et al., 2010). However, the Arctic region has undergone significant paleoenvironmental changes unrelated to human impact throughout most of the Pleistocene, and these fluctuations are archived in the sediments covering the Arctic Ocean floor. These geological archives have been, and still are, extensively studied by a number of geoscientific and geochemical approaches (e.g., Clark et al., 1980; Stein et al., 1994; Knies et al., 2000; Schoster et al., 2000; Phillips and Grantz, 2001; Polyak et al., 2004; Spielhagen et al., 2004; Löwemark et al., 2008; Polyak et al., 2009; März et al., 2010, 2011; for recent review see Stein, 2008). In this study, three short cores from the Mendeleev Ridge recovered during Expedition ARK-XXIII/3 by the icebreaker Polarstern in 2008

(Jokat, 2009) were studied in detail by inorganic geochemical methods. The main focus of this study is related to the occurrence of marked alternating dark brown and lighter olive brown intervals in Arctic Ocean sediments. These layers are characterized by variable Mn contents (e.g., Jakobsson et al., 2000; Löwemark et al., 2008). However, it is still debated whether these Mn layers represent primary environmental signals, allowing their use as stratigraphic tools to reconstruct climatic events in the Arctic, or whether diagenesis has the potential to

disrupt these primary signals. Regional correlations exclusively based on these Mn layers are complicated by their variable numbers in different Arctic sediment cores in response to varying sedimentation rates or diagenetic overprint (Stein et al., 2010a,b; März et al., 2011).

Manganese in the Arctic Ocean is delivered to the sediments mostly by riverine input and coastal erosion. While Macdonald and Gobeil (2012) proposed coastal erosion as the dominant Mn source, the composition of the eroded coastal deposits delivered to the Arctic Ocean basins during sea level rises is unknown, and quantitative estimates are missing. The circum-Arctic rivers carry huge amounts of freshwater into the Arctic Ocean, and particularly the Siberian rivers drain extensive peat bogs and boreal forests rich in Mn (e.g., Jakobsson et al.,

2000). For example, the mean dissolved Mn concentration in the river Lena is twice the world river average (Hölemann et al., 1999). The riverine particulate and in part dissolved material is deposited on the shelf where diagenetic cycling occurs (Schoster, 2005; März et al., 2011). Several studies show the release of dissolved Mn to the water column (Hölemann et al., 1999; Schoster et al., 2000; Dellwig et al., 2007; Macdonald and Gobeil, 2012). The dissolved Mn may be subsequently oxidized and accumulated as amorphous to poorly crystalline oxyhydroxide.

Higher amounts of Mn in the basinal sediments appear to document interglacials with reduced sea ice cover, higher river runoff and coastal erosion, and well-oxygenated bottom waters (Jakobsson et al., 2000, 2001; Polyak et al., 2004; Löwemark et al., 2008; Löwemark et al., 2012). As discussed by Macdonald and Gobeil (2012), oscillating Siberian river discharge may be sufficient to produce Mn enrichments that propagate across the shelves to the deep basins. In contrast to this model of climate-controlled sedimentary Mn variations, early diagenesis has been discussed as another possible mechanism to cause Mn enrichments or depletions (Li et al., 1969; Gobeil et al., 1997, 2001; März et al., 2011). Changes to the Mn redox cycle due to differences in oxygen concentration in bottom waters, organic matter flux to the sea floor, or oxidation capacity may shift the position of redox zones in the sediment column, leading to dissolution of existing, and formation of new, Mn peaks in the sediment (e.g., Froelich et al., 1979; Klinkhammer, 1980; Burdige, 1993).

With our geochemical investigation, we will try to evaluate whether the specific composition of the brown layers in the studied sediments may serve as a paleoenvironmental tool. As our short cores were taken along a latitudinal transect across Mendeleev Ridge, we aim to document the variable effects of river discharge/coastal erosion, sea ice transport, sediment provenance and the dominant current systems in this specific area.

The Mendeleev Ridge is situated at the confluence of the two major Arctic current systems: The anti-cyclonic Beaufort Gyre (BG) in the Amerasian Basin (Bischof and Darby, 1997) and the Transpolar Drift (TD), originating from the Siberian shelf areas and heading across the central Arctic towards the Fram Strait. Mineralogical analyses, investigations of clast composition, and studies of ice-rafted debris (IRD) in Arctic sediments have successfully been conducted to recover information about the lithological composition of detrital material originating from different source areas, and hence to reconstruct variable current patterns especially in the western Arctic Ocean (e.g., Bischof et al., 1996; Bischof and Darby, 1997; Spielhagen et al., 1997; Vogt, 1997; Phillips and Grantz, 2001; Spielhagen et al., 2004; Vogt, 2009; Stein et al., 2010a,b).

Here we present a geochemical investigation based on specific elemental patterns to trace the delivery of Siberian versus North American detritus to the Mendeleev Ridge, and hence to document the variable influence of the BG and TD current systems over the late Pleistocene.

### 3.3 Material and methods

Three multicorer sediment cores (PS72/408-4, PS72/410-2 and PS72/422-4, here referred to as 408, 410 and 422) from a transect across the Mendeleev Ridge at around 80° northern latitude were collected during RV Polarstern expedition ARK-XXIII/3 in 2008 (Abb. 5, Tab. 2; Jokat, 2009; Stein et al., 2010a,b). Sampling was carried out continuously at a depth resolution of 1 cm, and around 100 samples were stored frozen in plastic bags. Back onshore the samples were freeze-dried and finely ground in an agate ball mill for further analysis.

Analysis of Al, As, Ca, Co, Cu, Fe, K, Mg, Mn, Mo, Ni, Si, Sr, Ti and Zr was performed by wavelength-dispersive X-ray fluorescence (XRF, Philips PW 2400) on

fused borate glass beads. Additionally, inductively coupled plasma mass spectrometry (ICP-MS, Thermo Finnigan Element 2) of selected samples was applied to quantify Mo contents after acid digestion of the sediment powder (1 ml HNO<sub>3</sub>, 1 ml HClO<sub>4</sub>, 3 ml HF, 9 ml semi-concentrated HCl). Total carbon (TC) and total sulfur (TS) were determined via combustion analysis using an ELTRA CS Analyzer. Total inorganic carbon (TIC) was measured coulometrically with an UIC Coulometer. Total organic carbon (TOC) was calculated as the difference between TC and TIC.

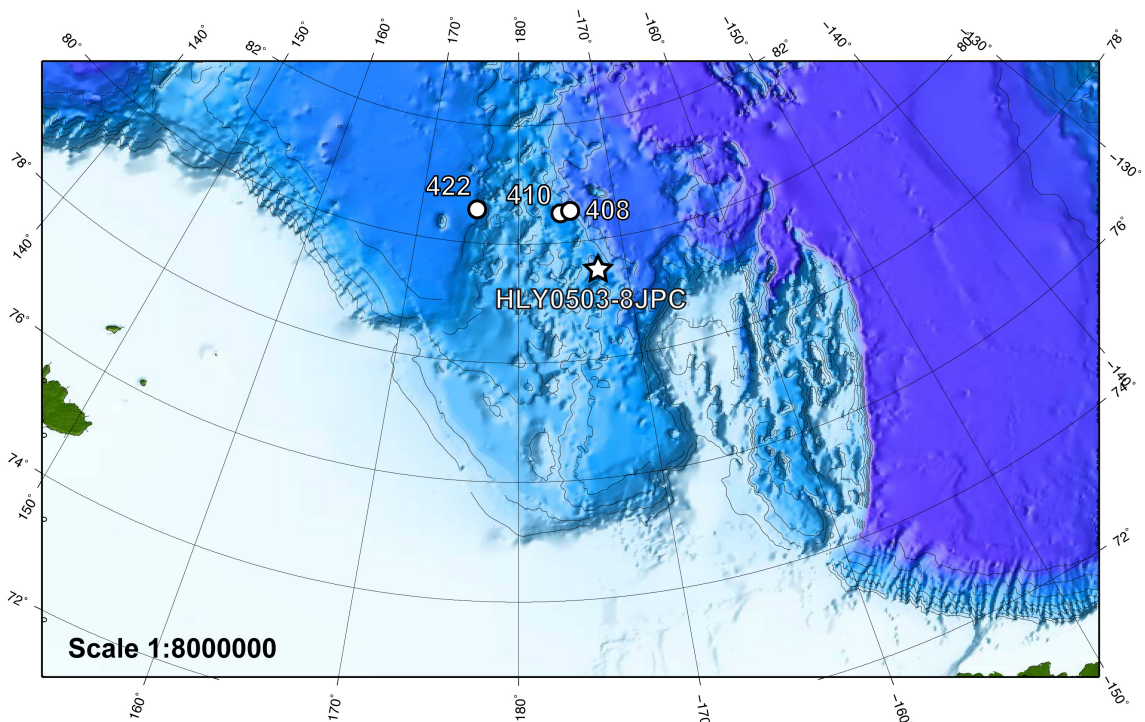


Abb. 5: Map of the Arctic Ocean with investigated core sites 408, 410 and 422, and coring site HLY0503-8JPC from Polyak et al. (2009, based on IBCAO 2.0; Jakobsson et al., 2008).

Accuracy and precision were checked with several inhouse standards (Babu et al., 1999). Errors in accuracy were <3% for TC and TIC and <5% for TS. Errors in precision were <2% for TC and TIC and <9% for TS. For XRF and ICP-MS analyses, accuracy and precision were checked with several international (SCO-1, SDO-1, STSD-3) and inhouse (CAST, Loess, TW-TUC, UT-S) standards. For major elements, the errors in accuracy were <3% and in precision <1%. For trace elements, errors in accuracy were <6% and in precision <3%.

Tab. 2: Core locations.

Station	Position	Water depth (m)	Core length (cm)
PS72/408-4	80° 32,94' N 174° 40,41' W	2577	33
PS72/410-2	80° 30,89' N 175° 44,27' W	1816	31
PS72/422-4	80° 32,88' N 175° 44,37' E	2545	35

All data are salt-corrected to eliminate dilution effects resulting from sea salt enclosed in interstitial waters. The water content of each sample, determined as the difference between wet and dry sediment weight, was used to calculate the content of each sea salt constituent. Element contents are displayed in weight % for major elements or ppm ( $\mu\text{g/g}$ ) for trace elements. Variations in the element content of detrital material can arise from variable input of biogenic material or the formation of authigenic phases. Aluminum is almost exclusively of terrigenous origin and hardly affected by biogenic or diagenetic processes. To compensate for variable dilution of the detrital record, element contents are normalized to Al (Brumsack, 2006). Enrichments of elements are described by using enrichment factors (EF), which are calculated by the following equation:

$$EF_{\text{element}} = \frac{(\text{element} / \text{Al})_{\text{sample}}}{(\text{element} / \text{Al})_{\text{reference}}} \quad (4)$$

Average shale (AS; Wedepohl, 1971, 1991), which represents the mean composition of weathered upper continental crust, was used as reference value.

To compare enrichments of certain elements relative to the local terrigenous input, which does not necessarily have an AS composition, we defined the lowest values attained in the cores ( $(\text{element}/\text{Al})_{\text{min}}$ ) as respective background values and calculated excess contents according to Brumsack (2006):

$$\text{element}_{\text{xs}} = \text{element}_{\text{sample}} - \text{Al}_{\text{sample}} \times (\text{element} / \text{Al})_{\text{min}} \quad (5)$$



## 3.4 Results

### 3.4.1 General geochemical characteristics and terrigenous elements

A first geochemical classification of the sediments can be done by using a ternary plot (Abb. 6) with the end members  $\text{Al}_2\text{O}_3$  and  $\text{SiO}_2$ , representing terrigenous clay minerals, aluminosilicates and quartz, and  $\text{CaO}$ , representing carbonate (modified from Brumsack, 1989). As seen in Abb. 6, the samples are dominantly composed of terrigenous material similar to AS. A significant number of samples show higher carbonate contents and plot along the mixing line from AS to the carbonate end member.

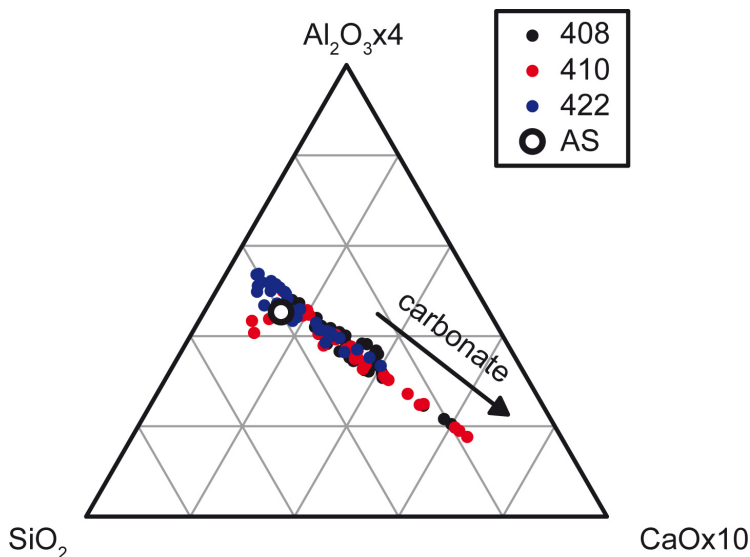


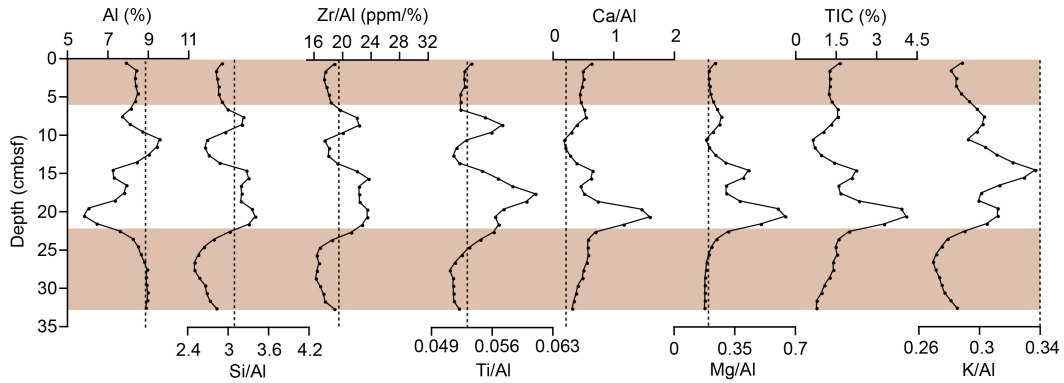
Abb. 6: Ternary plot of major components in samples from cores 408 (black symbols), 410 (red symbols), and 422 (blue symbols) in comparison with average shale (AS) (modified after Brumsack, 1989).

Aluminum contents are mostly below AS values (8.8%) in cores 408 and 410 and slightly elevated in core 422, where they roughly match AS (Abb. 7). Notably, deviations from the AS value are largely caused by detrital carbonate diluting the fine-grained siliciclastic material (Abb. 6). Values vary between 5.4 and 9.6%, with distinct peaks that are less pronounced in core 422. The profiles of Si/Al, Zr/Al and to a lesser degree Ti/Al parallel each other (Fig. 3); Si/Al and Zr/Al especially display a high positive linear correlation ( $R^2 = 0.94, 0.95$  and  $0.75$  for cores 408, 410 and 422). Background values of Ti/Al and Zr/Al are in the range of AS (Ti/Al =

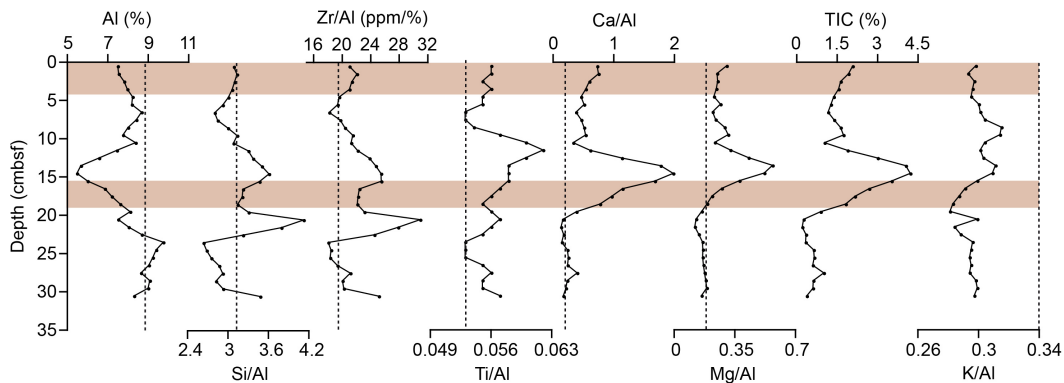
### 3. Regional variations in sediment geochemistry

0.053, Zr/Al = 18.1 ppm/%) or are slightly elevated, while the Si/Al background ratio is depleted in the sediments compared to AS (Si/Al = 3.1).

#### A PS72/408-4



#### B PS72/410-2



#### C PS72/422-4

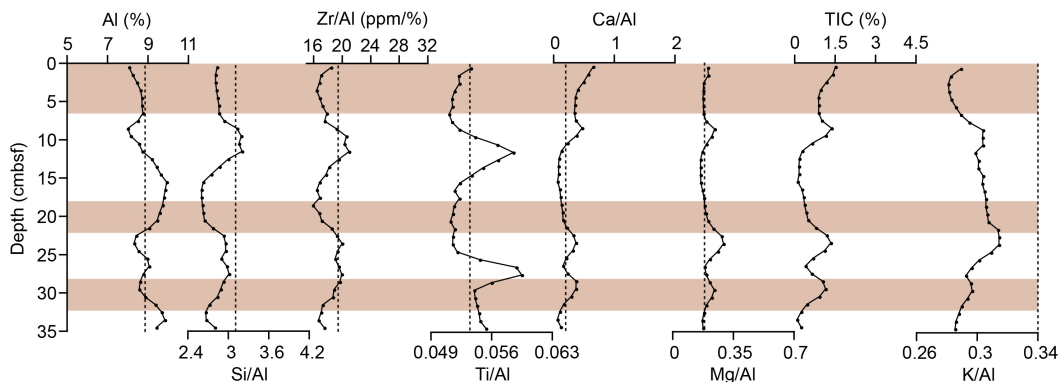


Abb. 7: Element/Al ratios of Si, Zr, Ti, K, Ca, Mg and element contents of Al and TIC for cores 408 (A), 410 (B) and 422 (C) (dashed line: AS; horizontal brown bars: brown layers).

Distinct peaks occur in every profile, and are again more pronounced in cores 408 and 410 than in 422. Peaks also occur in the K/Al profiles, but these depth profiles mostly deviate from those of the other detrital element ratios and do not

show well-correlated patterns (Abb. 7). Generally, K/Al is consistently depleted in all three cores compared to AS (0.34).

The peaks in Si/Al, Ti/Al and Zr/Al parallel the Ca/Al and Mg/Al records (Abb. 7), with one exception in core 410 (~20 cm) where corresponding Ca/Al and Mg/Al maxima are missing. These rather synchronous patterns do not imply a genetic or geochemical relationship, but rather document a specific mineralogical or sedimentological association, e.g., regarding settling velocities of grains.

Spatially, Ca/Al background ratios decrease westward from ~0.2 in core 408 to ~0.1 in core 422. There are distinct maxima with high values of up to 1.6 and 2.0 in cores 408 and 410, whereas in core 422 maximum values are up to ~0.4. In comparison to AS (0.18), Ca is mostly enriched in the sediment. The Mg/Al profiles are in general similar regarding the depths of the maxima, but the contents are lower than those of Ca. The Mg/Al ratios fluctuate between 0.12 and 0.64, background ratios are in the range of AS (0.18). In all cores, Ca and Mg patterns parallel TIC profiles (Abb. 7), indicating the occurrence of mixed Ca–Mg carbonates like dolomite. Like for Ca and Mg, TIC background values are higher in cores 408 and 410 (~1%), but lower in core 422 (~0.5%). The pronounced TIC peaks have higher values in the east (up to 4%) than in the west (up to 1.5%). Most carbon is present as carbonate (inorganic carbon), as indicated by the low organic carbon contents (see below) and the good correlation of TC and TIC for the three sites ( $R^2 = 0.96, 0.99$  and  $0.93$ ). Calcium and TIC are highly correlated ( $R^2 = 0.94$ ), whereas this is not the case for Ca and Mg ( $R^2 = 0.50, 0.54$  and  $-0.01$  for cores 408, 410 and 422, respectively).

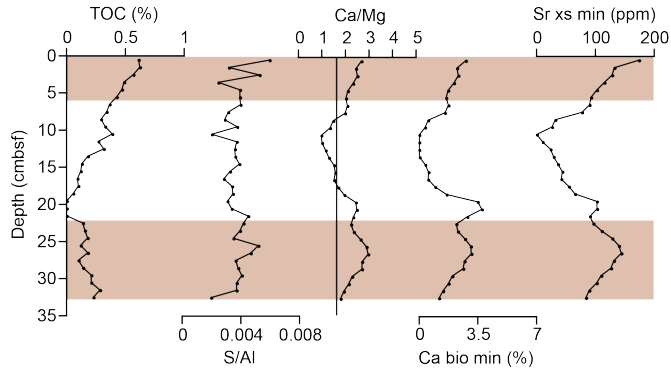
### 3.4.2 Elements related to organic matter and carbonate

As shown above, most of the carbon in the analyzed samples is inorganic. Organic carbon contents are below 0.9% in all three cores (Abb. 8). In the shallowest of the investigated cores (410), TOC values are lower (up to 0.4%) than in cores taken from the ridge flanks (cores 408 and 422). The low surface TOC contents further decrease with depth and show no significant peaks that would document events of enhanced productivity/biogenic input. Salt-corrected S/Al ratios are very low in comparison to AS (0.027), and only minor fluctuations with

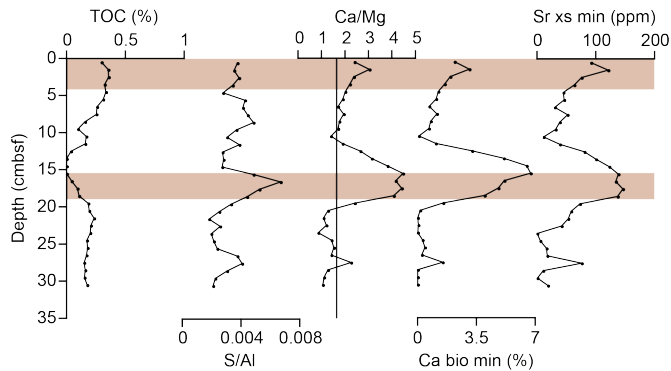
### 3. Regional variations in sediment geochemistry

core depth are discernible (Abb. 8). One should note that such low S values are close to the detection limit of the analytical method.

#### A PS72/408-4



#### B PS72/410-2



#### C PS72/422-4

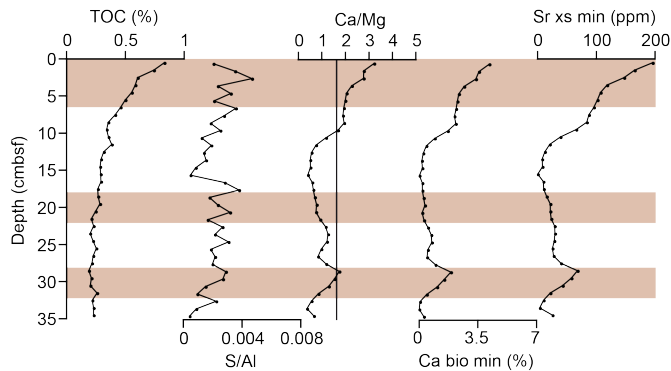


Abb. 8: TOC, S,  $Ca_{bio}$  and  $Sr_{xs}$  contents, and Ca/Mg ratios for cores 408 (A), 410 (B) and 422 (C) (solid line: molar Ca/Mg ratio in dolomite: 1.65; horizontal brown bars: brown layers).

Calcium/Mg weight ratios (Abb. 8) are mostly higher than stoichiometric dolomite (1.65) for core 408, and exhibit one minimum at ca. 10 cm and a broad maximum at ca. 20–30 cm. In core 410, Ca/Mg ratios fluctuate around 1.65 with

one broad maximum at ca. 10–20 cm with values of  $>5$ . In core 422, the upper 10 cm show higher Ca/Mg ratios, which decrease with depth.

### 3.4.3 Elements related to Mn and Fe (oxyhydr)oxides

Background Mn/Al ratios are in the range of 0.020, therefore higher than AS (0.009; Abb. 9). These values are slightly higher than those reported by März et al. (2011) in deeper ( $>1$  m) sediments from the southern Mendeleev Ridge, possibly indicating that the more distal sediments analyzed in this study received less detrital Al-rich minerals. The shapes of the Mn/Al profiles are variable, but overall smoother than the profiles of the detrital elements, and sharp maxima or minima are missing.

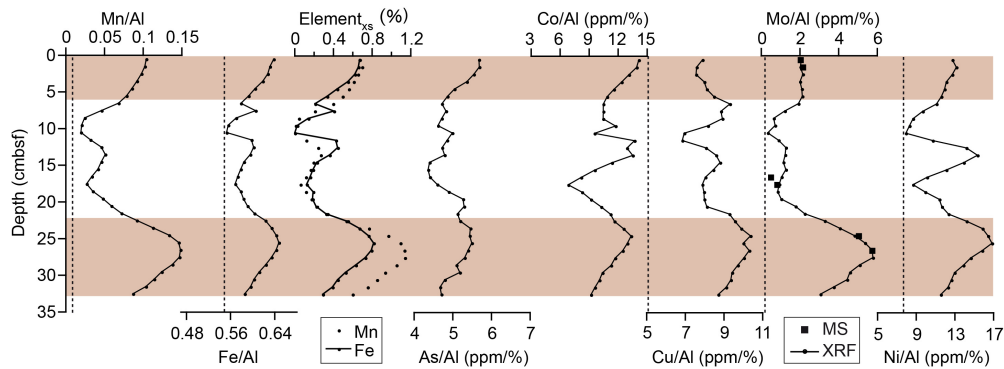
Nevertheless, samples within the Mn/Al maxima are highly enriched relative to AS (max. EF = 15 in core 408). Iron/Al shows a pattern similar to Mn/Al, and Fe/Al ratios are in most cases higher than AS (0.55), with values ranging from 0.48 to 0.68 (Abb. 9). The low value of 0.48 in core 410 (20–23 cm) is not paralleled in the respective Mn/Al profile. This sediment interval seems to have a different lithology (coarser-grained, see Jokat, 2009), representing an exotic sediment layer with unknown provenance, and is excluded from further interpretation in this study. Iron concentrations of this layer were not chosen as background values for the later determination of Fe excess contents due to these lithological differences, which we think do not represent water column or diagenetic signals. Generally, the element/Al ratios of both, Mn and Fe, are elevated near the sediment/water interface, which can be attributed to climatically enhanced input of these two elements during the present warm period. Maximum Mn/Al and Fe/Al ratios are higher in the eastern (core 408) than in the western (core 422) section of the transect.

Enrichment factors of Fe are about an order of magnitude lower than those of Mn in the selected Mn-rich layers (Abb. 10). However, the Fe content of AS is about 50 times higher than Mn (4.8% and 0.09%, respectively). Because the absolute Fe enrichment in our cores relative to the local background might be much higher, excess contents according to Brumsack (2006) were calculated for Fe and Mn (see Eq. (5)) to correct for the dilution of this potential water column

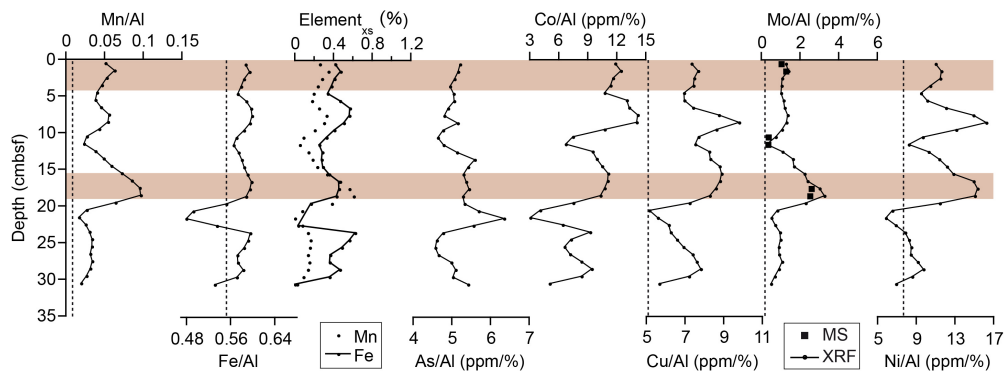
### 3. Regional variations in sediment geochemistry

signal by the terrigenous background material (Abb. 9). Interestingly, the Mn and Fe patterns resemble each other in all studied cores, and Mn and Fe excess contents are on the same order of magnitude (Abb. 9).

#### A PS72/408-4



#### B PS72/410-2



#### C PS72/422-4

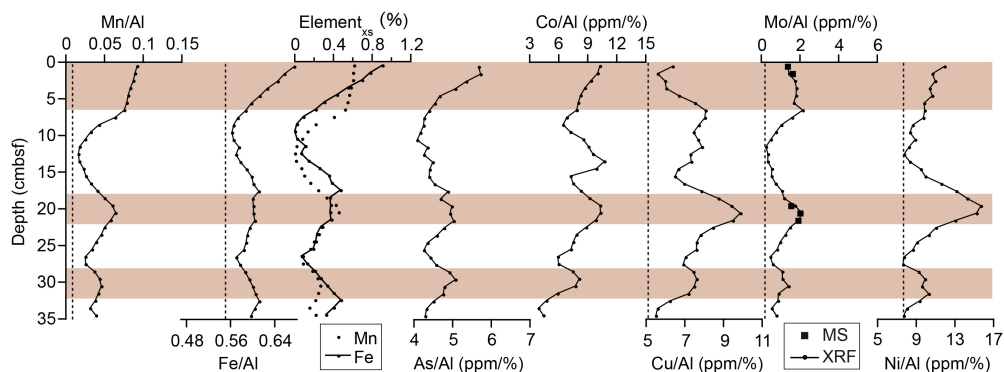


Abb. 9: Element/Al ratios of Mn, Fe, As, Co, Cu, Mo and Ni and excess contents of Mn and Fe for cores 408 (A), 410 (B) and 422 (C) (filled squares: ICP-MS results; dashed line: AS; AS for As/Al and Co/Al ( $1.13 \cdot 10^4$  and  $2.15 \cdot 10^4$ ) not shown; horizontal brown bars: brown layers).

Several trace metals show depth distribution patterns similar to Mn/Al and Fe/Al, namely the element/Al ratios of As, Co, Cu, Mo and Ni (Fig. 9). Differences are visible in the background trace metal contents. The background ratios of Mo/Al

and Ni/Al are in the range of AS. Both are significantly elevated in the Mn-rich layers. In contrast, As/Al and Cu/Al background ratios are elevated relative to AS (As/Al = 1.13 ppm/%; Cu/Al = 5.09 ppm/%), and are even more enriched in the Mn-rich layers.

Enrichment factors encompass a broad range of values, with highest enrichments seen for Mo (EF = 12–39 in the Mn-rich layers) and for As (EF = ~ 4 in the background, ~ 5 in the Mn-rich layers; Abb. 10). Although the geochemical profiles resemble each other, not all respective correlation coefficients of Mn with other trace metals are high. In most cases, the element/Al ratios correlate better than the respective element contents. Correlations are most significant for Mn/Al and Mo/Al ( $R^2 = 0.98$  for core 410 and 0.80 for core 408), and for Mn/Al and Ni/Al in core 410 ( $R^2 = 0.73$ ). Correlating normalized values may lead to spurious correlations (Van der Weijden, 2002), and should be considered carefully.

### 3.4.4 Geochemical trends along the transect

Along the sampling transect, we observe a progressive change in the geochemical composition of the core material. Manganese/Al ratios associated with the Mn-rich layers are highest at the eastern-most station (core 408) and lowest at the western-most site (core 422). Not all trace metals associated with the brown layers follow this geographical trend. The enrichment factors of Mn, Fe and trace metals in the following Mn-rich sediment sections are shown in Abb. 10: core 408, 24–29 cm; core 410, 16–19 cm; core 422, 19–22 cm.

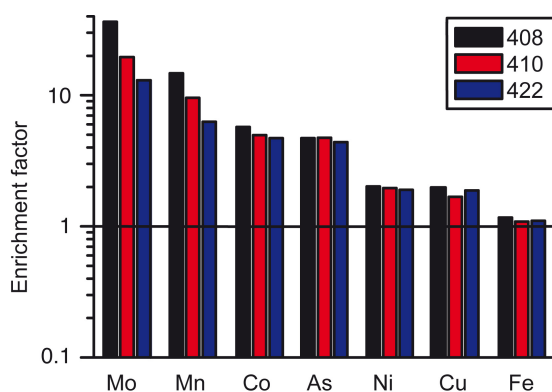


Abb. 10: Enrichment factors of Mo, Mn, Co, As, Ni, Cu and Fe in selected Mn-rich layers of the three cores.

Along the transect, the enrichments of Mn, Co, Mo and Ni are highest in core 408 and lowest in core 422, while Fe and Cu deviate from this trend with lowest enrichment factors in core 410. For all studied cores, the sequence of enrichment for individual elements in the Mn-rich layers is: Mo > Mn > Co > As > Ni > Cu > Fe.

### 3.5 Discussion

#### 3.5.1 Preliminary age model

Conventional radiocarbon dating of Arctic Ocean sediments is complicated by the usually very limited abundance of biogenic carbonate. Nevertheless, various age models exist for western Arctic sediment cores comparable to ours, based on <sup>14</sup>C dating, amino-acid racemization, magnetostratigraphy or Be isotopes (Darby et al., 1997; Adler et al., 2009; Polyak et al., 2009; Sellén et al., 2009). Furthermore, detrital carbonate layers are useful litho- and chemostratigraphic marker horizons as well as sediment provenance indicators. They are composed of material from the Canadian Archipelago that was distributed across the western Arctic Ocean after disintegration of the Laurentide Ice Sheet (e.g., Clark et al., 1980; Bischof and Darby, 1997; Hinrichs et al., 2001; Phillips and Grantz, 2001).

Stein et al. (2010a,b) correlated the new sediment cores recovered during Polarstern Expedition ARK-XXIII/3, including cores PS72/408, PS72/410, and PS72/422, to the dated sediment cores NP-26 and HLY0503-8JPC (Polyak et al., 2004, 2009) using the dark brown horizons, sandy intervals, and prominent detrital carbonate layers (pink-white layers) to obtain a preliminary age model (Abb. 11).

Following this approach, we compare core 408 to the published core HLY0503-8JPC retrieved from the Mendeleev Ridge ~100 km south of the RV Polarstern transect (Polyak et al., 2009). The authors used grain size, radiocarbon ages of planktic foraminifers, and variations in Ca and Mn to establish an age model (Abb. 12). The uppermost brown interglacial layer is dated to be 10.2 or 12 ka old (onset of the Holocene, MIS 1). The second brown layer represents MIS 3 and is dated to 32 or 43 ka. Between these two layers, the Last Glacial Maximum (LGM) is probably represented by a very fine-grained gray layer.



### 3. Regional variations in sediment geochemistry

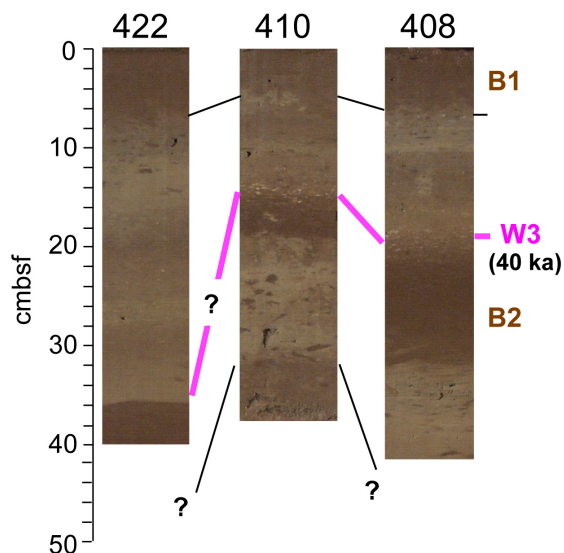


Abb. 11: Photographs of giant box corer (GKG) cores PS72/408-3, PS72/410-1, and PS72/422-3, recovered at the same locations than the corresponding multicorer cores. Dark brown layers B1 and B2 and the dolomite-rich “white layer” W3 are indicated (Figure from Stein et al. 2010b; age of W3 according to Polyak et al., 2004, 2009).

A comparison of HLY0503- 8JPC with the Ca and Mn profiles of core 408 (Abb. 12) shows a close re- semblance of the geochemical patterns, with three high-Mn intervals, two low-Mn intervals, and one dominant Ca peak.

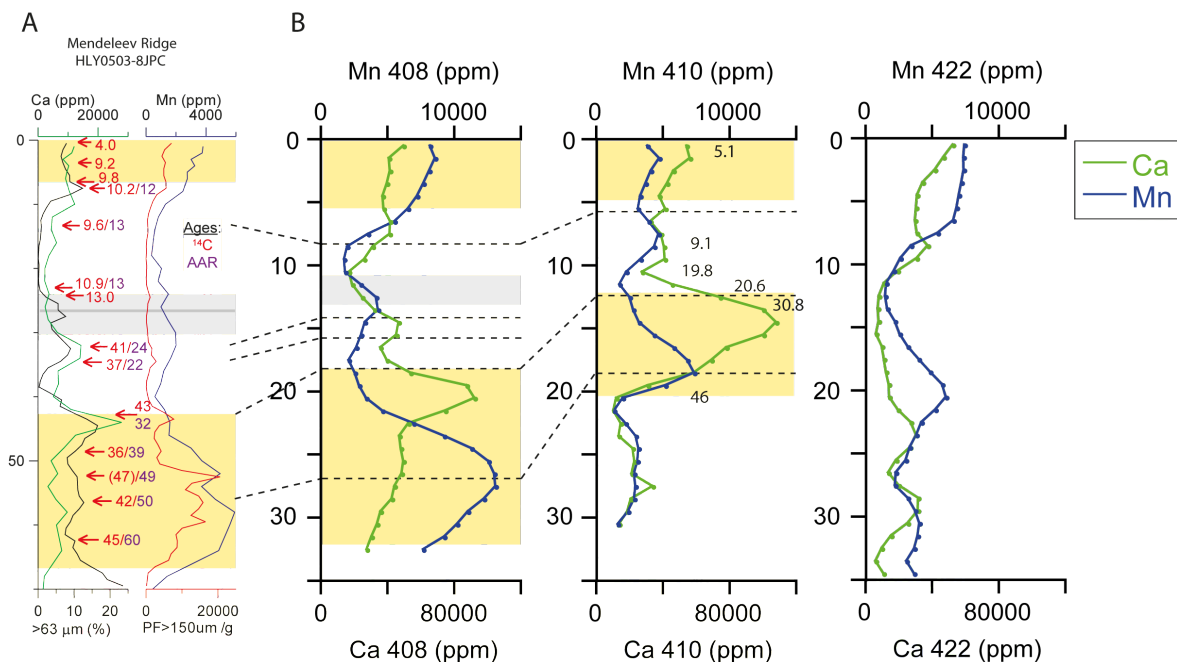


Abb. 12: (A) XRF calcium (green) and manganese (blue) contents, sand content (>63 μm; black), planktonic foraminifers (>150 μm/g; red), <sup>14</sup>C ages (red) and AAR ages (purple) of sediment core HLY0503-8JPC (Polyak et al., 2009). (B) XRF Mn (blue) and Ca (green) contents of cores 408, 410 and 422. Yellow shading: interglacial/interstadial units, light gray: interval with clastic IRD, dark gray: fine grained LGM sediment. Ages for core 410 from Jang et al. (2013).

In detail, the uppermost ~ 6 cm of core 408 have elevated Mn and Ca contents, which decrease to a minimum at ~10 cm depth. This minimum probably represents the LGM. At ~20 cm depth, Mn displays a minimum and Ca shows a prominent maximum. Compared with HLY0503-8JPC, this may be indicative for the end of MIS 3. Thus, the 33 cm of sediment in core 408 probably represent ~60 ky. The same time span is covered by 70 cm of sediment in core HLY0503-8JPC. Thus, sedimentation rates of core 408 (north of HLY0503-8JPC) are ~50% lower, supporting the finding of decreasing sedimentation rates from marginal areas to the deep basins and ridges of the Arctic Ocean (Phillips and Grantz, 2001; Polyak et al., 2009; Stein et al., 2010a,b).

By linking the age model of Polyak et al. (2009) to our short cores via Mn and Ca profiles, sedimentation rates can be estimated for the other cores as well (Tab. 3). Additionally, AMS <sup>14</sup>C dating was recently performed for core 410-1, a parallel core of 410-2 (Jang et al., 2013). Despite minor deviations in the upper section of core 410-2, the results of Jang et al. (2013) are in good agreement with our correlation-based ages for core 410 (Abb. 12). For core 422, the result of the geochemical profiles may be interpreted in two different ways, as the Mn peak at 20 cm depth in core 422 may either correspond to the Mn peak at 13 cm depth in core 408 or, due to its stronger Mn enrichment, to the Mn peak at 26 cm depth.

Tab. 3: Estimated sedimentation rates of the 3 cores by means of an age model determined by Polyak et al. (2009). Values in parentheses are from Stein et al., 2010b for corresponding longer cores 408-5, 410-3 and 422-5, respectively.

Core	Depth (cm)	Age (ka)	Sedimentation rate (cm/ka)	
408	6.0	10.2/12	0.50-0.59	(0.91)
	8.5	9.6/13	0.65-0.89	
	14.5	41/24	0.35-0.60	
	16.5	37/22	0.45-0.75	
	18.0	43/32	0.42-0.56	
	27.0	42/50	0.54-0.64	
410	7.5	41/24	0.18-0.31	(0.75)
	14.0	43/32	0.33-0.44	
	18.0	42/50	0.36-0.43	
422	8.5	41/24 10.2/12-9.6/13	0.21-0.35 0.65-0.89	(2.01)
	19.5	42/50 41/24	0.39-0.46 0.48-0.81	
	23.0	43/32	0.53-0.72	

In general, sedimentation rates of the investigated near-surface sediments are less than 1 cm/ka. However, the alternative interpretation of core 422 records would result in higher sedimentation rates. These higher sedimentation rates for core 422 agree with the mean sedimentation rates calculated by Stein et al. (2010b) for the last 110 ka using longer gravity cores recovered from the same station PS72/422 (Tab. 3). Higher sedimentation rates at this coring site would be in accordance with its location at the intersection of the Mendeleev Ridge and the Makarov Basin, an area that may have acted as a regional sediment trap. Apart from this specific coring site, our results fit into the compilation of Polyak et al. (2009), with average sedimentation rates of 2 cm/ka for core HLY0503-8JPC further to the south, and 0.3 cm/ka for sediment cores further to the north.

### 3.5.2 Input of terrigenous material and IRD

The composition of AS may be used to define the background contents of most elements in the studied sediment cores. However, some element background values deviate from the AS composition, presumably due to contributions from the hinterland with a specific lithology. The overall low values of Si/Al and K/Al suggest the influence of a more mafic detrital component. Low sedimentary K contents were reported from the central Lomonosov Ridge (Schoster, 2005; Backman et al., 2006; Martinez et al., 2009; März et al., 2010), and are attributed to material derived from the basaltic Siberian Putoran Massif. A local source of basaltic volcanic material to the southern Mendeleev Ridge is the vast Cretaceous Okhotsk–Chukotka volcanic belt (e.g., Tikhomirov et al., 2006) that has already been suggested as basaltic source to the Chukchi and East Siberian shelves by Viscosi-Shirley et al. (2003). Thus, the K record may potentially document a distinct terrigenous component of the sediment that is derived from East and/or West Siberia.

The parallel peaks in the profiles of Si/Al, Zr/Al, Ca/Al, Mg/Al and TIC suggest a similar way of enrichment in the sediments for both detrital carbonates and coarse/high-density siliciclastic components (März et al., 2011). The source of detrital carbonates (mainly dolomite) was related to the Canadian Archipelago, specifically Banks Island and Victoria Island (Bischof et al., 1996; Bischof and

Darby, 1997). Dolomites were identified during the expedition using light microscopy, giving direct evidence of their presence in the sediment cores (Jokat, 2009). Coarse material from the Canadian Archipelago, embedded in icebergs and/or sea ice, is transported across the Canadian Basin via the clockwise-turning BG current system. The BG crosses the Mendeleev Ridge from east to west, which is reflected in the sediment geochemistry by increased ratios of the elements related to ice transport (Si, Zr, Ca, Mg) in cores 408 and 410. This supports similar reconstructions based on Fe oxide grain composition and distribution in the Amerasian Basin (Darby, 2003), and the distribution patterns of dolomite-rich pink layers (e.g., Clark et al., 1980; Stein et al., 2010a,b). The markedly lower element ratios in core 422 lead to the assumption that less material delivered by the BG reached the western Mendeleev Ridge. This part of the ridge is probably more influenced by the Transpolar Drift and by deposition of rather fine-grained material from the Siberian Arctic (e.g., Polyak et al., 2004; Stein et al., 2010a,b). The drift pattern of IRD-related elements is similar to the drift of modern sea ice (e.g., Darby, 2003).

### 3.5.3 Biogenic material

Although primary productivity is generally low in the central Arctic Ocean (e.g., Sakshaug, 2004), our geochemical records can be used to identify a biogenic component preserved in the Mendeleev Ridge deposits. Biogenic material is either delivered in the form of organic carbon (TOC) or carbonate (calcite, aragonite) remains of foraminifera and coccolithophorids. However, organic carbon in marine sediments is quickly degraded during early diagenesis, and the biogenic carbonate record in the western Arctic Ocean is biased by the deposition of detrital carbonates (mostly dolomite). In the following, we will attempt to overcome this latter bias through the consideration of the elemental composition of different carbonate phases, i.e., contents of Ca, Mg and Sr in biogenic calcite/aragonite versus detrital dolomite.

Calcium is a major element in both calcite/aragonite and dolomite. In contrast, Mg contents are much higher in dolomite than in biogenic carbonate, where Mg only occurs in trace amounts (Weber, 1964; Renard, 1986; Cl eroux et al., 2008).

Stoichiometric dolomite exhibits the same molar amounts of Ca and Mg with an ideal Ca/Mg weight ratio of 1.65. In other words, a pure carbonate sample with a Ca/Mg ratio of  $>1.65$  should represent a mixture of dolomite and Mg-poor biogenic carbonate. Such Ca/Mg of  $>1.65$  are found in the upper 10 cm of all three studied cores, and also in two deeper sections of cores 408 and 410 (Abb. 8), providing a first indication for the deposition and preservation of biogenic carbonate in these layers.

However, the assumption of purely carbonate-controlled Ca and Mg records is too simplistic for Arctic sediments, which are dominantly composed of detrital siliciclastic material that contains Ca and Mg as well. To correct for the Ca and Mg contribution of the siliciclastic background, we calculate their excess contents (see Eq. (5)), resulting in  $Ca_{xs}$  and  $Mg_{xs}$  records. Assuming that all excess Mg ( $=Mg_{xs,tot}$ ) is accounted for by dolomite, we can use the ideal Ca/Mg ratio of 1.65 to calculate the amount of Ca that is bound in this dolomite (" $Ca_{xs,dol}$ " =  $Mg_{xs,tot} * 1.65$ ). The remaining, non-dolomitic fraction of  $Ca_{xs}$  should then represent Ca in calcite/aronite of tentatively biogenic origin (" $Ca_{bio}$ " =  $Ca_{xs,tot} - Ca_{xs,dol}$ ).

To test this way of calculating the amount of biogenic carbonate, we compare the records of  $Ca_{bio}$  and  $Sr_{xs}$  (Abb. 13). During the formation of biogenic carbonate (especially aragonite; e.g., Rickaby et al., 2002), the  $Sr^{2+}$  ion partly substitutes for  $Ca^{2+}$  in the mineral structure, leading to Sr contents in biogenic carbonates that are usually an order of magnitude higher than in dolomite (Weber, 1964; Renard, 1986; Hodell et al., 2008).

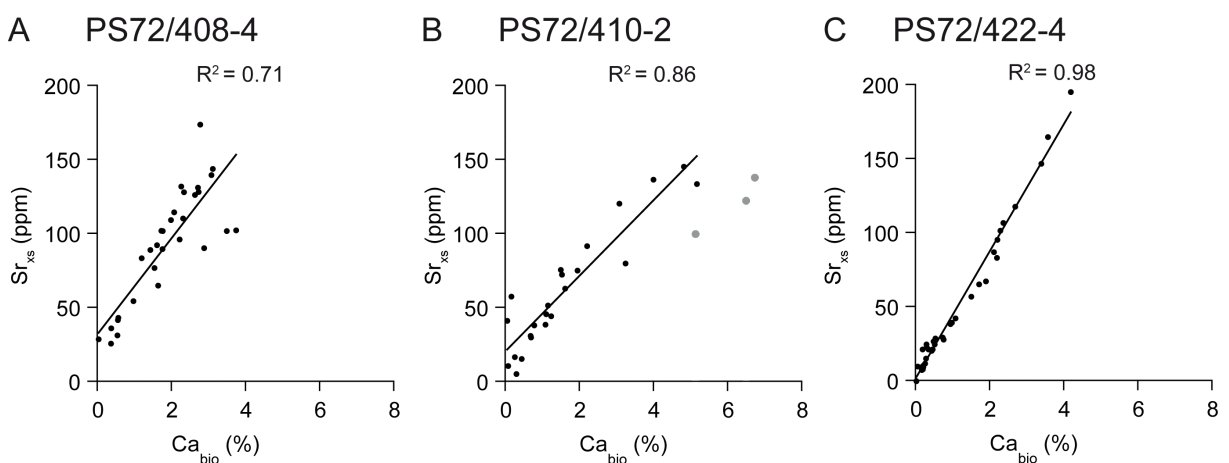


Abb. 13: Linear correlations of  $Sr_{xs}$  and  $Ca_{bio}$  for cores (A) 408, (B) 410 and (C) 422. Gray dots were omitted for calculating the correlation factor.

Thus, the  $Sr_{xs}$  record will mostly document biogenic carbonate deposition, and should as such be similar to the  $Ca_{bio}$  record. This assumption is supported by high to very high correlation coefficients between  $Ca_{bio}$  and  $Sr_{xs}$  (0.71, 0.86 and 0.98 for cores 408, 410 and 422, respectively) and the close similarity of the vertical distribution patterns, indicating the occurrence of biogenic carbonate in addition to dolomite in these sediments (Abb. 13). The lowest Ca/Al and Mg/Al ratios do not necessarily occur at the same depth, therefore  $Ca_{bio}$  may become negative in the calculation. These values were omitted for the comparison in Abb. 13.

It should be mentioned that our geochemistry-based attempt to calculate biogenic carbonate contents in the studied cores includes the simplification that (a) detrital dolomite has the ideal stoichiometric composition  $CaMg(CO_3)_2$ , and that (b) calcite/aragonite are solely biogenic and not detrital in origin. The few deviations seen in our otherwise good correlations of  $Ca_{bio}$  and  $Sr_{xs}$  (Abb. 13) may result from these simplifications. Despite these minor uncertainties, our results provide a good first-order estimate for biogenic carbonate deposition in Arctic sediments even when coarse-grained carbonate components are missing, as the detrital carbonates also occur in the fine fraction of the sediments. Our method does not intend to replace direct analyses of foraminifera tests, but should ideally be combined with micropaleontological studies. Geochemical screening by fast XRF scanning may help to quickly identify dolomite- or calcite-rich horizons in sediments (Hanslik et al., 2013). For the studied cores, the geochemically deduced presence of biogenic carbonate is confirmed by the occurrence of foraminifera tests in parallel cores from the same Multicorer cast (Nam, 2009; Stein et al., 2010a,b).

When comparing the  $Ca_{bio}$  and  $Sr_{xs}$  records to other geochemical parameters in the studied cores, it is noteworthy that their down-core trends are very similar to the respective Mn/Al records (Abb. 8; 9). Thus, high  $Ca_{bio}$  and  $Sr_{xs}$  values seem to occur during periods with enhanced bioproductivity and river runoff and/or coastal erosion (see also Abb. 12), which in the Arctic Ocean are usually associated with interglacial/interstadial climate conditions (e.g., Polyak et al., 2004, 2009; März et al., 2011; Macdonald and Gobeil, 2012). In conclusion, we suggest that  $Ca_{bio}$  and  $Sr_{xs}$  records in western Arctic Ocean sediments are useful proxies to trace

changes in biogenic carbonate deposition over glacial/interglacial climate changes.

### 3.5.4 Elements related to Mn and Fe oxyhydroxides: Temporal and spatial trends

The behavior of Mn in the aquatic environment is coupled to an intense redox cycle (e.g., Burdige, 1993). Under oxic conditions, poorly soluble  $Mn^{4+}$  precipitates and accumulates in the sediment mainly as oxyhydroxide ( $MnOOH$ ) or oxide ( $MnO_2$ ). Suboxic to anoxic conditions lead to the reduction of  $Mn^{4+}$  to highly soluble  $Mn^{2+}$ , which is then released into the pore or bottom waters (Li et al., 1969; Klinkhammer, 1980; Burdige, 1993, and references therein). The overall enrichment of Mn in the studied Arctic sediments indicates oxic depositional conditions. Iron shows synchronous patterns with the Mn profiles, indicating a concurrent way of delivery to the Arctic sea floor or a similar behavior during early suboxic diagenesis. Like Mn, Fe is present in oxic seawater mostly as insoluble particulate oxyhydroxide. As noted by März et al. (2011, and references therein), the major difference between Fe and Mn records in Arctic sediments seems to be the phases in which they are delivered to the Arctic Ocean. The input of Mn is dominantly related to coastal erosion (Macdonald and Gobeil, 2012) and the riverine input of dissolved/colloidal/organically complexed Mn under certain climatic conditions, leading to repeated sedimentary Mn enrichments significantly above the detrital background. While Fe is delivered in dissolved/colloidal/organically complexed form as well, these Fe fractions are outcompeted by the high Fe contents in the detrital background material, preventing significant Fe enrichments in the marine sediments (Hölemann et al., 1999; Gordeev et al., 2007).

To date, the typical color changes in Arctic sediments have mostly been attributed to varying Mn contents, with dark brown segments displaying high Mn (oxyhydr)oxides contents (Jakobsson et al., 2000; Löwemark et al., 2008). Our data set reveals for the first time that excess Mn and Fe contents in these sediments can be on the same order of magnitude. Therefore, the question arises if  $Fe_{xs}$  in these sediments is bound to specific phases that may contribute to the

brown sediment color as well. Grygar et al. (2007) investigated Fe species in sediments from the Mendeleev Ridge and suggested poorly crystalline or organically complexed Fe(III) species play a more important role for sediment color than previously assumed. Although we did not investigate the exact nature of the sedimentary Fe component in our study, the calculated  $Fe_{xs}$  contents and their relation to  $Mn_{xs}$  imply that not only Mn, but also Fe phases contributed to both trace metal scavenging in the water column and the characteristic sediment color.

Pore water data (dissolved Mn and Fe) are available for cores 410 and 422 (11 pore water samples for each core, depth range 0–26 cm). Concentrations are consistently low (Mn: 0.1–0.2  $\mu\text{mol}$ ; Fe: 0.2– 2.5  $\mu\text{mol}$ ) with no significant changes. The data do not indicate Mn or Fe remobilization. Therefore, the sediment geochemistry is currently not influenced by diagenetic signals and support a primary origin of the Mn and Fe enrichments in the sediments.

Several trace metals like As, Co and Mo are known to precipitate in the sediments as monosulfides, or are incorporated into pyrite if  $H_2S$  is present (Huerta-Diaz and Morse, 1992, and references therein; Calvert and Pedersen, 1993). However, the very low S/Al ratios in cores 408, 410 and 422 reveal that metal sulfides in our case are negligible as trace metal carriers, and that the sediments were deposited under oxic conditions without significant diagenetic alteration related to microbial sulfate reduction (März et al., 2011). Another potential pathway to enrich trace metals in marine sediments is by association with Fe/Mn-oxyhydroxides that scavenge As, Co, Mo, Ni and other metals from the overlying water column (Goldberg, 1954). Trace metal scavenging in the Arctic water column is clearly documented by very similar patterns of Mn, Fe and trace metals in the studied cores from Mendeleev Ridge (Abb. 9). The same Mn–trace metal relationship was already seen in older Arctic sediments from Mendeleev Ridge and Lomonosov Ridge (März et al., 2010, 2011). The evident co-occurrence of Mn with various trace metals is in contrast to XRF core scanner studies on Lomonosov Ridge sediments, where a correlation between Mn and any other element was not detected (Löwemark et al., 2008).

Considering the element EFs in the different cores (Abb. 10), Mn shows strong similarities with Co, Mo and Ni (with EFs decreasing from core 408 over 410 to 422), indicating that these trace metals are mainly bound to Mn phases. In



contrast, the spatial distribution of the EFs of As and Cu is rather similar to Fe (without a characteristic spatial trend), indicating that they are not predominantly bound to Mn, but instead to Fe phases. These specific associations of trace metals with either Mn or Fe (oxyhydr)oxides are only tentative for the studied Arctic sediments, but are in agreement with detailed studies on marine trace metal cycling (e.g., Goldberg, 1954; Belzile and Tessier, 1990; Devitre et al., 1991; Müller et al., 2002; Crowe et al., 2007).

### 3.6 Conclusions

(1) Manganese-rich layers in the studied cores from Mendeleev Ridge seem to reflect primary paleoenvironmental signals documenting warmer periods, making them applicable for stratigraphic correlations in shallow sediments unaffected by early diagenetic processes. However, geochemical differences even between closely spaced cores indicate a strong environmental control (e.g., sea ice extent, distance to shelf break) on the characteristics of the brown layers. Further investigations of surface and deeper sediments (multicorer and gravity/piston corer including their pore waters) throughout the Arctic Ocean are necessary to fully resolve this issue.

(2) Both flanks of the Mendeleev Ridge are influenced in different ways by various sedimentation processes. The profiles of Ca/Al, Mg/Al and TIC confirm the input of a dolomitic IRD component from the East (Canadian Archipelago) via the BG, and similar spatial patterns are seen in Mn and associated trace metal EFs. A different, probably mafic sediment component likely originates from the Siberian hinterland, as documented by low Si/Al and K/Al records.

(3) Little biogenic material is present in these Arctic Ocean sediments as shown by the TOC record. We propose  $Ca_{bio}$  and  $Sr_{xs}$  records as additional indicators for biogenic input by calcareous plankton. These records document a biogenic component in the top layers of the studied cores, and in two deeper layers in cores 408 and 410.

(4) The overall enrichments in Mn and low S contents indicate deposition of the sediments under fully oxic conditions and negligible microbial sulfate reduction.

(5) Several trace elements (As, Co, Cu, Mo, Ni) are related to Mn and Fe via

scavenging and show comparable distribution patterns. Additionally, similar spatial patterns in EFs indicate that Co, Mo and Ni are predominantly bound to Mn phases, while As and Cu are most probably bound to Fe phases.

(6) Iron may contribute to the characteristic brown color of the sediments, as excess Fe and Mn contents are on the same order of magnitude. At the same time, these Fe phases (most probably oxyhydroxides) are important for trace metal scavenging.

### 3.7 Acknowledgments

The authors would like to thank the master, crew, and shipboard scientists onboard RV Polarstern during the ARK-XXIII/3 expedition. We are grateful to S. Eckert, P. Monien and B. Schnetger for constructive discussions, and to E. Gründken, C. Lehnert and M. Schulz for substantial analytical assistance. The comments of Editor-in-Chief C. Koretsky and four anonymous reviewers considerably improved the manuscript. This study was supported by the German Research Foundation (DFG grants MA 4791/1-1 and BR 775/27-1), which is gratefully acknowledged.

## 4. Climate change and response in bottom water circulation and sediment provenance in the Central Arctic Ocean since the Last Glacial Maximum

A.-K. Meinhardt<sup>1\*</sup>, K. Pahnke<sup>2</sup>, P. Böning<sup>2</sup>, B. Schnetger<sup>1</sup>, H.-J. Brumsack<sup>1</sup>

<sup>1</sup> Institute for Chemistry and Biology of the Marine Environment (ICBM), Carl von Ossietzky University Oldenburg, P.O. Box 2503, 26111 Oldenburg, Germany

<sup>2</sup> Max Planck Research Group for Marine Isotope Geochemistry, Institute for Chemistry and Biology of the Marine Environment (ICBM), Carl von Ossietzky University Oldenburg, P.O. Box 2503, 26111 Oldenburg, Germany

Dieses Kapitel wurde eingereicht bei: Chemical Geology

### 4.1 Abstract

In this study, Arctic Ocean patterns of deep water circulation and sediment provenance during the Last Glacial Maximum (LGM) were compared with the recent situation by investigating the Nd and Sr isotopic composition ( $^{143}\text{Nd}/^{144}\text{Nd}$ , expressed as  $\epsilon_{\text{Nd}}$ ,  $^{87}\text{Sr}/^{86}\text{Sr}$ ) of the leachable and lithogenic sediment fractions as well as the elemental composition (Mn, Ca, Mg, total inorganic carbon (TIC)) on a spatially extended scale encompassing 11 sediment cores from several Arctic Ocean basins and ridges.

The signature of the surface sediments implies a North Atlantic deep water source and a circulation regime that leads to well-mixed, mostly uniform,  $\epsilon_{\text{Nd}}$  values of -10.9 to -10.3. Sediments from the LGM have overall more variable authigenic  $\epsilon_{\text{Nd}}$  values (-13.9 to -7.4). Lower values specifically occur in the Amerasian and Amundsen Basins, documenting an enhanced flow of deep waters from the Makarov Basin to the Amundsen Basin probably via the Lomonosov Ridge intra-basin.

In terms of detrital provenance areas, the cores cannot be assigned to distinct source areas, but document a diverse mixture. Nevertheless, the Nd and Sr

isotope signatures of surface sediments from the Amerasian Basin are dominated by western Arctic sources ( $\epsilon_{\text{Nd}} = -12.8$  to  $-11.0$ ;  $^{87}\text{Sr}/^{86}\text{Sr} = 0.7214$  to  $0.7251$ ), while Eurasian Basin surface sediments are dominated by Eurasian sources ( $\epsilon_{\text{Nd}} = -10.9$  to  $-9.7$ ,  $^{87}\text{Sr}/^{86}\text{Sr} = 0.7178$  to  $0.7299$ ). Bulk element patterns (Ca, Mg, TIC) of the studied sediments support these differences in provenance. The LGM samples show the same trends with low  $\epsilon_{\text{Nd}}$  ( $-16.1$  to  $-13.7$ ) and high  $^{87}\text{Sr}/^{86}\text{Sr}$  ( $0.7294$ ) in the Canada Basin, and overall higher  $\epsilon_{\text{Nd}}$  ( $-12.6$  to  $-8.8$ ) and lower  $^{87}\text{Sr}/^{86}\text{Sr}$  ( $0.7154$  to  $0.7249$ ) in the Eurasian Basin sediments.

Our geochemical study shows that there are no significant differences in deep water circulation or sediment provenance in the Central Arctic Ocean during the LGM compared with the modern situation. The overall circulation pattern of the deep water masses was locally influenced by brine formation but generally similar to today. Although sediment transport during the LGM was influenced by different environmental conditions (e.g., lower sea level, extended ice sheets, more arid climate) that shifted the lithogenic sources to areas more proximal to the Arctic Ocean, the detrital sources are indistinguishable from today.

## 4.2 Introduction

The deep water circulation of the Arctic Ocean is very important for the global climate because it impacts North Atlantic deep water formation and therefore forms a crucial part of the global overturning circulation (Aagaard et al., 1985). A varying deep water circulation during the Last Glacial Maximum (LGM) may have contributed to the drop in global temperatures by decreasing the transport of heat around the global ocean (Driscoll and Haug, 1998).

Information about water mass circulation in the oceans can be derived from Nd isotopes. Depending on lithology and age, continents have different isotopic signatures ( $^{143}\text{Nd}/^{144}\text{Nd}$ , expressed as  $\epsilon_{\text{Nd}}$ ) and these signatures are imprinted on sea water by weathering and erosion (e.g., Frank, 2002). The Nd isotopic composition of the authigenic Fe-Mn oxide fraction obtained by sequential leaching represents the Nd fraction, which is exchangeable with seawater, and thus reflects the deep water signal at the time of deposition. In the Arctic Ocean,

several authors have investigated the Nd isotopic composition of authigenic sediment fractions (Winter et al., 1997; Haley et al., 2008a, 2008b; Maccali et al., 2013; Jang et al., 2013). It has been shown that the past deep water circulation varied over glacial/interglacial timescales with some excursions due to specific events (e.g., outburst of ice-dammed lakes, melting of ice sheets; Spielhagen et al., 2004; Jakobsson et al., 2014). Haley and Polyak (2013) made the first attempt to use Nd isotopes on a broader spatial scale and defined a “pre-anthropogenic baseline” of deep water circulation in the Arctic Ocean. In our study we follow this approach and use the recent deep water circulation signals of surface sediments from several Arctic basins and ridges to update and refine this baseline. Additionally, we define the authigenic Nd isotopic composition of the last glacial to determine the glacial deep water circulation pattern on a broad spatial scale.

In order to better understand the environmental conditions in the Arctic and their impact on, and significance for, the Arctic Ocean during the LGM compared to the modern, we studied the provenance of the lithogenic material using elemental concentrations and Nd and Sr isotopes. Investigation of sediment provenance in the Arctic is expected to reveal surface circulation patterns because sea ice drift forms the dominant distribution pathway of detritus from the Arctic coasts and shelves across the entire basin. It is therefore instrumental to use sediment archives to reconstruct sea ice patterns in different regions of the Arctic Ocean in order to compare LGM and modern conditions.

The Arctic Ocean is surrounded by a large variety of lithologies, whose Nd and Sr isotopic composition have partly been determined. Therefore, distinct source areas can be defined. Our results provide a spatial and temporal pattern of sediment input and offer insight into the environmental conditions in the Arctic during the LGM compared to the modern situation.

We hypothesize that glacial sediment provenance was different from today because of a lower sea level, exposed shelves, the existence of large ice sheets, and an overall more arid climate (e.g., Darby et al., 2006). Today the surface circulation in the Arctic Ocean is dominated by two major current systems: The anti-cyclonic Beaufort Gyre (BG) in the Amerasian Basin, and the Transpolar Drift (TPD) originating from the Siberian shelves and crossing the Arctic Ocean towards the Fram Strait. These currents transport sea ice – and sediments entrained in it –

from the shelves across the entire Arctic Ocean. With our geochemical approach, we try to evaluate the potentially varying influence of these current systems on the isotopic signal of the studied sediments under last glacial and modern conditions. This will lead to a better understanding of present and past environmental conditions in the Arctic Ocean.

### 4.3 Material and methods

During R/V *Polarstern* expedition ARK-XXVI/3 in 2011 (Schauer, 2012), 11 multicorer cores were collected (Abb. 14a, Tab. 4; here referred to as 201, 206, 211, 217, 225, 231, 237, 248, 275, 277, and 285). Shortly after core recovery, sampling was carried out at a depth resolution of 1 cm and sediment slides were stored at ~4°C. After freeze-drying on shore, the samples were finely ground in an agate ball mill for the determination of element concentrations. Isotopic measurements were done on the untreated bulk sediment.

#### 4.3.1 Major and trace elements

Sediment analysis of Al, Ca, Mg, and Mn was performed by wavelength-dispersive X-ray fluorescence (XRF, Philips PW 2400) on fused borate glass beads (detailed procedure in data repository of Eckert et al., 2013). Total inorganic carbon (TIC) was measured coulometrically with an UIC Coulometer. Accuracy and precision were checked with several inhouse standards (CAST, ICBM-B, Loess, PS-S, Peru, WAP; for TIC only Loess was used). For TIC, accuracy and precision were <1%. For XRF measurements, accuracy and precision were <4%. The water content of each sample, determined as the difference of wet and dry sediment weight, was used to correct the sediment content for each sea salt constituent to eliminate dilution effects resulting from sea salt enclosed in interstitial waters.

Element contents are displayed in weight % for major elements, ppm ( $\mu\text{g/g}$ ) for trace elements, and are typically normalized to Al whose origin is essentially terrigenous and which is not affected by biogenic or diagenetic processes

(Brumsack, 2006). Therefore, variable dilution of the terrigenous background can be excluded.

Tab. 4: Core locations, bulk element contents and Nd and Sr isotopic composition of the leachable and lithogenic fractions of modern and LGM (bold) samples.

Station	Latitude	Longitude	Water depth (m)	Depth in core (cm)	Leachable fraction				Lithogenic fraction				Bulk sediment						
					eNd	2σ SD	eNd	2σ SD	<sup>87</sup> Sr/ <sup>86</sup> Sr	±2σ	Mn	Al	Mg	Ca	Mn/Al				
PS78/201-7	85° 32,49' N	59° 25,01' E	3797	0-1	-9.2	0.24	-9.7	0.26	0.7299	0.0000239	0.256	9.60	1.86	1.40	0.027				
				<b>2-3</b>	<b>-8.8</b>	<b>0.31</b>	<b>-10.1</b>	<b>0.26</b>	<b>0.7249</b>	<b>0.0000279</b>	<b>0.164</b>	<b>9.66</b>	<b>1.80</b>	<b>1.31</b>	<b>0.017</b>				
PS78/206-2	86° 26,43' N	60° 5,75' E	1770	0-1	-10.5	0.25	-10.4	0.26	0.7178	0.0000239	0.217	7.02	1.06	3.31	0.031				
				<b>6-7</b>	<b>-7.4</b>	<b>0.31</b>	<b>-8.8</b>	<b>0.26</b>	<b>0.7154</b>	<b>0.0000190</b>	<b>0.081</b>	<b>7.39</b>	<b>1.03</b>	<b>1.13</b>	<b>0.011</b>				
PS78/211-1	87° 36,04' N	61° 3,23' E	4026	0-1	-10.9	0.16	-10.9	0.27	0.7204	0.0000239	0.510	8.29	1.44	2.64	0.062				
				<b>7-8</b>	<b>-11.4</b>	<b>0.31</b>	<b>-11.3</b>	<b>0.23</b>	<b>0.7172</b>	<b>0.0000183</b>	<b>0.331</b>	<b>8.64</b>	<b>1.42</b>	<b>1.51</b>	<b>0.038</b>				
PS78/217-1	89° 57,73' N	97° 41,59' E	4122	0-1	-10.3	0.16	-9.9	0.26	0.7224	0.0000239	0.658	8.53	1.72	1.37	0.077				
				<b>21-22</b>	<b>-12.1</b>	<b>0.31</b>	<b>-12.6</b>	<b>0.19</b>	<b>0.7219</b>	<b>0.0000183</b>	<b>0.137</b>	<b>9.55</b>	<b>1.70</b>	<b>0.65</b>	<b>0.014</b>				
PS78/225-4	87° 39,09' N	157° 43,61' W	2314	0-1	-10.6	0.23	-11.0	0.26	0.7214	0.0000239	0.580	8.83	1.58	1.53	0.066				
				<b>4-5</b>	<b>-11.5</b>	<b>0.29</b>	<b>-11.2</b>	<b>0.39</b>	<b>0.7214</b>	<b>0.0000212</b>	<b>0.355</b>	<b>7.51</b>	<b>2.09</b>	<b>4.53</b>	<b>0.047</b>				
PS78/231-1	84° 54,32' N	137° 48,54' W	1594	0-1	-10.6	0.21	-11.9	0.26	0.7251	0.0000239	0.403	5.06	2.39	10.81	0.080				
				<b>2-3</b>	<b>-12.2</b>	<b>0.29</b>	<b>-13.7</b>	<b>0.29</b>	<b>0.7224</b>	<b>0.0000212</b>	<b>0.286</b>	<b>4.80</b>	<b>2.94</b>	<b>12.28</b>	<b>0.060</b>				
PS78/237-1	83° 44,65' N	154° 24,88' W	2378	0-1	-13.9	0.31	-12.8	0.26	0.7247	0.0000239	0.385	5.50	2.36	9.82	0.070				
				<b>5-6</b>	<b>-10.3</b>	<b>0.16</b>	<b>-16.1</b>	<b>0.26</b>	<b>0.7294</b>	<b>0.0000183</b>	<b>0.182</b>	<b>4.44</b>	<b>4.23</b>	<b>12.12</b>	<b>0.041</b>				
PS78/248-4	84° 40,75' N	149° 59,41' E	1611	0-1	-10.3	0.16	-10.0	0.26	0.7194	0.0000263	0.565	8.60	1.57	1.65	0.066				
				<b>19-20</b>	<b>-10.5</b>	<b>0.18</b>	<b>-10.7</b>	<b>0.30</b>	<b>0.7166</b>	<b>0.0000183</b>	<b>0.339</b>	<b>9.00</b>	<b>1.37</b>	<b>0.81</b>	<b>0.038</b>				
PS78/275-1	80° 49,13' N	120° 58,26' E	3527	0-1	-10.5	0.18	-10.6	0.18	0.7204	0.0000239	0.396	8.12	1.45	2.28	0.049				
				<b>18-19</b>	<b>-10.5</b>	<b>0.31</b>	<b>-11.1</b>	<b>0.26</b>	<b>0.7161</b>	<b>0.0000183</b>	<b>0.189</b>	<b>8.79</b>	<b>1.34</b>	<b>0.68</b>	<b>0.022</b>				
PS78/277-2	80° 12,54' N	122° 12,20' E	3359								0.413	8.51	1.49	1.99	0.049				
				<b>19-20</b>	<b>-10.4</b>	<b>0.31</b>	<b>-11.1</b>	<b>0.27</b>	<b>0.7167</b>	<b>0.0000249</b>	<b>0.212</b>	<b>8.78</b>	<b>1.39</b>	<b>0.71</b>	<b>0.024</b>				
PS78/285-6	78° 29,97' N	125° 42,94' E	2805	0-1	-10.3	0.20	-10.2	0.18	0.7205	0.0000239	0.384	8.70	1.64	1.36	0.044				

#### 4. Variations of bottom water circulation and sediment provenance

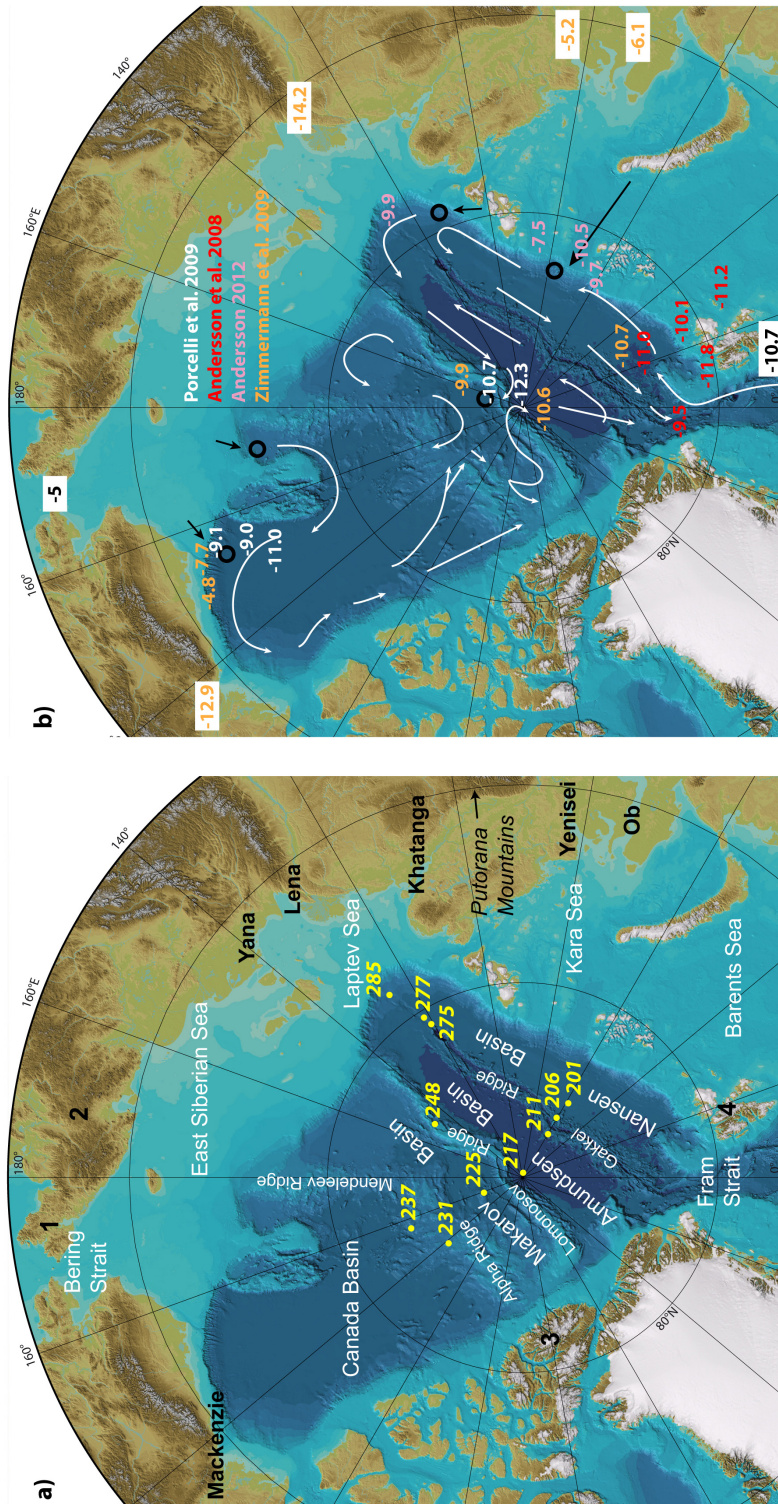


Abb. 14: (based on IBCAO, Jakobsson et al., 2008) a) Map of the Arctic Ocean with core locations and major rivers. Black numbers: 1: Chukchi Peninsula 2: Okhotsk-Chukotka volcanic belt 3: Arctic Archipelago; 4: Svalbard. b) Recent deep water currents (adapted from Rudels et al., 2012), literature values for deep water  $\epsilon_{ND}$  and river water  $\epsilon_{ND}$ . Black circles and arrows: possible sites of slope convection from cold, brine enriched shelf waters to the deep waters (Nansen, 1906; Rudels et al., 2012). Black numbers: Atlantic inflow from the Greenland Sea deep water (Piepgras and Wasserburg, 1987) and Pacific inflow (Dahlqvist et al., 2004).



### 4.3.2 Nd and Sr isotopes

Sample preparation for Nd and Sr isotope analysis was modified from Chester and Hughes, 1967. All chemicals were of ultrapure or distilled quality. Authigenic Fe-Mn oxides were leached from 500 mg of the bulk sediments using 10 ml of a 0.02 M solution of hydroxylamine hydrochloride (HH) in a weak 2% acetic acid matrix. The mixture was shaken for 1.5 hrs. After centrifuging, the supernatant was collected, centrifuged again, filled into a Teflon beaker and dried down at 160 °C. The samples were dissolved in 0.5 ml 1 N HNO<sub>3</sub> for separation of rare earth elements (REE) from Sr and other cations on Eichrom Tru-Spec resin (100-150 µm mesh; Pin and Zalduegui, 1997). Final isolation of Nd from other REE was achieved using Eichrom Ln-Spec resin (50-100 µm mesh; Pin and Zalduegui, 1997) and 0.24 N HCl as eluant. The residual sediment fraction (after the first leach, see above) was washed with demineralized water and then treated with 10 ml of buffered acetic acid (pH of 5.5) to remove carbonates. The suspension was agitated over night. After centrifuging, the supernatant was discarded and the sediment was again washed with demineralized water. The carbonate removal was repeated until no more CO<sub>2</sub> was released, followed by two more leaching steps with HH (0.02 M in 25% acetic acid, 6 hrs and 24 hrs) to remove any authigenic fraction.

Acid digestion was performed with about 40 mg of residual sediment, 0.5 ml conc. HClO<sub>4</sub>, 3 ml conc. HF and 3x3 ml 6M HCl. Pure MgO powder was added in excess (~20 mg) prior to dissolution to prevent the formation of AlF<sub>3</sub> (Takei et al., 2001). For separation of REEs from Sr and other cations, Eichrom Tru-Spec resin was used. The isolation of Nd followed the procedure described above, while Sr was isolated from Rb using Eichrom Sr-Spec resin (100-150 mm mesh).

Neodymium and Sr isotopes were measured with a multi-collector ICP-MS (Neptune Plus, Thermo Scientific) at the University of Oldenburg. For Nd isotope analyses, all samples were corrected for mass fractionation using  $^{146}\text{Nd}/^{144}\text{Nd} = 0.7219$  and an exponential law. Each measurement session was accompanied by multiple analyses of the Nd standard JNdi-1 (generally every 3 samples), and

$^{143}\text{Nd}/^{144}\text{Nd}$  ratios of all samples were normalized to the reported JNdi-1 value of  $^{143}\text{Nd}/^{144}\text{Nd} = 0.512115$  (Tanaka et al., 2000).

The Nd isotopic composition is expressed in  $\epsilon_{\text{Nd}}$  notation:

$$\epsilon_{\text{Nd}} = [({}^{143}\text{Nd}/{}^{144}\text{Nd})_{\text{sample}} / ({}^{143}\text{Nd}/{}^{144}\text{Nd})_{\text{CHUR}} - 1] * 10^4 \quad (6)$$

$({}^{143}\text{Nd}/{}^{144}\text{Nd})_{\text{CHUR}}$  is the Chondritic Uniform Reservoir with a value of 0.512638 (Jacobsen and Wasserburg, 1980).

The internal precision was better than 17 ppm ( $2\sigma$ ). The external reproducibility for Nd isotope analyses was determined by replicate measurements of the JNdi-1 standard and was  $\pm 0.000027$  (27 ppm) for  $^{143}\text{Nd}/^{144}\text{Nd}$  ( $\pm 0.3 \epsilon_{\text{Nd}}$ ;  $n = 36$ ;  $2\sigma$ ). The BCR-2 standard had an  $\epsilon_{\text{Nd}}$  value of 0.1 ( $\pm 0.3$ ;  $n = 5$ ;  $2\sigma$ ), which is well within the reported  $\epsilon_{\text{Nd}}$  value of  $0.0 \pm 0.2$  (Raczek et al., 2003). The addition of MgO to the acid digestion resulted in Nd blank levels of 2-3% of sample Nd. To check the potential influence of the MgO powder on the isotopic ratios of the samples, the  $\epsilon_{\text{Nd}}$  of the pure dissolved powder was measured to correct the  $\epsilon_{\text{Nd}}$  of the samples. As a result, the MgO powder caused a maximum change of 0.1  $\epsilon_{\text{Nd}}$  units of the isotopic composition of the samples. This is in the range of the standard deviation of the measurements and can therefore be neglected.

For Sr isotope analyses, all samples were corrected for mass fractionation using  $^{88}\text{Sr}/^{86}\text{Sr} = 0.1194$  and the exponential law. Measurements were accompanied by multiple analyses of NBS987 (generally every 7 samples), and  $^{87}\text{Sr}/^{86}\text{Sr}$  values of all samples were normalized to the reported NBS987 value of 0.710248 (Thirlwall, 1991). Further, Kr, Rb and Ba contents were monitored and found to be negligible. The external reproducibility for Sr isotopes determined through replicate analyses of NBS987 was  $\pm 0.000033$  for  $^{87}\text{Sr}/^{86}\text{Sr}$  (33 ppm;  $n = 11$ ;  $2\sigma$ ). The BCR-2 standard had a  $^{87}\text{Sr}/^{86}\text{Sr}$  value of  $0.70504 \pm 0.00002$  ( $n = 5$ ;  $2\sigma$ ), well within the reported value of 0.70496 (Raczek et al., 2003).

### 4.3.3 Sampling strategy for recent Holocene and LGM sediment samples

The age of the sediments was estimated based on the Mn/Al variations of the sediment cores (Abb. 15).

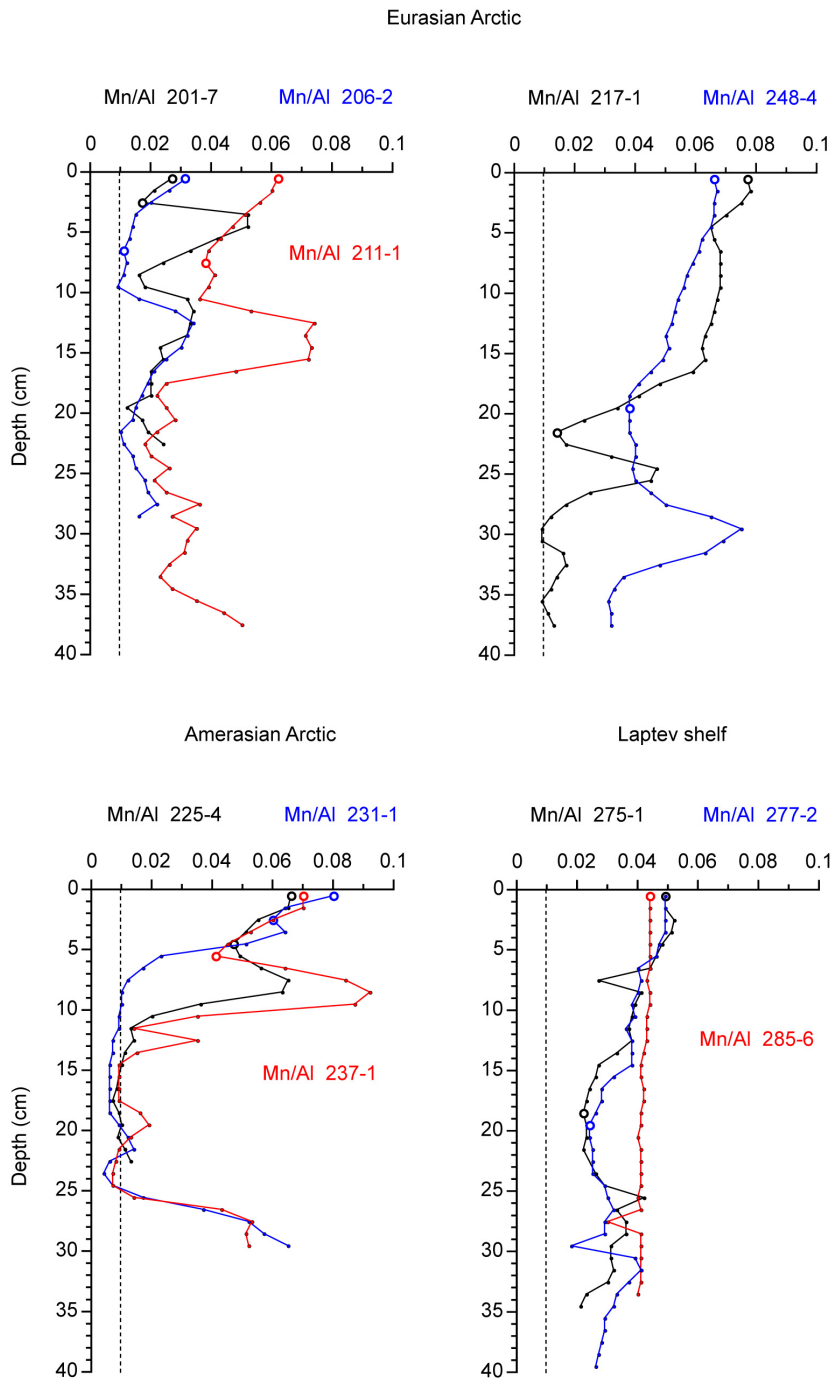


Abb. 15: Mn/Al ratios of the studied multicorer cores. Open circles mark samples for isotope measurements. Dashed line marks average shale (Wedepohl, 1971, 1991).

Close to the surface, the sediment cores show elevated Mn/Al ratios that decrease downcore until a minimum is reached. We chose the upper first centimeters of each core as a representative sample for recent Holocene sedimentation. As demonstrated by Meinhardt et al. (2014) for sediment cores from the Mendeleev Ridge, the first downcore minimum in Mn/Al reflects reduced fluvial and coastal erosion Mn input during glacial periods (Jakobsson et al., 2000), and corresponds to the LGM. Therefore we have chosen samples from the first Mn/Al minimum to represent the LGM. Conventional dating in Arctic Ocean sediments (e.g.,  $^{14}\text{C}$  dating,  $\delta^{18}\text{O}$  stratigraphy) is limited because of poor preservation of calcareous nanofossils and the varying riverine fresh water input, which prevents the correlation of foraminiferal oxygen isotopes to lower latitude oxygen isotope records (Backman et al., 2004; Spielhagen et al., 2004). Stratigraphic correlation based on elevated Mn contents can be applied for central Arctic Ocean sediments when diagenetic remobilization can be excluded (März et al., 2011; Löwemark et al., 2014). In the studied multicorer samples, additional pore water analyses (not shown) reveal  $\text{Mn}^{2+}$  concentrations below detection limit, suggesting that diagenetic Mn relocation is negligible. The correlation may not be valid for all parts of the Arctic Ocean and we therefore refer to Mn-poor/cold/LGM-like depositional conditions throughout the manuscript.

## 4.4 Results

### 4.4.1 Geochemical characteristics of the sediment cores

Compared to average shale ("AS", Wedepohl, 1971; 1991), all cores are enriched in Mn at the surface with highest enrichments in core 217 from the North Pole (Amundsen Basin) and cores 231 and 237 from the Alpha Ridge/Canada Basin (Abb. 15). The Mn/Al ratios decrease downcore towards lower ratios that mark the LGM (Meinhardt et al., 2014), before they sharply increase towards a maximum. In cores close to the Laptev Sea shelf (275 to 285), the minima and maxima are less pronounced compared to the other locations.

The surfaces of cores 201, 206, 211, 231, and 237 are also enriched in Ca, and parallel enrichments in Ca, Mg, and TIC are visible in the upper centimeters of cores 231 and 237 (Abb. 16).

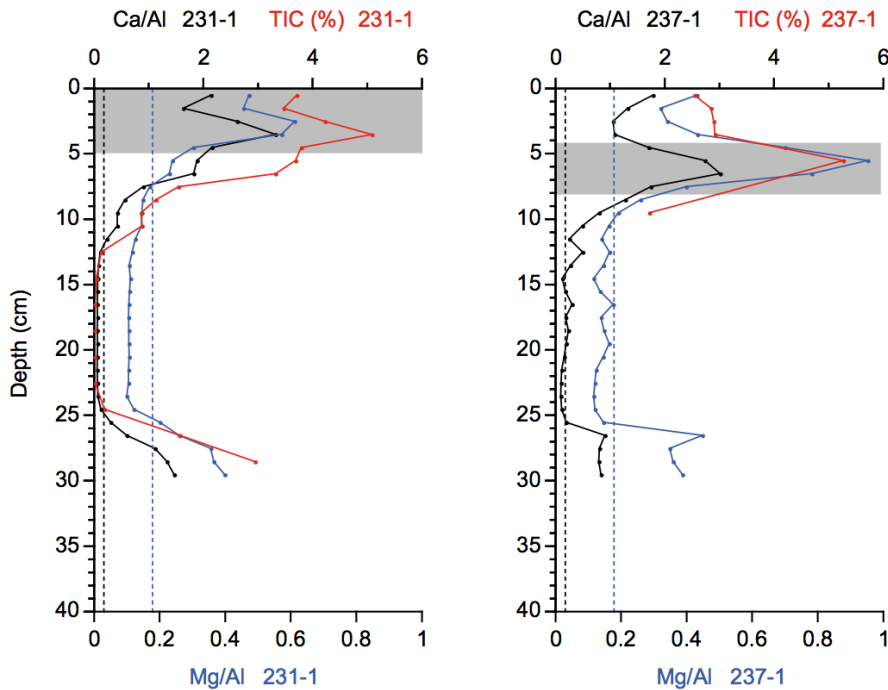


Abb. 16: Sedimentary Ca/Al (black), Mg/Al (blue), and TIC (red) data for cores 231 and 237 from the Canada Basin. Dashed lines: average shale. Gray bars indicate sediment layers with supposed occurrence of dolomite.

#### 4.4.2 Nd isotope ratios of authigenic Fe-Mn oxides (leachable fraction)

The Nd isotope signature of the surface sediment leachates is rather uniform. Except for station 201 in the Nansen Basin ( $\epsilon_{Nd} = -9.2$ ), the  $\epsilon_{Nd}$  values range from -10.9 to -10.3 (Abb. 17a, Tab. 4).

The samples from the LGM show larger spatial differences than the surface samples, with higher  $\epsilon_{Nd}$  in the Nansen Basin (-8.8 to -7.4) and lower  $\epsilon_{Nd}$  in the Canada (-13.9) and Amundsen Basins (-12.2 to -11.4) (Abb. 17b). Samples from the Lomonosov Ridge and near the Laptev shelf have values similar to the surface samples.

#### 4. Variations of bottom water circulation and sediment provenance

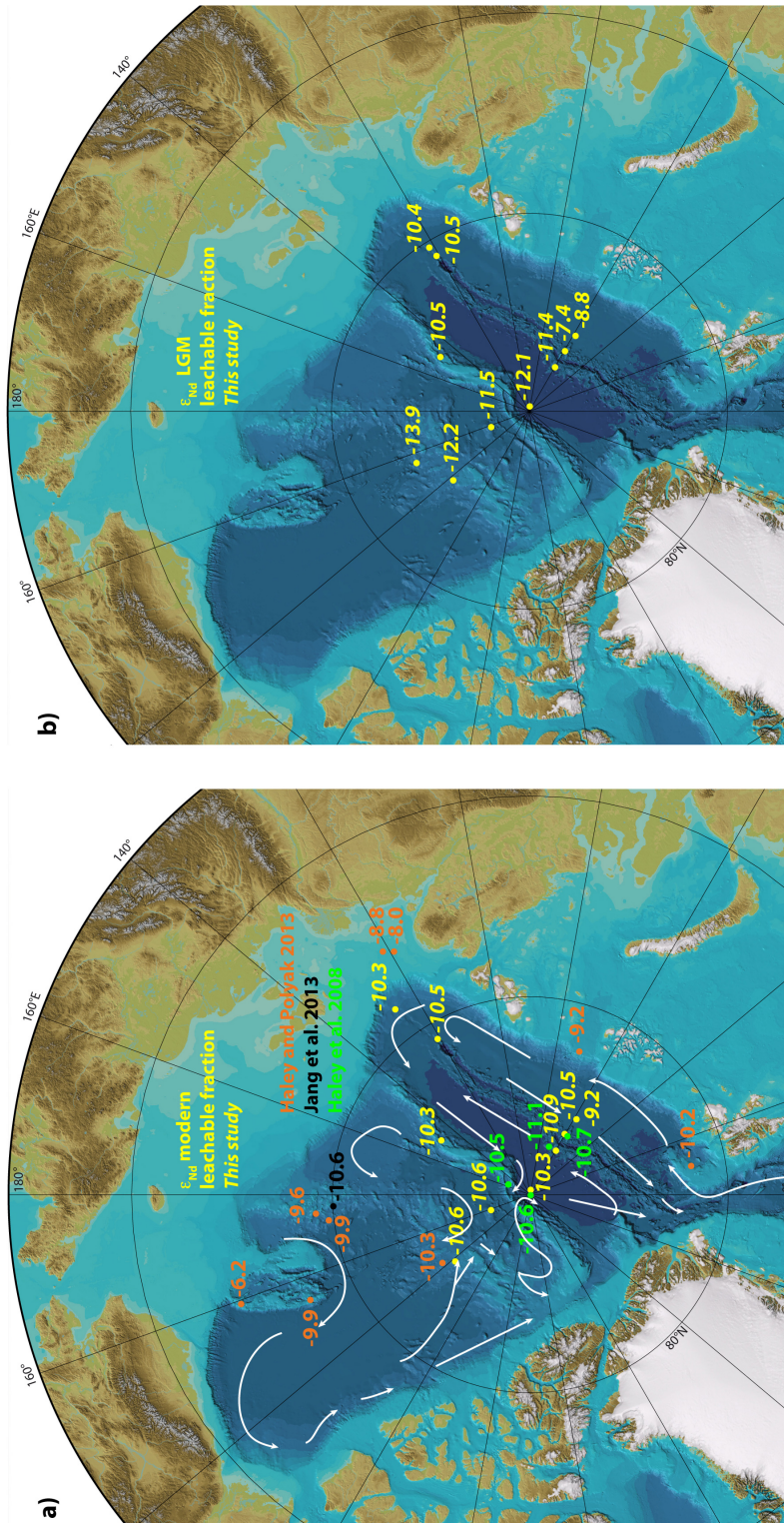


Abb. 17: (based on IBCAO, Jakobsson et al., 2008)  $\epsilon_{Nd}$  values of the leachates from a) surface sediments, b) sediments from the Last Glacial Maximum. Additional literature values of sediment leachates are given. Modern deep water circulation in white (adapted from Rudels et al., 2012).

#### 4.4.3 Nd and Sr isotopes of the terrigenous fraction

To distinguish between different source areas of the terrigenous material, we plot our Nd and Sr isotope results into  $\epsilon_{Nd}$  versus  $^{87}Sr/^{86}Sr$  diagrams together with Nd and Sr isotope compositions of the surrounding Arctic terrains as potential source endmembers (Abb. 18).

The lithogenic fraction of the surface samples shows  $\epsilon_{Nd}$  values of -12.8 to -9.7 (Abb. 18a, 19a; Tab. 4). The most negative values are found in samples closer to the Canadian Arctic (cores 231 and 237). The  $^{87}Sr/^{86}Sr$  values from the terrigenous fraction range from 0.7154 to 0.7299 (Abb. 18a, Tab. 4). Figure 4a shows, that no sample can be assigned to one distinct source area but that they plot between potential source areas. The  $^{87}Sr/^{86}Sr$  values of cores from the Eurasian Basin (206, 211, 275, 285) are located closer to the suspended particulate matter (SPM) of the Siberian rivers Khatanga, Yana, and Lena than samples 231 and 237 from the Amerasian Basin. Some distinct trends are visible for the surface sediments. Cores 231 and 237 from the Alpha Ridge/Canada Basin have the lowest  $\epsilon_{Nd}$  values of the surface sediments and plot closer to the Mackenzie particles. This is in accordance with their geographic location: Of all cores they are located closest to the North American continent. Core 201 from the Nansen Basin, which is located nearest to Svalbard, has the highest  $\epsilon_{Nd}$  and  $^{87}Sr/^{86}Sr$  values. Core 206 from the southern Gakkel Ridge has the lowest  $^{87}Sr/^{86}Sr$  value. Cores 211 from the northern Gakkel Ridge, 225 from the Makarov Basin, and 275 and 285 near the Laptev shelf plot closely together.

During the LGM,  $\epsilon_{Nd}$  values are mostly in the same range as the surface samples, except for core 206 with higher  $\epsilon_{Nd}$  (-8.8) and cores 231 and 237 with lower  $\epsilon_{Nd}$  (-13.7 and -16.1, respectively; Tab. 4). The most negative values are again found in the Canada Basin. Most of the LGM samples have lower  $\epsilon_{Nd}$  values and lower  $^{87}Sr/^{86}Sr$  values than the surface samples (Abb. 20).

#### 4. Variations of bottom water circulation and sediment provenance

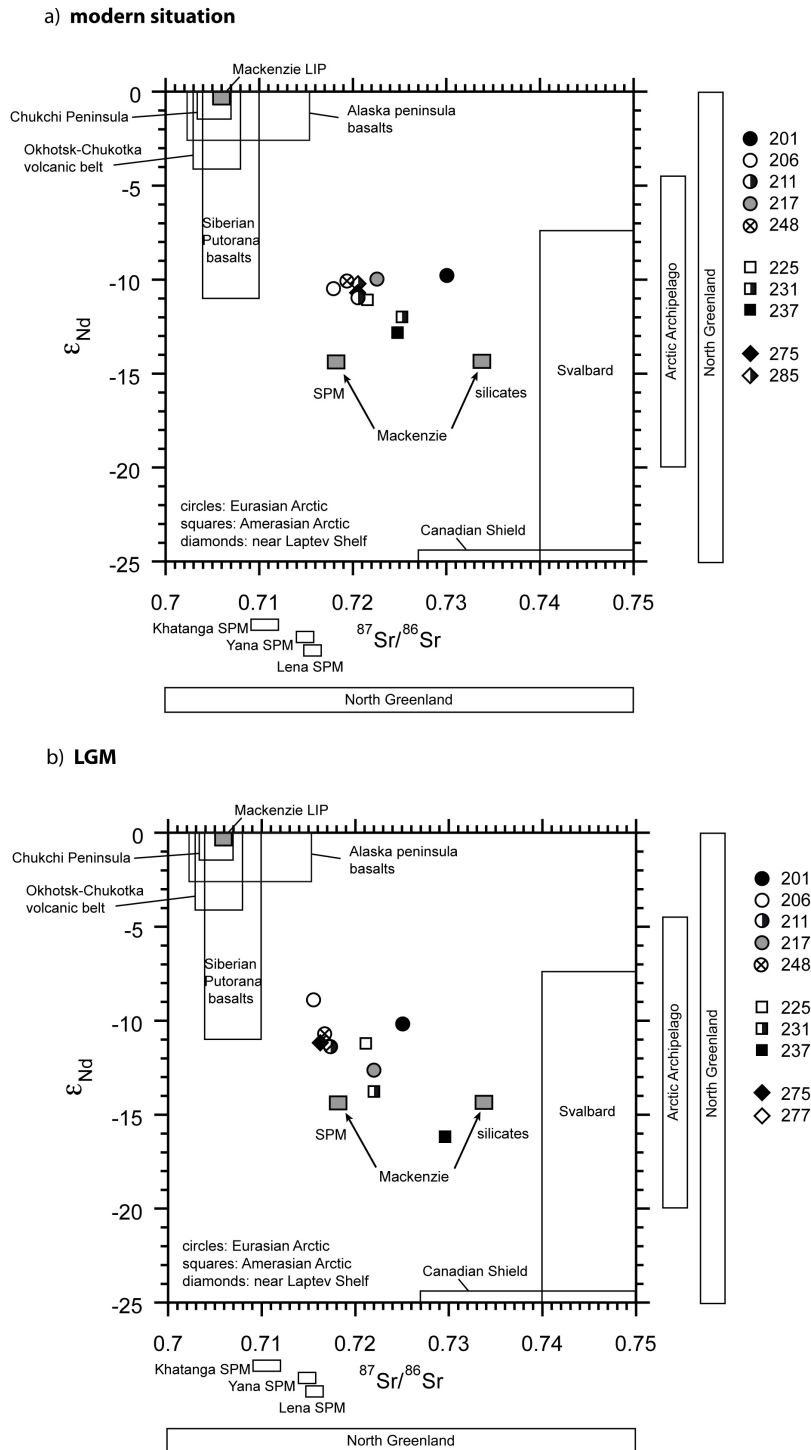


Abb. 18:  $\epsilon_{Nd}$  versus  $^{87}Sr/^{86}Sr$  diagram for the lithogenic fraction of a) surface sediments, b) sediments from the Last Glacial Maximum. Reference data for potential source areas: Siberian Putorana basalts: Lightfoot et al., 1993; Wooden et al., 1993. Chukchi peninsula: Ledneva et al., 2011 (from Georoc database); Akinin et al., 2013. Okhotsk-Chukotka volcanic belt: Tikhomirov et al., 2008. Alaska peninsula: Andronikov and Mukasa, 2010; Akinin et al., 2013. Mackenzie particles: Goldstein et al., 1984; Millot et al., 2003. Mackenzie LIP: Dupuy et al., 1992. Svalbard: Johansson et al., 1995; 1999. Canadian Shield: McCulloch and Wasserburg, 1978. North Greenland: Kalsbeek and Jepsen, 1983; 1984; Estrada et al., 2001; Upton et al., 2005; Kalsbeek and Frei, 2006; Thorarinsson et al., 2011. Arctic Archipelago: Patchett et al., 2004 (only  $\epsilon_{Nd}$  values). Khatanga/Lena/Yana suspended particulate matter (SPM): Eisenhauer et al., 1999 (only  $^{87}Sr/^{86}Sr$  values).



4. Variations of bottom water circulation and sediment provenance

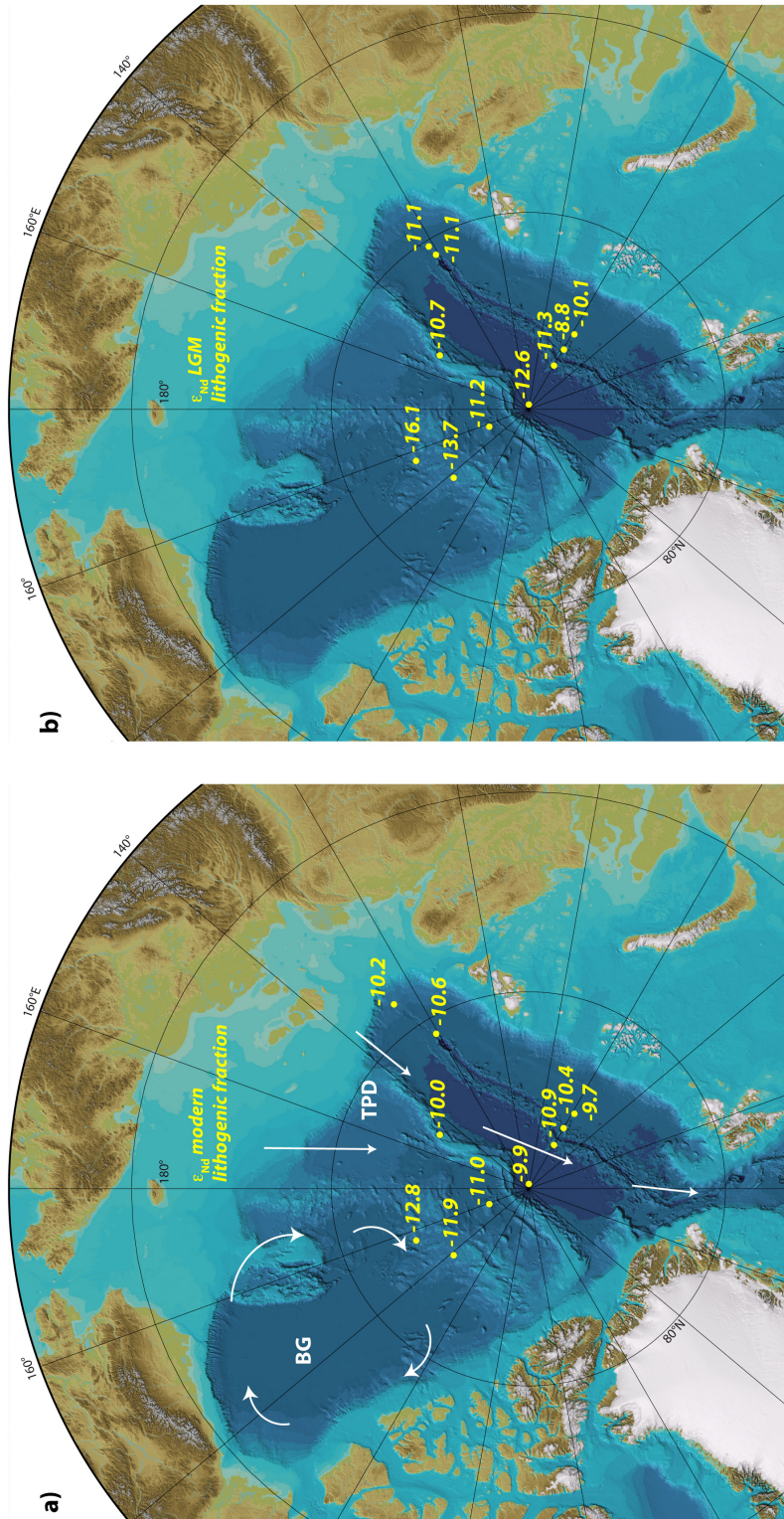


Abb. 19: (based on IBCAO, Jakobsson et al., 2008)  $\epsilon_{Nd}$  values of the lithogenic fraction from a) surface sediments, b) sediments from the Last Glacial Maximum. Modern surface water circulations (BG Beaufort Gyre and TPD Transpolar Drift) are shown schematically.

## 4.5 Discussion

### 4.5.1 Bulk sediment characteristics

In the oxic environment of the Arctic Ocean, Mn forms (oxyhydr)oxides with a high adsorption capacity for many elements. High enrichments of Mn are common in Arctic Ocean sediment cores (e.g., Jakobsson et al., 2000; März et al., 2011; Macdonald and Gobeil, 2012; Löwemark et al., 2014; Meinhardt et al., 2014). In the Central Arctic Ocean, dark brown, Mn-rich sediment layers alternate with lighter olive brown, Mn poor layers. The main reason for the occurrence of these Mn layers is the enhanced input from rivers and coastal erosion during interglacial/interstadial times (Jakobsson et al., 2000; Macdonald and Gobeil, 2012).

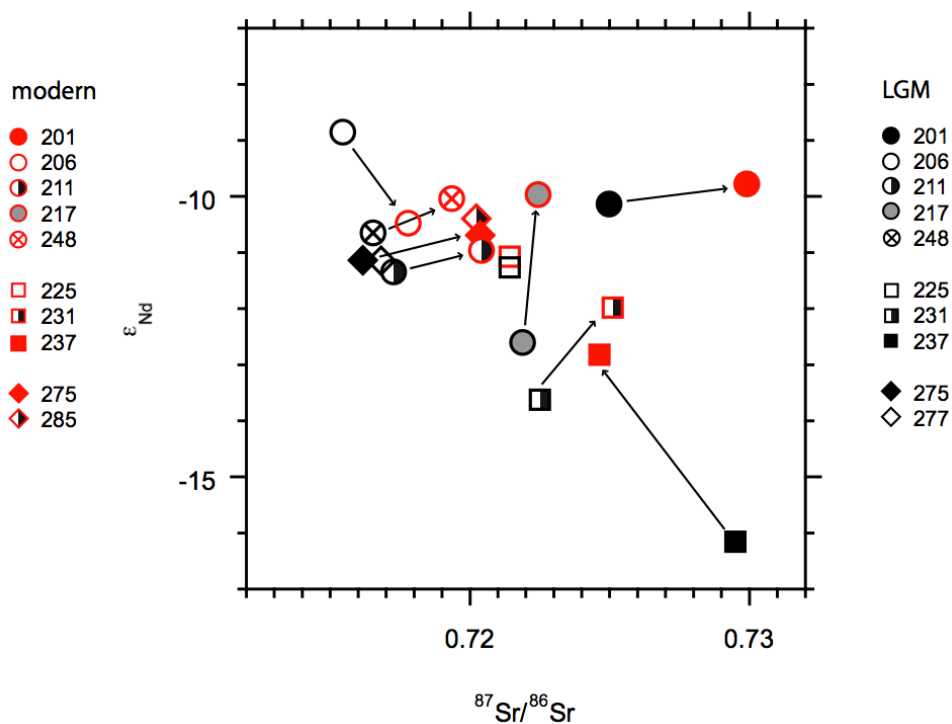


Abb. 20: Enlarged section of Abb. 18 with arrows pointing from the LGM values towards the modern values for each core. Red: modern samples, black: LGM samples.

The very high Mn/Al values especially in the surface samples of cores 231 and 237 may result from either enhanced fluvial/erosional Mn input in the recent warm

period compared to the LGM or enhanced diagenetic remobilization. Riverine input has been found to dominate over coastal erosion in the Canadian Beaufort Sea, and coastal erosion may only be important locally (Rachold et al., 2000). Secondary processes may redistribute Mn in the sediment after deposition (Li et al., 1969; Macdonald and Gobeil, 2012), but this can be excluded for surface sediments in the central Arctic Ocean (Meinhardt et al., submitted).

The enrichment in Ca in the upper intervals of sediment cores 231 and 237 indicates the presence of biogenic or terrigenous detrital carbonate (Abb. 16). Terrigenous carbonates (mostly dolomite) are characterized by synchronous enrichments in Ca, Mg, and TIC, as seen in the surface samples of the two sediment cores and the LGM sample of core 237. Dolomite is common in the western part of the Arctic and presumably originates from the Arctic Archipelago (Banks and Victoria Islands, Bischof et al., 1996; Bischof and Darby, 1997). It is transported by icebergs and sea ice as ice rafted debris (IRD) with the BG in the western Arctic Ocean. The element profiles therefore give evidence that locations 231 and 237 have been influenced by the BG and that TIC is indicative for Arctic Archipelago provenance. However, dolomite is not indicative for changes between modern and LGM conditions and can only be used for sediments from the Amerasian Basin.

Samples from the LGM have higher Mn contents than the local background, indicating the occurrence of additional authigenic Mn to the sediment even during the glacial period. But they generally have lower Mn contents than the modern samples due to reduced fluvial and erosional input. However, the authigenic sediment fraction is very large and biases the use of other bulk sedimentary trace metals as provenance indicators (e.g., Ni, Y), leading to ambiguous results. To overcome this bias we will focus on the Nd and Sr isotopic composition of the lithogenic sediment fraction after removal of the authigenic sediment fraction for provenance studies (chapter 4.4.3).

## 4.5.2 Nd isotope ratios of authigenic Fe-Mn oxides

### 4.5.2.1 Modern situation

Atlantic inflow is the primary source of Arctic Ocean deep water (Abb. 14b) with an  $\epsilon_{Nd}$  signature of -10.7 (from the Greenland Sea deep water, Piepgras and Wasserburg 1987). The surface samples from the Eurasian Basin (except for core 201 with  $\epsilon_{Nd}$  -9.2, discussed below) show values of  $\epsilon_{Nd}$  -10.6  $\pm$ 0.3, suggesting a clear influence of bottom water from the North Atlantic. This is in accordance with former studies (e.g., Haley and Polyak, 2013) and suggests well-mixed deep waters with an Atlantic origin in the Eurasian part of the Arctic Ocean.

Core 201 in the Nansen Basin is the only one with a slightly higher  $\epsilon_{Nd}$  value of -9.2, the same as a sediment sample from the Kara shelf (Haley and Polyak 2013; Abb. 17a). This may indicate the influence of shelf-seawater interaction and the transport of this signal into deep waters through brine formation.

The Nd isotope ratios of cores 275 and 285 near the Laptev Sea shelf ( $\epsilon_{Nd}$  -10.5 and -10.3, respectively) show the North Atlantic  $\epsilon_{Nd}$  signature and clearly differ from sediments directly on the shelf ( $\epsilon_{Nd}$  = -8.8 to -8.0, Haley and Polyak, 2013, Abb. 17a). This indicates that there is no direct transport of waters from the shelf to the deep basin in this region (as would be expected in case of brine rejection).

One deep water measurement of Porcelli et al. (2009) in the Amundsen Basin shows an  $\epsilon_{Nd}$  value of -12.3 (Abb. 14b), which is considerably lower than elsewhere in the Arctic Ocean. The authors explain this value by exchange between shelf sediments and overlying waters. They doubt simple mixing of North Atlantic derived water with shelf water or addition of Nd as explanation for lower values in the Amundsen Basin. Our data do not confirm this finding. Core 217 from the Amundsen Basin has a similar  $\epsilon_{Nd}$  (-10.3) as our other surface samples in the Eurasian Basin and the value of Zimmermann et al. (2009) from the Amundsen Basin (Abb. 14b), suggesting that this location is as well influenced by well-mixed deep water with a North Atlantic origin.

Pacific water enters the Arctic Ocean with an average  $\epsilon_{Nd}$  value of  $\sim$ -5 (Dahlqvist et al., 2007). Even core 237 closest to the Canada Basin shows no

change towards more positive values and is therefore apparently not influenced by Pacific water.

#### 4.5.2.2: LGM

The  $\epsilon_{Nd}$  results from the LGM show a less homogenous deep water  $\epsilon_{Nd}$  distribution in the Arctic Ocean compared to the modern situation, most likely suggesting stronger local influence (Abb. 17b). During the LGM, the sea level was lower than today and most of the Siberian shelf area was exposed. The core sites were therefore subject to more direct influence from land. Water from the Pacific Ocean with a more positive isotopic signature could not enter the Arctic Ocean.

Location 237 with a low  $\epsilon_{Nd}$  signature (-13.9) must have been influenced by water with a more negative signature. One possible source with negative signature is the Mackenzie River ( $\epsilon_{Nd} = -12.9$ ), whose isotopic signature is transported with the anti-cyclonic BG in the Canada Basin. Its isotopic signature must have been even more negative during the LGM by at least one  $\epsilon_{Nd}$  unit to cause the observed signal. In sediments close to the North Pole, Haley et al. (2008) explained low  $\epsilon_{Nd}$  values during glacial intervals with brine formation occurring on the Eurasian shelves. The isotopic signature of the Lena River ( $\epsilon_{Nd} = -14.2$ ) is a potential source for low  $\epsilon_{Nd}$  values and may be added to the deep water through brine rejection.

A higher  $\epsilon_{Nd}$  signal is seen in Nansen Basin samples from cores 201 and 206 ( $\epsilon_{Nd}$  values of -8.8 and -7.4, respectively), possibly indicating local river input to surface waters and subsequent brine rejection. A possible source for higher  $\epsilon_{Nd}$  values on land are the Putorana Mountains. Material from the Putorana Mountains ( $\epsilon_{Nd} \geq 0$ , Sharma et al., 1992), which is transported by rivers and coastal erosion to the shelf area, is incorporated into the Eurasian ice sheet. This ice sheet extended to the current shelf edge of the Kara and Barents Seas (Svendsen et al., 2004). Boundary exchange and brine rejection on the ice edge especially in the Kara Sea may have transferred this material to the deeper waters, as proposed by Aagaard et al. (1985), Tütken et al. (2002), and Haley et al. (2008). As the deep water from the Nansen Basin with its higher  $\epsilon_{Nd}$  flows towards the Laptev shelf, it must have mixed with local water with a lower  $\epsilon_{Nd}$  signature along its way, because samples

from the Lomonosov Ridge (core 248) and near the Laptev shelf (core 275 and 277) have lower  $\epsilon_{Nd}$  values (-10.5 to -10.4) than cores 201 and 206 (-8.8 to -7.4). In this area, the Lena River is a likely source and could have had a greater influence than today. It has been found that the very low Lena water signature of -14 does not propagate far onto the Laptev shelf today, but is diluted on the shelf by coastal currents eastward (Haley and Polyak, 2013). This dilution must have been absent during the LGM because of the exposed shelf area, which moved the river mouth closer to the core location.

At the Northern Gakkel Ridge and the North Pole (stations 211 and 217), LGM  $\epsilon_{Nd}$  values (-12.2 and -11.4, respectively) are lower than the surface samples. This may indicate an enhanced water flow from the Makarov Basin through an intra-basin on the Lomonosov Ridge. This water flow has been observed in the modern Arctic Ocean (Björk et al., 2007) and may have been active during the LGM as well. This is likely, because deep waters from the Canada and Makarov Basins (cores 225, 231, and 237) have low  $\epsilon_{Nd}$  value of -13.9 to -11.5. A reverse flow from the Amundsen Basin to the Makarov Basin has not been observed by Björk et al. (2007).

### 4.5.3 Lithogenic material

#### 4.5.3.1 Modern situation

The different Nd and Sr isotope compositions of the studied lithogenic fractions (Abb. 18, 19) show that the core sites are influenced by different sources. Possible transport mechanisms are erosion, river input, and sea ice transport and therefore surface currents. Eolian input plays only a minor role in the Arctic Ocean (Stein, 2008).

Individual source areas have a wide range of  $\epsilon_{Nd}$  and  $^{87}Sr/^{86}Sr$  signatures, making the assignment of our samples to distinct source areas difficult. All studied sediments most likely represent mixtures of material from the Eurasian and Amerasian Arctic. North Greenland source rock data ( $\epsilon_{Nd}$  and  $^{87}Sr/^{86}Sr$ ) encompass the whole scale shown in Abb. 18 and therefore all samples could

have been influenced by material from Greenland (Kalsbeek and Jepsen, 1983; 1984; Estrada et al., 2001; Upton et al., 2005; Kalsbeek and Frei, 2006; Thorarinsson et al., 2011). The same is valid for available  $\epsilon_{Nd}$  data from the Arctic Archipelago. However, based on their location and the prevailing surface currents it is more likely that cores from the Canada Basin (231, 237) received more material from the Arctic Archipelago than cores in the Eurasian Basin (201, 206, 211, 275, 285).

Core 201 in the Nansen Basin can be distinguished from the other cores (206, 211, 248, 275, 285) of the Eurasian Basin. The high  $^{87}Sr/^{86}Sr$  values are indicative of contributions from Svalbard. Svalbard source rocks have  $^{87}Sr/^{86}Sr$  values  $\geq 0.74$  and  $\epsilon_{Nd}$  from -25 to -7 (Johansson et al., 1995, 1999). The possible transport way is the West Spitsbergen Current, which enters the Arctic Ocean from the Atlantic and flows along the shelf break into the Nansen Basin (Rudels et al., 2012). This current may transport sea ice with entrained material from Svalbard to station 201.

Core 225 is slightly shifted to higher  $^{87}Sr/^{86}Sr$  values and lower  $\epsilon_{Nd}$  compared to the other Eurasian cores, in accordance with its location in the Makarov Basin closer to Canada.

Cores 201, 231, and 237 are least influenced by SPM from the Siberian rivers. This can be explained by enhanced inputs from Svalbard to core 201 and the large distance of cores 231 and 237 to the Siberian coast. Cores 231 and 237 plot closer to the Mackenzie particles. The Ca/Al, Mg/Al, and TIC data provide additional evidence that locations 231 and 237 have Canadian influence especially transported by the BG (see chapter 4.1).

#### 4.5.3.2. LGM

There are some clear deviations in sediment provenance from the LGM to today (Abb. 18, 20). Most of the LGM samples have lower  $^{87}Sr/^{86}Sr$  values and lower  $\epsilon_{Nd}$  values.

Core 201 has a smaller contribution from Svalbard. During the LGM, Svalbard was covered by the Svalbard-Barents Sea Ice Sheet (Landvik et al., 1998;

Svendsen et al, 2004), which, together with a lower sea level, limited sediment transport to the Arctic Ocean.

Higher  $\epsilon_{Nd}$  values and lower  $^{87}Sr/^{86}Sr$  in core 206 from the Gakkel Ridge may be explained by increased influence of basalts from this spreading ridge. Mühe et al. (1997) found  $\epsilon_{Nd}$  values of +7 for glasses from the Gakkel Ridge. This influence could have been higher during the LGM, when the external hydrological material input to the Arctic Ocean was smaller. Another possibility for higher  $\epsilon_{Nd}$  values is an increased influence of volcanic material. Volcanic contribution from circum-Arctic sources should have  $\epsilon_{Nd}$  values higher than -1.4 (Fagel et al., 2014 and references therein). However, the influence of basalts seems more likely because volcanic input probably would have influenced other locations as well.

Core 217 from the North Pole may have received more material from the western Arctic than today, because  $\epsilon_{Nd}$  is shifted to lower values, which is indicative for the Mackenzie.

Cores 211, 248, 275, and 277 plot closely together and can be discriminated from the other samples by their low  $\epsilon_{Nd}$  and  $^{87}Sr/^{86}Sr$ . They probably received higher contributions from Siberian basalts compared to today and compared to the other locations. The most probable transport pathway is sediment entrainment on the shelves into drifting pack ice with the TPD (Stokes et al., 2005).

The changes in  $\epsilon_{Nd}$  and  $^{87}Sr/^{86}Sr$  for core 225 from the Makarov Basin are within the measurement uncertainty. Either the transport ways of lithogenic material to this location has not changed since the LGM or varying contributions from different source areas yield the same values.

Cores 231 and 237 from the Canada Basin show a greater influence from particulate material from the Mackenzie and possibly the Canadian Shield during the LGM (Abb. 18). This material was most probably transported with the BG.

## 4.6 Conclusions

The Nd and Sr isotopic composition of the leachable and lithogenic fractions of modern and LGM Arctic Ocean sediments was investigated to document changes in deep water circulation and sediment provenance since the LGM. The modern



deep water in the Eurasian Basin of the Arctic Ocean originates mainly from the North Atlantic and carries a homogenous Nd isotopic signature ( $\epsilon_{Nd} = -11$  to  $-10$ ). The same signature is found in the authigenic fraction of the studied surface sediments ( $\epsilon_{Nd} = -10.6 \pm 0.3$ ; except for one value). We suggest that input from the shelf regions via brine rejection changed the isotopic signature of the deep water during the LGM. Therefore the large-scale deep water currents do not seem to have changed, but were locally influenced by brines. Additionally, the inflow from the Makarov (Canada) Basin to the Amundsen Basin through a Lomonosov Ridge intra-basin was enhanced.

Nd and Sr isotope ratios as well as bulk geochemical data indicate that the lithogenic sediment fraction represents a complex mixture from different source areas (North Greenland, Arctic Archipelago, Mackenzie area, Canadian Shield, Svalbard, as well as Eurasian sources like the Putorana basalts or the Okhotsk-Chukotka volcanic belt). The separation of the Arctic Ocean into the Amerasian and Eurasian Basins is clearly found in the isotopic signatures of the lithogenic sediment fraction. Cores located in the Amerasian Basin have higher  $^{87}\text{Sr}/^{86}\text{Sr}$  values and lower  $\epsilon_{Nd}$  indicating influence from the Mackenzie whereas cores from the Eurasian Basin have lower  $^{87}\text{Sr}/^{86}\text{Sr}$  values and higher  $\epsilon_{Nd}$  indicative of Siberian basalts. Additionally, higher contents of Ca, Mg, and TIC, indicative for the occurrence of dolomite from the Arctic Archipelago, and higher Mn/Al values, possible indicators for enhanced riverine input from the Mackenzie area, can be found in samples from the Amerasian Basin. Most of the lithogenic LGM samples have lower  $\epsilon_{Nd}$  and  $^{87}\text{Sr}/^{86}\text{Sr}$  values than the recent samples and a less homogenous provenance signature, suggesting enhanced local input. We propose that due to lower sea level and exposed shelves, the transport pathways of lithogenic material to the Arctic Ocean were shorter, creating a strong heterogeneity in Nd and Sr isotope signatures across the Arctic basins. This diverse  $\epsilon_{Nd}$  and  $^{87}\text{Sr}/^{86}\text{Sr}$  distribution became more uniform after the LGM as a result of retreating ice cover, enhanced hydrological and particle flux and deep water mixing. To further discriminate sources, studies of REE patterns of the lithogenic sediment fraction after leaching may give additional information.

## 4.7 Acknowledgements

The authors would like to thank the master, crew, and shipboard scientists onboard R/V *Polarstern* during the ARK-XXVI/3 expedition, M. Schulz, E. Gründken, and C. Lehnert for substantial analytical assistance, and C. März for helpful comments. This study was supported by the German Research Foundation (DFG grant, BR 775/27-1) within the IODP SPP, which is gratefully acknowledged.

## 5. Diagenetic regimes in Arctic Ocean sediments: Implications for sediment geochemistry and core correlation

A.-K. Meinhardt<sup>a\*</sup>, C. März<sup>b</sup>, S. Schuth<sup>c</sup>, K. A. Lettmann<sup>a</sup>, B. Schnetger<sup>a</sup>, J.-O. Wolff<sup>a</sup>, H.-J. Brumsack<sup>a</sup>

<sup>a</sup> Institut für Chemie und Biologie des Meeres (ICBM), Carl von Ossietzky Universität Oldenburg, 26111 Oldenburg, Germany (\* corresponding author: ann.k.meinhardt@uni-oldenburg.de, +49-441-798-2534)

<sup>b</sup> School of Civil Engineering and Geosciences, Newcastle University, NE1 7RU Newcastle upon Tyne, United Kingdom

<sup>c</sup> Institut für Mineralogie, Leibniz Universität Hannover, 30167 Hannover, Germany

Dieses Kapitel wurde eingereicht bei: *Geochimica et Cosmochimica Acta*.

### 5.1 Abstract

Dark brown sediment layers are a potential stratigraphic tool in Quaternary Arctic Ocean sediments. They are rich in Mn, Fe, and trace metals scavenged from the water column and were most likely deposited during interglacial intervals. In this study, we combine sediment and pore water data from sediment cores taken in different parts of the Arctic Ocean to investigate the influence of early diagenetic processes on sediment geochemistry. In most studied cores, Mn, Co, and Mo are released into the pore waters from Mn oxide dissolution in deeper (>1.5 m) sediment layers. The relationships between sedimentary Mn, Co, and Mo contents in excess of the lithogenic background ( $\text{element}_{\text{XS}}$ ) show that  $\text{Co}_{\text{XS}}/\text{Mo}_{\text{XS}}$  values are a diagnostic tool to distinguish between layers with diagenetic metal addition from the pore waters, and layers affected by Mn oxide dissolution and metal release. Steady-state calculations based on current pore water profiles reveal that in the studied cores, the diagenetic addition of these metals from the pore water pool alone is not sufficient to produce the sedimentary metal enrichments. A primary Mn- and Fe-rich layer must have been present before.

However, it is evident that dissolution of Mn oxides in the Mn reduction zone can permanently alter the primary geochemical signature of the dark brown layers. Therefore only layers above the topmost Mn reduction zone should be used for core correlation. In contrast to the mostly non-lithogenic origin of Mn in the dark brown layers, sedimentary Fe consists of a large lithogenic (80%) and a small non-lithogenic fraction (20%). Our pore water data show that diagenetic Fe remobilization within the sediment can largely be excluded. The dominant Fe sources are coastal erosion and river input. Budget calculations show that Fe seems to be trapped in the modern Arctic Ocean and accumulates in shelf and basin sediments.

The Fe isotopic signal  $\delta^{56}\text{Fe}$  is positive ( $\sim 0.2$  to  $0.3\text{‰}$ ) in samples defined as the lithogenic background without significant Fe enrichments. With increasing non-lithogenic Fe contents in the sediment,  $\delta^{56}\text{Fe}$  becomes more negative, which indicates a shelf-to-basin export of an isotopically lighter Fe fraction. We assume that the same transport process is true for Mn.

## 5.1 Introduction

The Arctic Ocean plays an important role for the global climate because it governs deep water formation in the North Atlantic and therefore the global overturning circulation (Aagaard et al., 1985). As the Arctic Ocean is very sensitive to climate change, research into the impacts of current global warming, sea ice melting and sea level rise has been intensified over the last decades (e.g., Lambeck et al., 2002; Anisimov et al., 2007). Sedimentary records are valuable archives of information about different climate conditions in the past, and the response of the Arctic Ocean to these changes. Hence, extraction of this information can provide unique insights into the past, and possibly future effects of changing environmental conditions in this highly sensitive environment. An important requirement for such studies is the establishment of an accurate age model for the sediments, which is an omnipresent problem in the Arctic environment (Alexanderson et al., 2014). The use of several conventional dating techniques in the Arctic (e.g.,  $^{14}\text{C}$  dating,  $\delta^{18}\text{O}$  stratigraphy) is hindered by low

organic matter contents in the basin sediments, poor preservation of calcareous tests, and problematic correlations of Arctic to lower latitude oxygen isotope records due to the changing fresh water contribution from Arctic rivers (Backman et al., 2004; Spielhagen et al., 2004). An alternative potential stratigraphic tool for core correlation in Quaternary Arctic sediments are widespread, cyclically occurring dark brown Mn-rich sediment layers. They seem to have formed during interglacial intervals by enhanced Mn input (Jakobsson et al., 2000; März et al., 2011; Meinhardt et al., 2014; recent review by Löwemark et al., 2014). In oxic waters Mn particles in the form of (oxyhydr)oxides are often associated with Fe (oxyhydr)oxides and during settling to the sea floor, these Mn- and Fe-rich particulates scavenge trace metals from the water column, creating parallel sedimentary enrichments in, e.g., Co, Mo, and Ni (Goldberg, 1954; März et al., 2011; 2012; Meinhardt et al., 2014). The dark brown layers may be used for core correlation if they were deposited synchronously across the whole Arctic Ocean during interglacials (Löwemark et al., 2012, 2014). However, this stratigraphic use of the brown layers is only justified when significant diagenetic modification can be excluded. Dissolution and re-precipitation of Mn or Fe (oxyhydr)oxides and other sediment components after deposition have the potential to erase primary Mn layers completely, and form new Mn layers at the redox boundary in the sediment (e.g., Li et al., 1969; Burdige, 1993; Macdonald and Gobeil, 2012). These processes may disrupt the climatically forced sequence of Mn enrichments, and therefore prevent their use for stratigraphic purposes (Sundby et al., 2015).

In addition to these marked Mn enrichments, another prominent feature of Arctic Ocean sediments is the enrichment of Fe relative to average shale in different sediment layers. In sediment cores from the Mendeleev Ridge, many dark brown Mn-rich layers have elevated Fe contents as well, although the variations in Fe contents are less pronounced (März et al., 2011, 2012; Meinhardt et al., 2014). Especially in the surface sediments on the Mendeleev Ridge, Fe contents in excess of the lithogenic background ( $Fe_{xs}$ ) are on the same order of magnitude as  $Mn_{xs}$  contents (Meinhardt et al., 2014). However, despite significant progress in our understanding of Arctic Mn-, Fe-, and trace metal-rich layers, a more systematic investigation of these particular geochemical features is still missing. In this study, we combine solid phase and pore water data of sediment cores from

different parts of the Arctic Ocean to determine which elements are currently influenced by dissolution/precipitation processes, and to what extent the location and composition of dark brown layers is modified by diagenesis. Analyses of Fe isotope ratios in selected sediment layers enables a further discussion of potential sources of the Fe enrichments in Arctic Ocean sediments. We also evaluate if diagenetic processes influence the sedimentary Fe and Mn records in the same way.

## 5.2 Material and methods

During R/V *Polarstern* expeditions ARK-XXIII/3 in 2008 and ARK-XXVI/3 in 2011 (Jokat, 2009; Schauer, 2012), five gravity corer (GC) and eight multicorer (MUC) cores were collected (Abb. 21, Tab. 5). Shortly after core recovery, the GC cores were cut into 1 m segments. Pore water sampling was performed immediately with rhizons (polymer filter with 0.1  $\mu\text{m}$  pore size, Rhizosphere; Seeberg-Elverfeldt et al., 2005) at 4°C. Every 20 cm, holes were drilled into the liners of the GC cores.

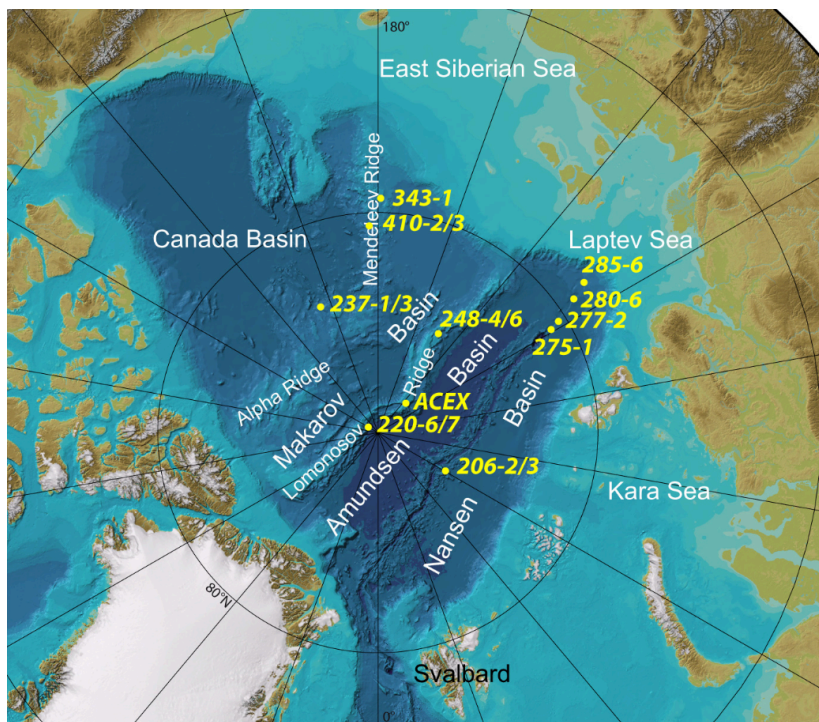


Abb. 21: Map of the core locations.

Tab. 5: Core locations,  $\delta^{56}\text{Fe}$  values, Fe/Al, and ratios of lithogenic and non-lithogenic Fe. Stars mark cores without  $\delta^{56}\text{Fe}$  measurement.

Sample	Latitude	Longitude	Water depth (m)	Depth in core (cm)	$\delta^{56}\text{Fe}$ (‰)	$\pm 2\text{sd}$	Fe/Al	Fe <sub>Lith</sub> /Fe <sub>NL</sub>
PS78/206-2 MUC	86° 26,43' N	60° 5,75' E	1770	0-1	0,109	0,031	0,51	31,9
PS78/206-3 GC	86° 26,55' N	60° 9,27' E	1791	41-42	0,082	0,026	0,46	2,1
PS78/206-3 GC				49-50	-0,220	0,019	0,85	0,6
PS78/206-3 GC				141-142	0,167	0,029	0,32	46,5
PS78/206-3 GC				251-252	0,160	0,034	0,66	0,9
PS78/237-1 MUC	83° 44,65' N	154° 24,88' W	2378	1-2	0,052	0,034	0,57	4,2
PS78/237-3 GC	83° 44,85' N	154° 25,64' W	2369	15-16	0,119	0,013	0,52	3,8
PS78/237-3 GC				25-26	0,059	0,019	0,60	3,7
PS78/237-3 GC				37-38	0,104	0,031	0,58	4,4
PS78/237-3 GC				46-47	0,085	0,01	0,58	4,6
PS78/248-4 MUC	84° 40,75' N	149° 59,41' E	1611	0-1	0,030	0,009	0,64	6,0
PS78/248-6 GC	84° 40,37' N	149° 47,79' E	1620	44-45	0,034	0,047	0,61	1,5
PS78/248-6 GC				120-121	0,235	0,039	0,38	26,9
PS78/248-6 GC				463-464	-0,072	0,033	0,86	0,8
PS78/248-6 GC				481-482	0,274	0,011	0,37	124,9
PS78/275-1 MUC	80° 49,13' N	120° 58,26' E	3527	0-1	-0,006	0,022	0,62	8,4
PS78/277-2 MUC	80° 12,54' N	122° 12,20' E	3359	0-1	0,035	0,034	0,63	8,8
PS78/280-6 MUC	79° 8,97' N	124° 2,11' E	3077	0-1	0,069	0,006	0,58	5,4
PS78/285-6 MUC	78° 29,97' N	125° 42,94' E	2805	0-1	-0,057	0,074	0,67	6,4
PS72/410-2 MUC	80° 31,04' N	175° 44,07' W	1828	0-1	0,083	0,03	0,59	4,5
PS72/410-2 MUC				11-12	0,074	0,075	0,57	5,6
PS72/410-3 GC	80° 31,39' N	175° 43,18' W	1854	18-19	0,014	0,023	0,60	4,1
PS72/410-3 GC				34-35	0,103	0,026	0,50	68,9
PS72/410-3 GC				38-39	0,059	0,032	0,59	4,6
PS72/410-3 GC				55-56	0,052	0,031	0,53	only Lith
PS72/410-3 GC				64-65	0,032	0,039	0,60	9,8
PS78/220-7 GC*	89° 14,86' N	115° 11,34' W	1668					
PS72/343-1 GC*	77° 18,3' N	179° 3,00' E	1227					

The rhizons were stuck into the holes, syringes were attached and vacuum was applied with the help of a spacer. Pore water sampling of the MUC cores was performed in the same way on pre-drilled holes of the MUC tube (1-5 cm intervals). Variable amounts of pore water were retrieved (~5-10 ml) and stored in PP tubes. For later analyses the pore water was acidified with distilled HNO<sub>3</sub> to a pH of <2. Sediment samples were taken with plastic spatula at a resolution of 1-5 cm and stored in plastic bags at 4°C. Sediments from all MUC cores and one GC core (248-6) were taken on board. For later on-shore sampling of GC cores 206-3, 220-

7, and 237-3, plastic U-channels were used. After freeze-drying at the University of Oldenburg, the samples were finely ground (< 0.125 mm) in an agate ball mill for further analyses. Analysis of pore water ammonia was performed on board with the untreated pore water via photometry using a microtiter plate reader (Spectra Tecan; modified protocol based on Benesch and Mangelsdorf, 1972). Nitrate was analyzed on shore with a microtiter plate reader as well (Multiskan Go, Thermo Scientific; Schnetger and Lehnert, 2014). Dissolved Mn ( $Mn_{diss}$ ) and S (calculated as  $SO_4^{2-}$ ) were analyzed by inductively coupled plasma-optical emission spectrometry (ICP-OES, Thermo-Fisher iCAP 6000). Dissolved Co, Fe, and Mo ( $Co_{diss}$ ,  $Fe_{diss}$ ,  $Mo_{diss}$ ) were analyzed in medium resolution (4500) by ICP-mass spectrometry (Element 2, Thermo-Finnigan) with Lu and Y as internal standards. Sediment analyses of Al, Co, Fe, Mn, Mo, and Ni were performed by wavelength-dispersive X-ray fluorescence (XRF, Philips PW 2400) on fused borate glass beads (detailed method in data repository of Eckert et al., 2013). For ICP-OES analyses, accuracy and precision were determined with the standard NASS-5 ( $n = 7$ ) and Mn-spiked Atlantic Sea Water ( $n = 23$ ), and were <5%. For ICP-MS analyses, accuracy and precision were monitored with the standard CASS-5 ( $n = 10$ ) and were <8% for Fe, Co, and Mo. Precision of Fe measurements was higher than 10%, likely due to sample concentrations close to the detection limit. Several in-house standards (CAST, ICBM-B, Loess, PS-S, Peru) were used to determine accuracy and precision for XRF measurements, which were <4% for major elements and <9% for trace elements.

The water content of each sample, determined as the difference between wet and freeze-dried sediment weight, was used to calculate the content of each sea salt constituent. All data were then salt-corrected to eliminate dilution effects resulting from sea salt enclosed in interstitial waters. Element contents are displayed in weight-% for major elements or ppm ( $\mu\text{g/g}$ ) for trace elements, and are normalized to Al (according to Meinhardt et al., 2014). Average shale (AS; Wedepohl, 1971, 1991), which represents the mean composition of weathered upper continental crust, was used as a reference value.

For later calculations, excess contents were calculated according to Brumsack (2006):

$$\text{element}_{xs} = \text{element}_{\text{sample}} - Al_{\text{sample}} \cdot (\text{element}/Al)_{\text{min}} \quad (7)$$



where  $(\text{element}/\text{Al})_{\min}$  displays the lowest ratio in the respective core to compare the authigenic enrichments of certain elements relative to the local terrigenous input.

For analyses of Fe isotope ratios, ~100 mg of each sample were dissolved in a mixture of 1.5 ml distilled conc. HNO<sub>3</sub> and 7.5 ml conc. HF (Merck® Suprapure) in PFA vessels heated in a microwave (CEM Mars 5 Express; operated at 1200 W, 190°C, for 2 h). The clear solutions were transferred into Savillex® beakers and evaporated at ~100°C. To remove potential fluoride compounds, the samples were treated subsequently step-wise with distilled hot conc. HNO<sub>3</sub>, aqua regia, and 6 M HCl overnight. Separation of Fe employed 1.8 ml AG1 X8 anion resin (100-200 mesh; Bio-Rad®) loaded into columns made of polypropylene (Bio-Rad®). Iron was separated quantitatively after a slightly modified protocol from Dauphas et al. (2009) by using 3 M HNO<sub>3</sub> instead of 0.4 M HCl for resin cleaning prior to column separation. The procedure was repeated to obtain a pure Fe fraction (see Mansfeldt et al., 2012). Concentrated distilled HNO<sub>3</sub> and H<sub>2</sub>O<sub>2</sub> (30%, Merck® Suprapure) were added to remove potential organic compounds leached from the resin, and dried at 105°C. The dry Fe fraction was dissolved in 1 ml 3 M HNO<sub>3</sub>. Measurements of Fe isotope ratios were carried out via high resolution-multi collector-ICP-MS (Neptune Plus, Thermo-Scientific; see e.g., Weyer and Schwieters, 2003) at the University of Hannover, Germany. The sample solutions were diluted to yield 3% HNO<sub>3</sub> and ~7 ppm Fe. A Ni standard solution (NIST 986, National Institute of Standards and Technology, USA) was added to samples and standards for instrumental mass bias correction as outlined by Oeser et al. (2014). The signal intensity was ~20 V for <sup>56</sup>Fe and ~4 V for <sup>60</sup>Ni. The interference of <sup>54</sup>Cr on <sup>54</sup>Fe was corrected for by measurement of <sup>53</sup>Cr. Analyses followed the standard-sample-standard bracketing protocol.

The results are given in the delta notation:

$$\delta^{56}\text{Fe} (\text{‰}) = \left[ \left( \frac{{}^{56}\text{Fe}}{{}^{54}\text{Fe}}_{\text{sample}} \right) / \left( \frac{{}^{56}\text{Fe}}{{}^{54}\text{Fe}}_{\text{IRMM-14}} \right) \right] \cdot 10^3 \quad (8)$$

relative to the international Fe isotope standard IRMM-14 that was analyzed before and after each sample.

The average reproducibility (2 standard deviation, 2s.d.) of the measurements was  $\pm 0.05\text{‰}$  for  $\delta^{56}\text{Fe}$ , determined by triplicate analyses of each sample (Tab. 5). The reference materials SDO (Devonian shale) and BCR-2 (basalt), and the in-house standard Fe-ETH (a Fe salt from the ETH Zürich; see, e.g., Kiczka et al., 2011) were used to determine the analytical accuracy of the Fe separation procedure. Results for the SDO ( $\delta^{56}\text{Fe} = 0.024\text{‰}$ , 2s.d. =  $\pm 0.05\text{‰}$ ,  $n = 6$ ), the BCR-2 ( $\delta^{56}\text{Fe} = 0.107\text{‰}$ , 2s.d. =  $\pm 0.02\text{‰}$ ,  $n = 3$ ), and the Fe-ETH ( $\delta^{56}\text{Fe} = -0.711\text{‰}$ , 2s.d. =  $\pm 0.06$ ,  $n = 6$ ) are in excellent agreement with reference values of 0.008-0.036‰ for SDO, 0.022-0.098‰ for BCR-2 (GeoRem references), and -0.71‰ for Fe-ETH (e.g., Kiczka et al., 2011; Fehr et al., 2008).

## 5.3 Results and Discussion

### 5.3.1 Preliminary stratigraphy

An age model for the studied sediment cores has not been published so far, but there are prominent sediment features that may serve as stratigraphic marker horizons. Here we refer to distinct, wide-spread dark gray sediment layers which occur in different parts of the Arctic Ocean (Jakobsson et al., 2000; Löwemark et al., 2014). They are mostly centimeters to meters thick and interpreted as diamicts synchronously deposited by either freshwater discharges from Eurasian ice-dammed lakes (Spielhagen et al., 2004) or the release of large quantities of icebergs from the extended Barents-Kara ice sheet (Jakobsson et al., 2014). Two distinct gray diamicts have been identified in the upper meters of several sediment cores from the Lomonosov Ridge (Abb. 22). They are characterized by generally lower Mn concentrations and elevated total organic carbon (TOC) concentrations. However, these characteristics may vary within the diamicts (Löwemark et al., 2014). The first gray layer was usually found at ~100-200 cm depth and was attributed to Marine Isotope Stage (MIS) 4/3 (Jakobsson et al., 2001; Löwemark et al., 2012). The second gray layer was typically located at ~250-400 cm depth and attributed to MIS 6 (Löwemark et al., 2012; 2014). In core 248-6 from the Lomonosov Ridge, two distinct dark gray sediment layers are located at ~220 cm

and ~480 cm depth, and we tentatively assign them to MIS 4/3 and MIS 6, respectively (Abb. 22). There are some other layers in the sediment core with mixed grayish/brownish color, but for our age correlation we only refer to distinct very dark gray layers of more than 1 cm thickness.

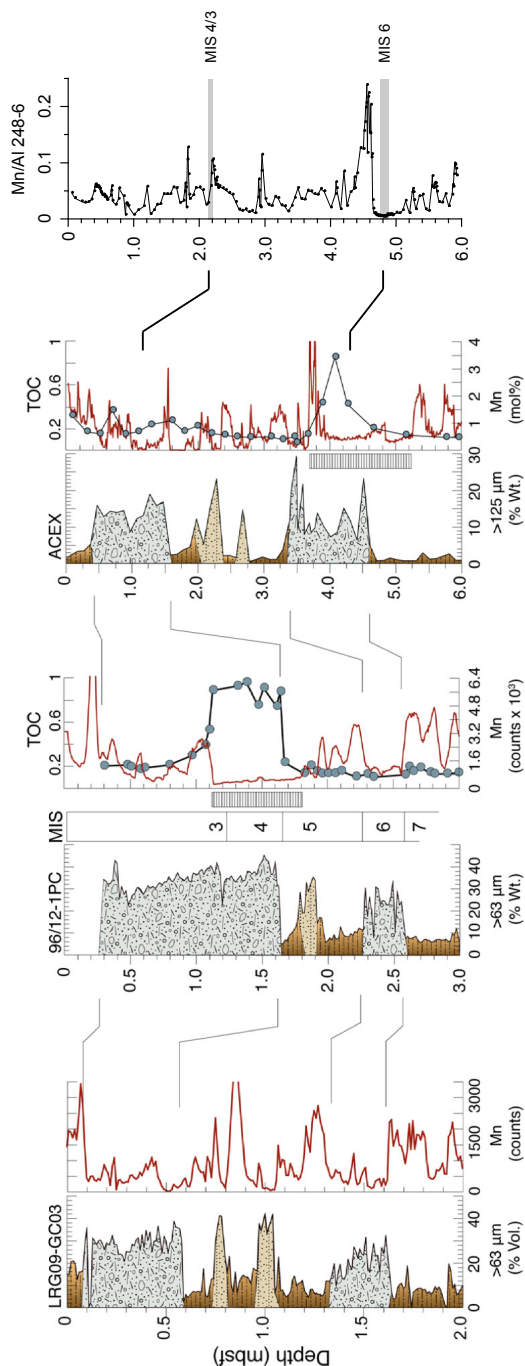


Abb. 22: Stratigraphic correlation of core 248-6 to three sediment cores (LRG09-GC03; 96/12-1PC; ACEX core) from the central Lomonosov Ridge (from Löwemark et al., 2014). Horizontal gray bars: gray sediment layers in core 248-6. Gray patterned intervals mark coarse-grained diamicts. Stippled vertical gray bar: zone of low Mn abundance in the diamicts.

### 5.3.2. Sedimentary characteristics and potential origin of the Mn enrichment in core 248-6

Core 248-6 is mostly composed of alternating dark brown and olive brown sediment layers. The dark brown layers have elevated ratios of Mn/Al, Fe/Al, Co/Al, Mo/Al, and Ni/Al (Abb. 23).

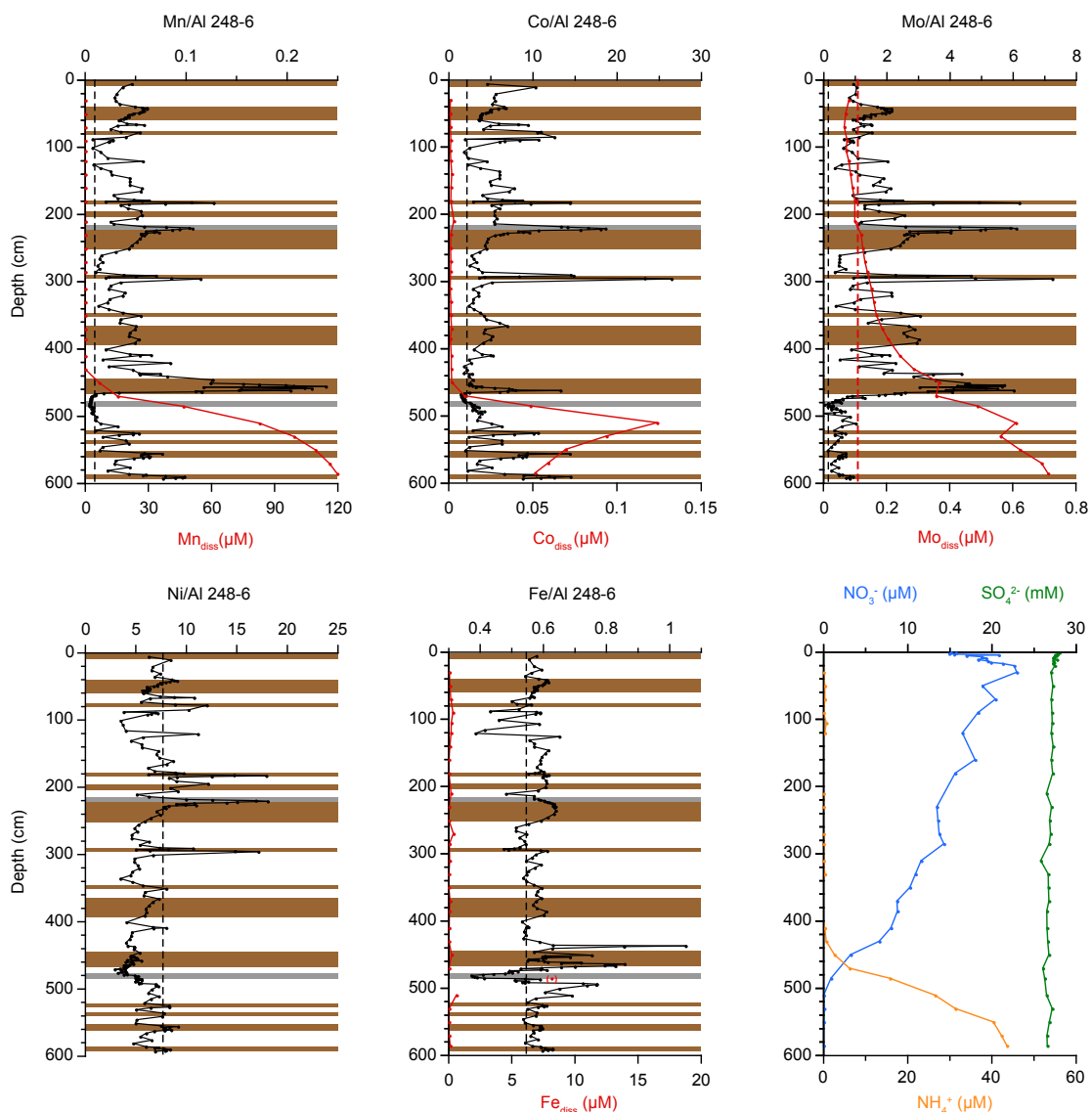


Abb. 23: Sedimentary Mn/Al, Fe/Al, Co/Al, Mo/Al, and Ni/Al values (black) and pore water Mn<sup>2+</sup>, Co<sup>2+</sup>, Mo<sup>6+</sup> (all red), NO<sub>3</sub><sup>-</sup> (blue), SO<sub>4</sub><sup>2-</sup> (green) and NH<sub>4</sub><sup>+</sup> (orange) concentrations in core 248-6. Dashed black line represents average shale (Wedepohl 1971, 1991), dashed red line represents mean Arctic seawater Mo value (Tovar-Sánchez et al., 2010), gray bars represent gray sediment layers, brown bars represent dark brown sediment layers.

This is in accordance with previous geochemical studies in Arctic Ocean sediment cores (März et al., 2011; Meinhardt et al., 2014) and demonstrates scavenging of Mn/Fe (oxyhydr)oxides and associated trace metals from the water column (Goldberg, 1954; Bertine and Turekian, 1973).

Olive brown sediment layers have usually lower ratios of these elements. The dark brown layers are partly enriched in other elements like As, Cu, and V (not shown), but in this study we will focus on the selected elements above. Background ratios for Mn/Al, Fe/Al, Co/Al, and Mo/Al are comparable to average shale (Wedepohl 1971; 1991) whereas Ni/Al background ratios of ~4 are lower than the average shale ratio of 7.7.

Coastal erosion and river input are considered to be the two dominant sources for non-lithogenic Mn to the open Arctic Ocean today (Macdonald and Gobeil, 2012), with an intermittent diagenetic shuttling mechanism across the shelves (Löwemark et al., 2014). The lithogenic component,  $Mn_{Lith}$ , represents Mn that is incorporated into the mineral matrix and does not participate in redox reactions. The non-lithogenic component,  $Mn_{NL}$ , may be mobilized by redox reactions either within sediments of the continental shelf or within sediments in the deep ocean. This fraction is of interest in terms of possible diagenetic modification in the sediment. It is currently unknown if these present-day Mn inputs for the Arctic Ocean were different in the geological past, or if the values by Macdonald and Gobeil (2012) can be applied to calculate past Arctic Mn budgets as well. We will approach this question by calculating the cumulative excess Mn in the open marine core 248-6 from the sediment surface to 480 cm depth (dark gray layer tentatively attributed to MIS 6 in Abb. 22, with an age of ~135,000 years) and compare it with the amount that could have been derived exclusively from river input, coastal erosion, and additional sources like hydrothermal or eolian input. We first calculate the Mn accumulation rate in the sediment core ( $ar_{Mn248}$ ), and then compare this rate with the modern Mn input rate via coastal erosion and rivers given, as determined by Macdonald and Gobeil (2012). A detailed calculation and the used parameters can be found in the Appendix and Tab. 6. The resulting average Mn accumulation rate in core 248-6 over the last 135,000 years (0 to 480 cm sediment depth) is  $ar_{Mn248} = 1.6 \cdot 10^{-5} \text{ g cm}^{-2} \text{ a}^{-1}$ .

Tab. 6: Sedimentary  $Mn_{xs}$  and  $Fe_{xs}$  calculations for five different sediment cores.

	248-6	206-3	220-7	343-1	ACEX
mean $Mn_{xs}$ ( $g \cdot kg^{-1}$ )	4135	1000	820	2630	1940
sedimentation rate ( $cm \cdot a^{-1}$ )	0.0036	0.0018	0.0010	0.0042	0.0024
Mn accumulation rate ( $g \cdot cm^{-2} \cdot a^{-1}$ )	$1.69 \cdot 10^{-5}$	$2.11 \cdot 10^{-6}$	$9.08 \cdot 10^{-7}$	$1.26 \cdot 10^{-5}$	$5.40 \cdot 10^{-6}$
Mn from external sources (rel-%)	48	>100	>100	65	>100
mean $Fe_{xs}$ ( $mg \cdot kg^{-1}$ )	18757	12520	33010	10000	23210
Fe accumulation rate ( $g \cdot cm^{-2} \cdot a^{-1}$ )	$7.67 \cdot 10^{-5}$	$2.64 \cdot 10^{-5}$	$3.66 \cdot 10^{-5}$	$4.79 \cdot 10^{-5}$	$6.46 \cdot 10^{-5}$
Fe from external sources (rel-%)	>100	>100	>100	>100	>100

The terrigenous background composition of the sediment may vary, and the definition of the lowest Mn/Al value in the core as a background implies that the calculated  $ar_{Mn248}$  represents a maximum estimate. However, our background Mn concentration of 0.028% is close to the lithogenic background value of 0.032% from Macdonald and Gobeil (2012) for other Arctic Ocean sediment cores.

The total Mn input flux to the Arctic basins and submarine ridges (excluding shelf areas) was calculated with the following parameters: total non-lithogenic Mn from coastal erosion and river input under present conditions:  $334.5 \text{ kt a}^{-1}$  Mn ( $= 3.35 \cdot 10^{11} \text{ g a}^{-1}$ , Macdonald and Gobeil, 2012); area of Arctic Ocean seafloor excluding shelf areas:  $4.5 \cdot 10^{16} \text{ cm}^2$  (Jakobsson et al., 2003). The Mn accumulation for the Arctic basins and submarine ridges under current input conditions gives therefore  $ar_{MnInput} = 7.4 \cdot 10^{-6} \text{ g cm}^{-2} \text{ a}^{-1}$ .

This value explains only 46% of the  $ar_{Mn248}$ .

Other non-lithogenic Mn sources to the open Arctic Ocean (hydrothermal input at Gakkel Ridge; atmospheric deposition by rain water; inflow from groundwater, Pacific or Atlantic Oceans) amount to  $32.1 \text{ kt a}^{-1}$  (Edmonds et al., 2003; Middag et al., 2011; Macdonald and Gobeil, 2012), hence delivering another  $7.12 \cdot 10^{-7} \text{ g cm}^{-2} \text{ a}^{-1}$  of non-lithogenic Mn to the deep Arctic Ocean, and accounting for a further ~4% of  $ar_{Mn248}$ . Taken together, all these sources explain only 50% of the cumulative non-lithogenic Mn accumulated at coring site 248-6 over the last 135,000 years. Three different processes may have resulted in this low Mn accumulation.

1) The coastal erosion and river Mn input fluxes determined by Macdonald and Gobeil (2012) for the modern Arctic Ocean were much higher in the past,

especially during deglacial sea level rises when coastal erosion and the hydrological cycle were strongly intensified.

2) The studied core 248-6 is not representative, i.e., it received a significantly higher input of non-lithogenic Mn than the “average” Arctic basin and submarine ridge environments. Indeed, in four other cores from different parts of the Arctic Ocean (Lomonosov Ridge, southern Mendeleev Ridge, Gakkel Ridge; Abb. 21, Tab. 6), 65-100% of  $Mn_{xs}$  in sediments younger than MIS 6 can be explained by non-lithogenic input fluxes according to Macdonald and Gobeil (2012). Overall, in three of five selected cores, the modern non-lithogenic Mn input is sufficient to explain cumulative  $Mn_{xs}$  contents over the last ~135,000 years, providing support for the validity of the modern Arctic Mn budget at least for the last glacial cycle.

3) A significant fraction of non-lithogenic Mn in the sediment interval from 0 to 480 cm depth in core 248-6 is derived from deeper sediment layers where it was released during diagenesis. This latter explanation is supported by the pore water profiles (Abb. 23) and specific sediment structures (Abb. 24), as will be discussed in the following chapters.

### 5.3.3 Pore water characteristics and diagenetic trace metal cycling in core 248-6

To assess the contribution of diagenetic processes on sediment geochemistry, the pore water composition can provide valuable information. Microbially mediated redox reactions usually alter the sediment composition after deposition by following the catabolic sequence of electron acceptors during microbial degradation of organic matter:  $O_2$ ,  $NO_3^-$ , Mn (oxyhydr)oxides, Fe (oxyhydr)oxides,  $SO_4^{2-}$  and  $CH_4$  (Froelich et al., 1979). The activation of a specific electron acceptor in a sediment succession depends on its availability, the energy gain of the reaction, and the microbial community present in the sediments. These electron acceptors (e.g.,  $NO_3^-$ ,  $SO_4^{2-}$ ) or their metabolic products (e.g.,  $Mn^{2+}$ ,  $Fe^{2+}$ ,  $NH_4^+$ ) can be detected and analyzed in the pore waters.

Compared to other parts of the global ocean,  $NO_3^-$  pore water measurements from the Arctic Ocean are rare. Hulth et al. (1996) calculated a  $NO_3^-$  penetration

depth of up to 8 cm in marine sediments around Svalbard. Concentrations of  $\text{NO}_3^-$  in pore waters from giant box corer sediments (max. 50 cm depth) from the Kara Sea indicate  $\text{NO}_3^-$  reduction at these depths as well (Damm, 1999). To our knowledge, our data represent the first published deeper  $\text{NO}_3^-$  pore water profiles for the central Arctic Ocean. In core 248-6, the  $\text{NO}_3^-$  concentration is  $\sim 15 \mu\text{M}$  at the core top and has a subsurface maximum at  $\sim 30$  cm (Abb. 23) resulting from  $\text{O}_2$  reduction (Emerson et al., 1980). The  $\text{NO}_3^-$  concentrations reach the detection limit at  $\sim 5$  m depth, following an almost linear concentration gradient down to  $\sim 4$  m depth. The linear gradient indicates that no significant organic matter re-mineralization via nitrate reduction is occurring in the upper  $\sim 4$  m of the sediments at site 248. This is corroborated by the pore water profile of  $\text{NH}_4^+$ , the possible metabolic product of nitrate reduction and suboxic organic matter re-mineralization, which is below detection limit in the upper  $\sim 4$  m of the sediment. Ammonia only starts to increase in core 248-6 below 4 m depth, where the  $\text{NO}_3^-$  profile deviates from its linear gradient, and reaches a maximum of  $44 \mu\text{M}$  at the bottom of the core ( $\sim 6$  m; Abb. 23). Similar to  $\text{NH}_4^+$ , the  $\text{Mn}_{\text{diss}}$  concentration increases downcore from below detection limit at  $\sim 4$  m depth to  $120 \mu\text{M}$  at the bottom of the core, most likely induced by dissimilatory Mn reduction at depth (Froelich et al., 1979). Collectively, the pore water profiles imply that in these Arctic sediments, 1)  $\text{NO}_3^-$  has a very deep sediment penetration depth of  $\sim 5$  m, 2)  $\text{NO}_3^-$  reduction does not contribute significantly to organic matter re-mineralization and  $\text{NH}_4^+$  production, 3) dissimilatory  $\text{Mn}^{\text{IV}}$  reduction below  $\sim 5$  m depth is likely the dominant pathway of organic matter re-mineralization and  $\text{NH}_4^+$  production, and 4) the top of the  $\text{Mn}^{\text{IV}}$  reduction zone is determined by the  $\text{NO}_3^-$  penetration depth.

Regarding diagenetic Mn redistribution within the sediments, it seems evident that a  $\text{Mn}_{\text{diss}}$  sink is located just below 4 m depth in core 248-6 (Abb. 23). The source of  $\text{Mn}_{\text{diss}}$  must be located deeper in the sediment, and was not fully recovered by the GC. At  $\sim 460$  cm, where  $\text{Mn}_{\text{diss}}$  concentrations start to increase, a peak in sedimentary Mn/Al is observed, most likely caused by precipitation of Mn (oxyhydr)oxides at the Mn redox boundary upon contact with nitrate (Lovley and Phillips, 1988; Hulth et al., 1999), as suggested by März et al. (2011). Pore water  $\text{Mn}_{\text{diss}}$  may precipitate at or adsorb on existing (oxyhydr)oxide surfaces (Murray, 1975) or form new authigenic Mn (oxyhydr)oxides (Li et al., 1969; Burdige 1993).



The pore water data prove that the sedimentary Mn peak at 460 cm includes a diagenetic component due to precipitation/adsorption of  $\text{Mn}^{\text{IV}}$  compounds from the pore water  $\text{Mn}_{\text{diss}}$  pool.

Pore water  $\text{Mn}_{\text{diss}}$  increases concomitantly with  $\text{Co}_{\text{diss}}$  and  $\text{Mo}_{\text{diss}}$ , indicating that Co and Mo seem to be diagenetically recycled along with Mn (Abb. 23). The  $\text{Co}_{\text{diss}}$  profile shows a sharp peak, whereas the  $\text{Mo}_{\text{diss}}$  profile increases smoothly from around the Arctic seawater value (Tovar-Sánchez et al., 2010) downcore to higher concentrations. This process of Co and Mo release into pore waters, their vertical migration, and possible adsorption/precipitation further upcore in close association with the diagenetic Mn cycle has already been described in other oxic sedimentary environments (e.g., Knauer et al., 1982; Gendron et al., 1986; Shaw et al., 1990; Morford and Emerson, 1999).

Another indication for diagenetic Mn recycling is the occurrence of very thin, closely spaced layers that appear dark in the core, but white (i.e., with a high density) in the x-ray radiographs of core 248-6 between 430 and 470 cm depth (Abb. 24).

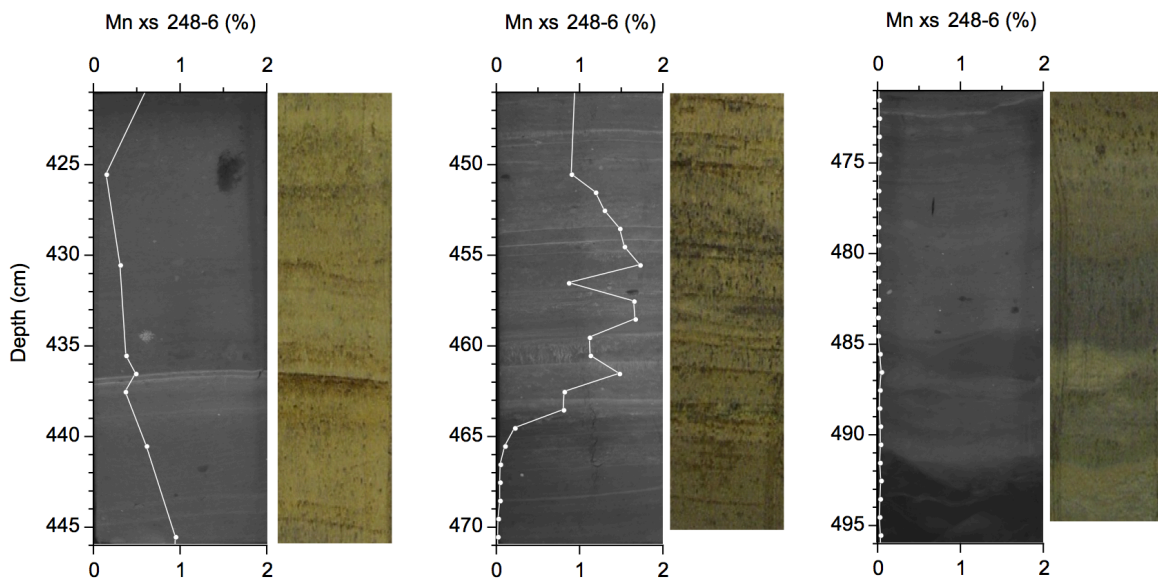


Abb. 24: X-ray radiographs,  $\text{Mn}_{\text{xs}}$  contents, and core photos of core 248-6 (x-ray radiographs and photos: Matthiessen, 2011). Thin white bands in the x-ray radiographs correspond to higher  $\text{Mn}_{\text{xs}}$  contents and dark brown sediment color.

The spacing of discrete XRF samples is too low to resolve these layers individually, but the respective sediment interval is overall enriched in Mn, Co, and Mo, especially above 465 cm (Abb. 23, 24). Some of the dense layers show dendritic, “frosted” structures in the x-ray radiograph (455 and 460 cm, Abb. 24).

This phenomenon has been reported in another sediment core from the Lomonosov Ridge by Löwemark et al. (2012), and is explained to represent purely authigenic Mn precipitates (see also März et al., 2011; Löwemark et al., 2014). Mobilization of  $Mn_{diss}$  from deeper sediment layers and reprecipitation at the Mn redox boundary may form these layers under steady-state conditions, in a depth interval that depends on factors like organic matter availability and sedimentation rate. The proposed dissolution-reprecipitation process is in agreement with our pore water data: Both  $Mn_{diss}$  and  $Co_{diss}$ , which show elevated concentrations near the core bottom, decrease to minimum concentrations in the sediment interval around 460 cm depth, indicating precipitation of these elements within this interval (Abb. 23). Interestingly,  $Mo_{diss}$  needs a much longer diffusion pathway than Mn and Co to reach background concentrations, possibly because the sedimentary Mn surfaces are saturated with Mo. The thin dendritic layers have a dark brown sediment color (Abb. 24), which indicates that they may consist of Mn oxides.

In contrast to Mn, dissolved Fe is mostly below quantitation limit in core 248-6, except for one sample where dissolved Fe is slightly increased (Abb. 23). The concentrations are much lower than for Mn and there is no similar smooth profile. This one value does not necessarily show a recent significant pore water Fe flux that may influence the solid phase Fe distribution, and is therefore considered as an outlier. In the sediment interval below the  $NO_3^-$  reduction zone, the redox potential seems to be sufficiently low for Mn(oxyhydr(oxide) reduction, but still too high for significant Fe(oxyhydr(oxide) reduction.

The  $SO_4^{2-}$  concentration is constant in the core, and consequently a significant sulfate-reduction can be excluded.

Based on pore water and sedimentological patterns in core 248-6, we found that the brown layer at ~445-470 cm depth has experienced, and still is experiencing, diagenetic addition of Mn, Co, and Mo. To further evaluate if these diagenetic additions have impacted the sediment geochemistry in a particular way, we will compare the fractions of the excess contents of Mn, Co, and Mo in this

brown layer with each other. Differences in the behavior of specific trace metals during Mn diagenesis in the Arctic were first reported for sediments from the Mendeleev Ridge by März et al. (2011). They proposed the use of Co/Mo values to distinguish between authigenic and diagenetic Mn layers. Higher Co/Mo in layers indicate diagenetic loss of Mn and Mo from the solid phase, and lower Co/Mo indicate post-depositional addition of Mn and Mo. This is in accordance with the results in Abb. 25a, where  $Co_{xs}/Mo_{xs}$  values of all Mn-enriched layer in core 248-6 are illustrated. The highest ratios of  $\sim 10$  are found in those layers located in the Mn and Mo reduction zone deeper than 500 cm, whereas lowest ratios of  $\sim 1$  are found in the layer at  $\sim 460$  cm depth with diagenetic Mo addition, supporting the findings of März et al. (2011). Samples with  $Co_{xs}/Mo_{xs}$  between 1 and 10 are considered to be primary layers. Considering  $Co_{xs}/Mo_{xs}$  values is therefore a promising tool for the identification of diagenetically overprinted sediment intervals when pore water data are missing.

The use of this proxy is enabled by the different behavior of Co and Mo during diagenesis. In Mn-rich layers Mo and Co are adsorbed to the surface of Mn oxides. During partial dissolution of Mn oxides Mo is preferentially released to the pore water. This is because Co has a high specific adsorption potential to  $MnO_2$  surfaces (Murray, 1975; Murray and Dillard, 1979) and the reduced  $Mn_{diss}$  can partly re-adsorb to the remaining Mn oxides whereas  $Mo_{diss}$  remains in solution (Shimmield and Price, 1986). Therefore Co remains preferentially in the sediment layers, whereas Mo and Mn are released to the pore water. Similar observations were found by März et al., 2011.

5. Diagenetic regimes in Arctic Ocean sediments

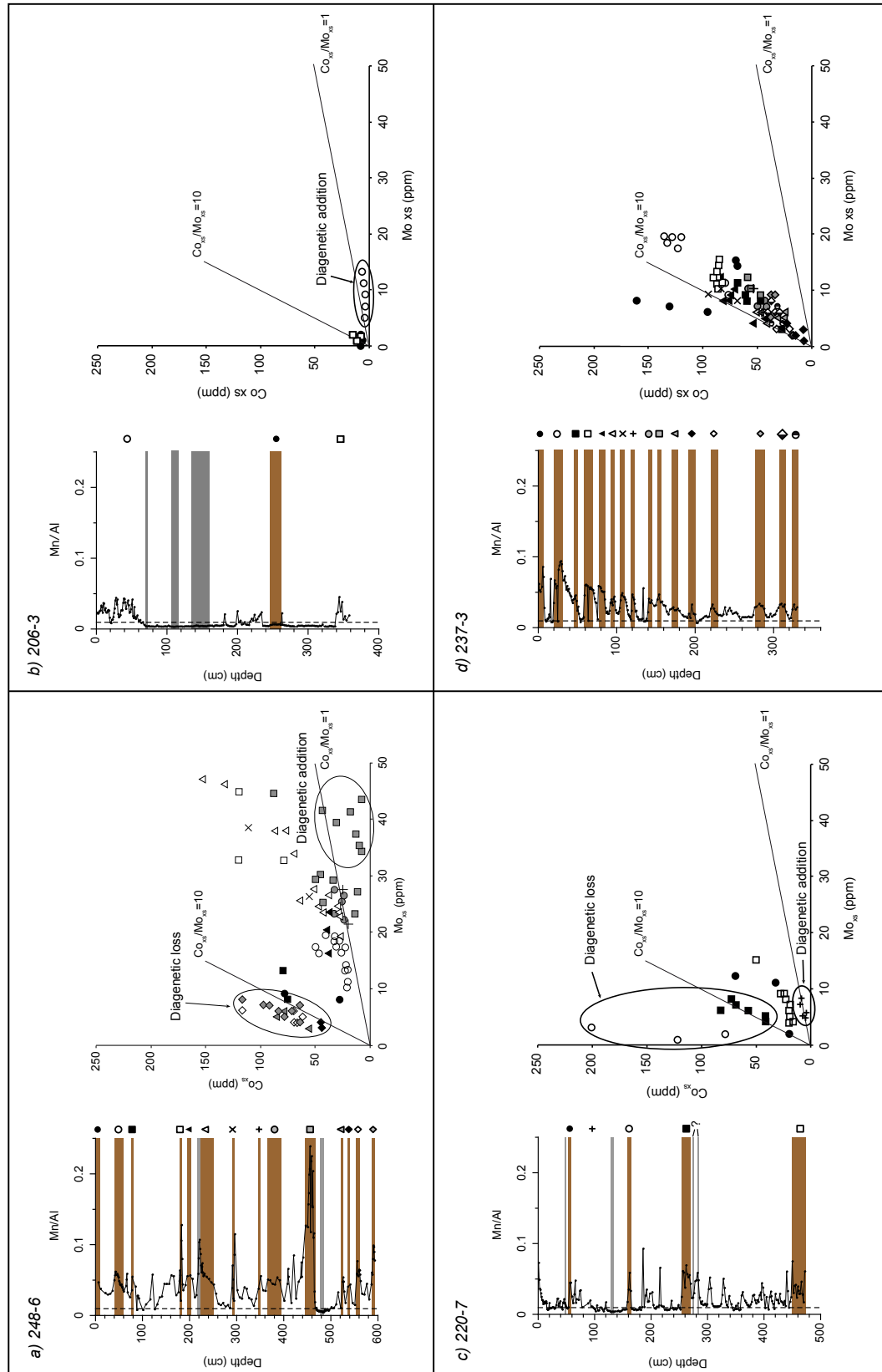


Abb. 25:  $Co_{xs}$  versus  $Mo_{xs}$  relationship of different dark brown sediment layers. a) core 248-6, b) core 206-3, c) core 220-7, d) core 237-3. Layers with diagenetic addition of Mn from the pore water have lower  $Co_{xs}/Mo_{xs}$ . Layers that were subjected to Mn reduction have higher ratios.

### 5.3.4 Pore water flux calculation and Mn<sub>diss</sub> reduction rate for core 248-6

We have previously concluded that at site 248 around 50% of excess Mn accumulated over the past ~135,000 years (0-480 cm sediment depth) cannot be explained by coastal erosion and river input (Macdonald and Gobeil, 2012) and that the brown layer at ~445-470 cm is diagenetically accumulating Mn, Co, and Mo. To constrain if the current pore water fluxes of Mn, Co, and Mo into the brown layer at ~445-470 cm alone could have generated the observed post-depositional element enrichments, we performed simple pore water flux calculations (assuming steady state conditions) based on Fick's first law of diffusion (Schulz, 2006), following an approach by März et al. (2011; 2015):

$$J_{\text{sed}} = -\Phi \cdot D_{\text{sed}} \cdot dC/dx \quad (9)$$

with  $J_{\text{sed}}$  = diffusive pore water flux,  $\Phi$  = sediment porosity,  $D_{\text{sed}}$  = diffusion coefficient, and  $dC/dx$  = concentration gradient.

The detailed calculations and boundary parameters can be found in Tab. 7 and in the Appendix (A1.2). The calculated advective pore water flux is three orders of magnitude lower and can be neglected (Appendix (A1.3)).

For Mn<sub>diss</sub>, the concentration gradient is calculated from the linear part of the pore water profile between 470 and 485 cm, directly below the Mn-rich layer at 445 to 470 cm (Abb. 23). We chose a mean porosity of 0.6 referring to published data from Lomonosov Ridge sediments (Stein et al., 2004). The resulting  $J_{\text{sedMn}}$  is  $-0.59 \cdot 10^{-3} \text{ mol m}^{-2} \text{ a}^{-1}$ .

The sediment layer at ~445-470 cm depth has a tentative age of ~120,000 years (located above the MIS 6 deposit), which is the maximum time that might have been available for diagenetic Mn enrichment.

Assuming that the pore water flux was stable for the last 120,000 years,  $13.5 \text{ g kg}^{-1} \text{ Mn}_{\text{xs}}$  could have been produced by this flux (Appendix (A1.4); Tab. 7).

Tab. 7: Boundary parameters used for the calculation of diffusive fluxes of cores 248-6, 206-3, and 220-7.  $D_{sw}$  for Mn and Co from Boudreau (1997).  $D_{sw}$  for Mo estimated from Li and Gregory (1974). See chapter 5.3.4 and Appendix for details.

Core	element	$\Phi$	$\theta^2$	$D_{sw}^{0^\circ C}$ ( $m^2*s^{-1}$ )	$D_{sed}$ ( $m^2*s^{-1}$ )	gradient ( $mol*m^{-4}$ )	$J_{sed}$ (mol* $m^{-2}*a^{-1}$ )	representative time for flux (ka)	total element <sub>xs</sub> ( $g*kg^{-1}$ )	flux- derived element <sub>xs</sub> ( $g*kg^{-1}$ )	flux- derived element <sub>xs</sub> (rel-%)
248-6	Mn	0.6	2.02	$3.0*10^{-10}$	$1.5*10^{-10}$	$2.1*10^{-1}$	$0.6*10^{-3}$	120	9.1	13.5	149
								12	9.1	1.3	15
	Co	0.6	2.02	$3.2*10^{-10}$	$1.6*10^{-10}$	$2.6*10^{-4}$	$0.8*10^{-6}$	80	0.021	0.013	61
								12	0.021	0.002	9
	Mo	0.6	2.02	$4.0*10^{-10}$	$2.0*10^{-10}$	$8.7*10^{-4}$	$3.3*10^{-6}$	80	0.029	0.087	303
								12	0.029	0.013	45
206-3	Mn	0.6	2.02	$3.0*10^{-10}$	$1.5*10^{-10}$	$2.2*10^{-2}$	$6.2*10^{-5}$				
220-7	Mn	0.6	2.02	$3.0*10^{-10}$	$1.5*10^{-10}$	$5.6*10^{-2}$	$1.6*10^{-4}$				

However, the average  $Mn_{xs}$  content of the respective interval is only  $9.1 \text{ g kg}^{-1}$ , which implies that the current Mn flux into this sediment layer was only established significantly after its deposition. Under steady-state conditions, it would have taken at least  $\sim 80,000$  years to accumulate the measured  $Mn_{xs}$  content (Appendix (A1.5)). Even if the current Mn flux was only established at the onset of the Holocene ( $\sim 12,000$  years BC), it could still have contributed up to  $\sim 15\%$  of the total  $Mn_{xs}$  inventory between 445 and 470 cm depth at site 248-6 (Appendix (A1.6); Tab. 7). Pore water fluxes for Co and Mo were calculated as well, analogous to the calculations for Mn (Tab. 7). Cobalt and Mo pore water fluxes are three orders of magnitude lower than for Mn, which is in accordance with the pore water concentrations of  $Co_{diss}$  and  $Mo_{diss}$ . After 80,000 years at steady-state conditions, the current pore water fluxes of Co and Mo can explain 61% and  $>100\%$  of the sedimentary Co and Mo enrichments in the sediment layer, respectively (Tab. 7). After 12,000 years, still 9% of the Co enrichment and 45% of the Mo enrichment can be explained by the pore water flux. The Co addition from the pore water flux is similar to that of Mn, whereas Mo is marked by an elevated diagenetic addition. These simple steady-state calculations only provide relatively rough estimates of the potential diagenetic Mn (as well as Co and Mo) contribution to a specific brown sediment layer, and more advanced reaction-transport modelling simulating non-steady state conditions would be required to better constrain these numbers. However, our data still confirm earlier and recent studies

of relatively fast diagenetic Mn redistribution in open Arctic Ocean sediments (Sundby et al., 2015). We therefore recommend that Mn layers within the Mn reduction or precipitation zone in Arctic sediments should not be used for correlation purposes, as they will have lost or gained  $Mn_{xs}$  by diagenesis, respectively.

To further constrain rates of  $Mn_{diss}$  release into, and precipitation from, the pore waters at site 248-6, we applied the REC (Rate Estimation from Concentrations) model from Lettmann et al. (2012, Abb. 26).

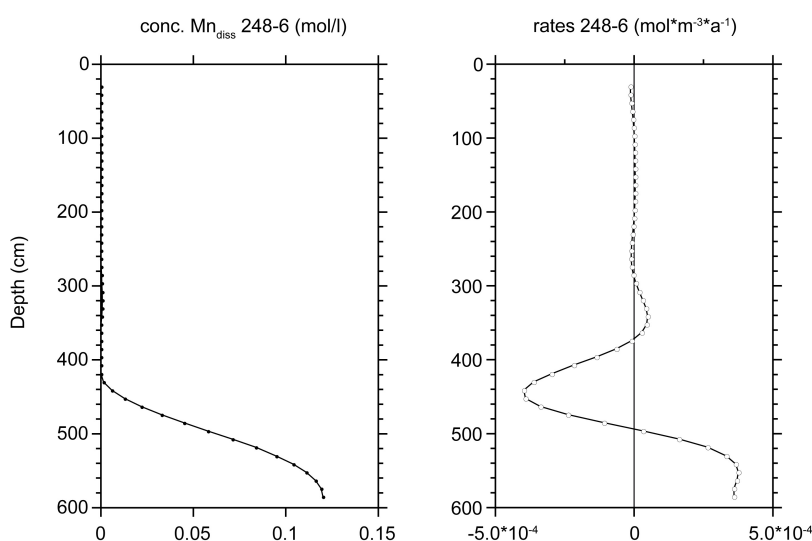


Abb. 26: Net  $Mn^{2+}$  rate of core 248-6 from the REC model (Lettmann et al., 2012). Positive values indicate  $Mn^{2+}$  production and negative values indicate  $Mn^{2+}$  consumption.

For this model, we used the pore water  $Mn_{diss}$  concentrations, porosity  $\Phi$  (estimated from Stein et al., 2004), diffusion coefficient  $D_{sed}$ , and sedimentation rate  $sr$ . The bioturbation coefficient  $D_b$  and the bioirrigation factor were set to zero. In the interval above  $\sim 370$  cm, net rates are around zero, implying neither consumption nor production of  $Mn_{diss}$ . The rate is negative in the interval from  $\sim 370$  to 500 cm, implying consumption of  $Mn_{diss}$ , i.e., precipitation from the pore water. Below 500 cm depth, positive values indicate the production of  $Mn_{diss}$ . This is in agreement with the observation discussed in chapter 5.3.2 that the source of  $Mn_{diss}$  is located at greater depths than the recovered sediment interval. The most negative rate values in the dark brown layer at  $\sim 450$  cm depth are indicative for an

enhanced Mn oxide precipitation in this layer. The integrated  $Mn_{diss}$  reduction rate over the interval from 4 to 5 m was  $-2.64 \cdot 10^{-4} \text{ mol m}^{-2} \text{ a}^{-1}$ . This value is in good agreement with the calculated pore water flux value  $J_{sedMn}$  for the interval from 445 to 470 cm ( $-5.9 \cdot 10^{-4} \text{ mol m}^{-2} \text{ a}^{-1}$ ), supporting our hypothesis of Mn diagenesis at coring site 248-6.

### 5.3.5 Diagenetic conditions and their diagnostic parameters in sediment cores from different parts of the central Arctic Ocean

Having studied and discussed core 248-6 from the Lomonosov Ridge in detail, we will now compare diagenetic conditions and processes at this site with other parts of the Arctic Ocean, including the Gakkel Ridge (core 206-3), the Lomonosov Ridge near the North Pole (core 220-7), the Canada Basin (core 237-3), and the southern Mendeleev Ridge (core 343-1).

Core 206-3 from the Gakkel Ridge has only one dark brown sediment layer at ~250 cm depth and three dark gray sediment layers (Abb. 27). The element ratios of Mn/Al, Co/Al, and Mo/Al are mostly around average shale with only slight enrichments, while Ni/Al values are lower (~5) than average shale (7.7). In contrast to core 248-6, the dark brown layer in core 206-3 is not enriched in Mn, Co, Mo, or Ni. The color may therefore rather result from higher Fe oxide contents, as indicated by higher Fe/Al (Abb. 27).

Pore water characteristics are similar to core 248-6, with  $NO_3^-$  decreasing from the sediment-water interface to ~1 m depth, only very slightly decreasing  $SO_4^{2-}$  concentrations, and broad maxima in  $Mn_{diss}$  and  $Co_{diss}$  (Abb. 27). The Mn redox boundary (~1 m) is located closer to the sediment/water interface compared to core 248-6 (~4.5 m), and again seems to be related to the  $NO_3^-$  penetration depth. Both the sediment interval at ~350 cm depth without brown coloration and the brown layer at ~250 cm depth have elevated  $Co_{xs}/Mo_{xs}$ , indicating loss of Mn (Abb. 25b). As the pore water  $Mn_{diss}$  starts to increase at ~350 cm depth and Mn/Al is elevated here (Abb. 27), this interval seems to be the source for dissolved Mn. In contrast, the Mn-rich interval from 38 to 45 cm, where the pore water gradient ends, has lower  $Co_{xs}/Mo_{xs}$ , comparable to the diagenetically influenced dark brown



layer at 460 cm in core 248-6 (Abb. 25a). This indicates that despite the lack of dark brown coloration, diagenetic Mn and Mo addition from the pore waters likely influenced this Mn- and Mo-rich interval in core 206-3. Interestingly, pore water data (Abb. 27) show no current flux of  $\text{Mo}_{\text{diss}}$  into this sediment layer, so it can be assumed that the precipitation of remobilized  $\text{Mo}_{\text{diss}}$  at this site has occurred in the past.

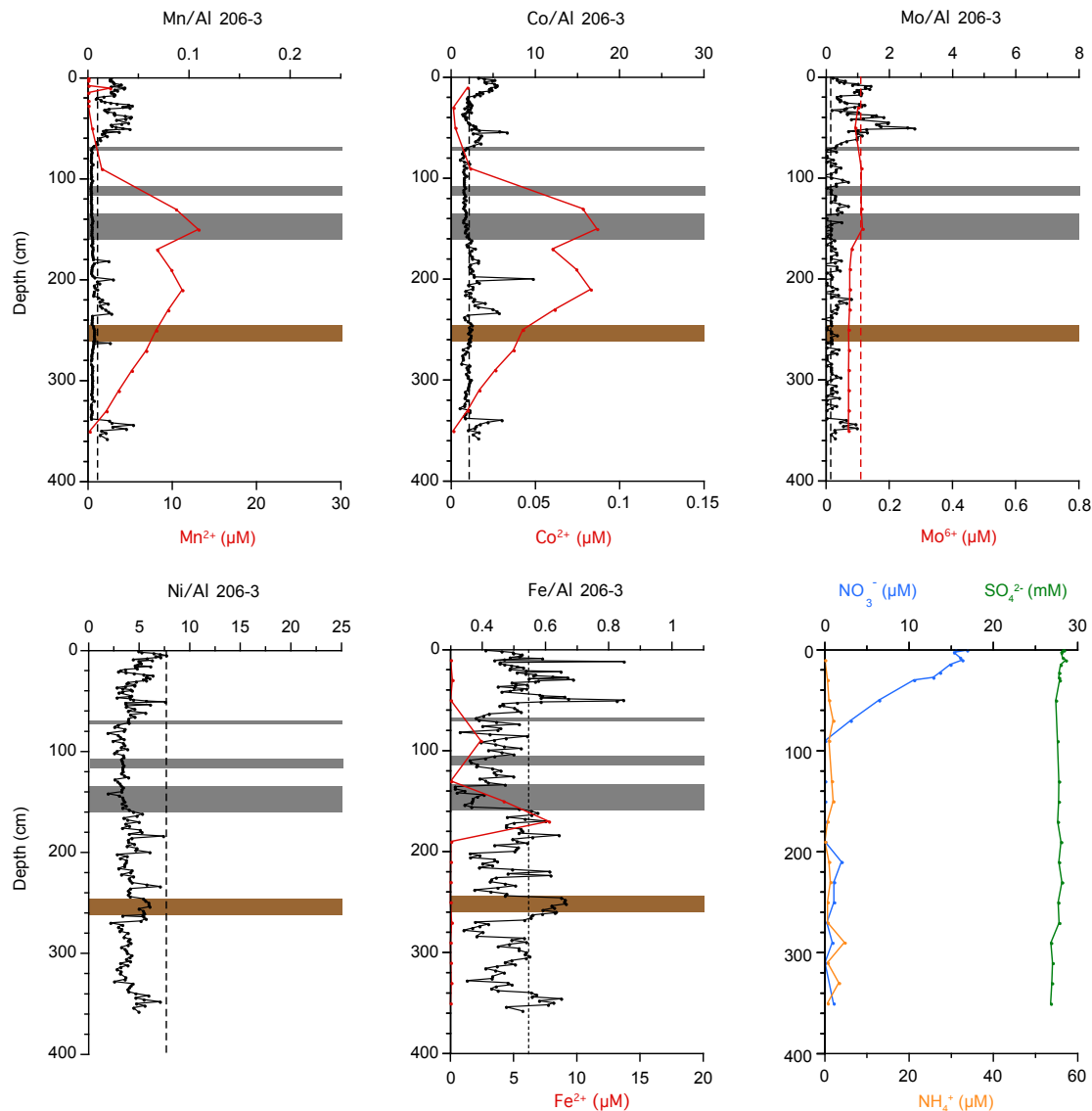


Abb. 27: Sedimentary Mn/Al, Fe/Al, Co/Al, Mo/Al, and Ni/Al values (black) and pore water  $\text{Mn}^{2+}$ ,  $\text{Co}^{2+}$ ,  $\text{Mo}^{6+}$  (all red),  $\text{NO}_3^-$  (blue),  $\text{SO}_4^{2-}$  (green) and  $\text{NH}_4^+$  (orange) concentrations in core 206-3. For additional information see Abb. 23.

Pore water concentrations of  $\text{Co}_{\text{diss}}$  in core 206-3 are comparable to core 248-6, but  $\text{Mn}_{\text{diss}}$  concentrations are ten times lower, and  $\text{Mo}_{\text{diss}}$  concentrations range

around the seawater value without any indication of  $\text{Mo}_{\text{diss}}$  release into the pore waters. Overall, Mn and Mo remobilization seem to be less pronounced in this core. This may be due to the fact that sedimentary Mn (oxyhydr)oxide contents are lower as well, implying that the sparse availability of  $\text{Mn}^{\text{IV}}$  as an electron acceptor in combination with low organic matter contents limits the degree of Mn diagenesis. There is no systematic increase in pore water  $\text{Fe}_{\text{diss}}$  concentration in this core, indicating no significant diagenetic  $\text{Fe}^{\text{III}}$  reduction either.

Core 220-7 from the Lomonosov Ridge near the North Pole has four dark brown sediment layers enriched in Mn, Co, Mo, Ni, and partly Fe (Abb. 28).

The profiles of  $\text{NO}_3^-$ ,  $\text{SO}_4^{2-}$ , and  $\text{Mn}_{\text{diss}}$  are similar to core 206-3. A narrow maximum for  $\text{Co}_{\text{diss}}$  is recorded in the upper part of the Mn reduction zone. The  $\text{Mo}_{\text{diss}}$  profile is similar to the  $\text{Mn}_{\text{diss}}$  profile,  $\text{Fe}_{\text{diss}}$  is below detection limit. The pore water gradients of  $\text{Mn}_{\text{diss}}$ ,  $\text{Co}_{\text{diss}}$ , and  $\text{Mo}_{\text{diss}}$  in cores 206-3 and 220-7 do not terminate in distinct brown layers (as they do in core 248-6), therefore pore water flux calculations were not performed. However,  $\text{Co}_{\text{xs}}/\text{Mo}_{\text{xs}}$  values in the interval from 90 to 100 cm depth where the pore water gradient ends are very low ( $\sim 1$ ), and thus indicate diagenetic addition of Mo from the pore water pool (Abb. 25c). In addition, Mn/Al is slightly increased above this interval. The  $\text{Co}_{\text{xs}}/\text{Mo}_{\text{xs}}$  values of the brown layers show that the first one (at  $\sim 50$  cm depth) is of primary origin, and that the two layers at 160 cm and 260 cm experienced diagenetic loss of Mn. The lowermost brown layer has elevated Mn/Al and Mo/Al and intermediate  $\text{Co}_{\text{xs}}/\text{Mo}_{\text{xs}}$ , which indicates that this layer is currently not influenced by diagenesis.

In core 237-3 from the Canada Basin, enrichment patterns of sedimentary Mn and trace metals in the dark brown sediment layers are very similar to core 248-6, whereas the ratios of Fe/Al are almost constant plotting close to the average shale ratio (Abb. 29). In this core, Mn oxides with adsorbed Co, Mo, and Ni clearly seem to be responsible for the dark brown color of these layers. However, the pore water data of core 237-3 are different compared to the other cores (Abb. 29).

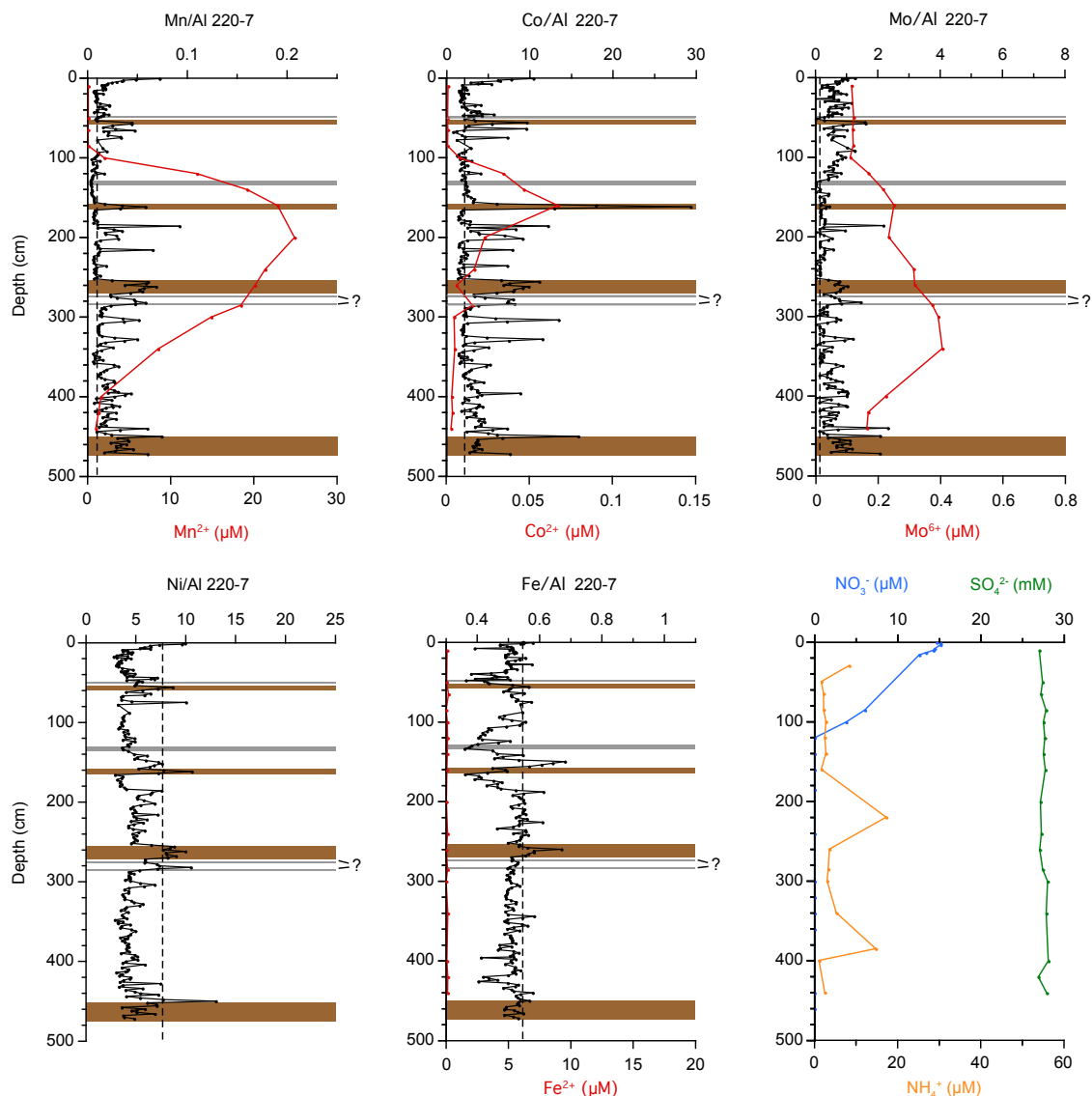


Abb. 28: Sedimentary Mn/Al, Fe/Al, Co/Al, Mo/Al, and Ni/Al values (black) and pore water  $\text{Mn}^{2+}$ ,  $\text{Co}^{2+}$ ,  $\text{Mo}^{6+}$  (all red),  $\text{NO}_3^-$  (blue),  $\text{SO}_4^{2-}$  (green) and  $\text{NH}_4^+$  (orange) concentrations in core 220-7. For additional information see Abb. 23

Nitrate only slightly increases from  $\sim 15 \mu\text{M}$  at the top further downcore. Ammonia,  $\text{Mn}_{\text{diss}}$ ,  $\text{Fe}_{\text{diss}}$ , and  $\text{Co}_{\text{diss}}$  are mostly below quantitation limit. There is neither a decrease in  $\text{SO}_4^{2-}$  nor an increase in  $\text{Mo}_{\text{diss}}$  with depth. These data show that the sediment geochemistry of core 237-3 is presently not overprinted by diagenetic processes. Both  $\text{NO}_3^-$  and  $\text{Mn}^{\text{IV}}$  are available as electron acceptors, and it seems very likely that the low availability of reactive organic matter is limiting diagenesis at this distal site in the Canada Basin. The ratios of  $\text{Co}_{\text{xs}}/\text{Mo}_{\text{xs}}$  (Abb. 25) of the brown layers are almost constant between 1 and 10, and suggest that the

Mn-rich layers in this core are of primary origin, which is in agreement with the pore water profiles (Fig. 29). The topmost samples have higher  $\text{Co}_{\text{XS}}/\text{Mo}_{\text{XS}}$ , but a potential diagenetic loss is not reflected in the pore water data.

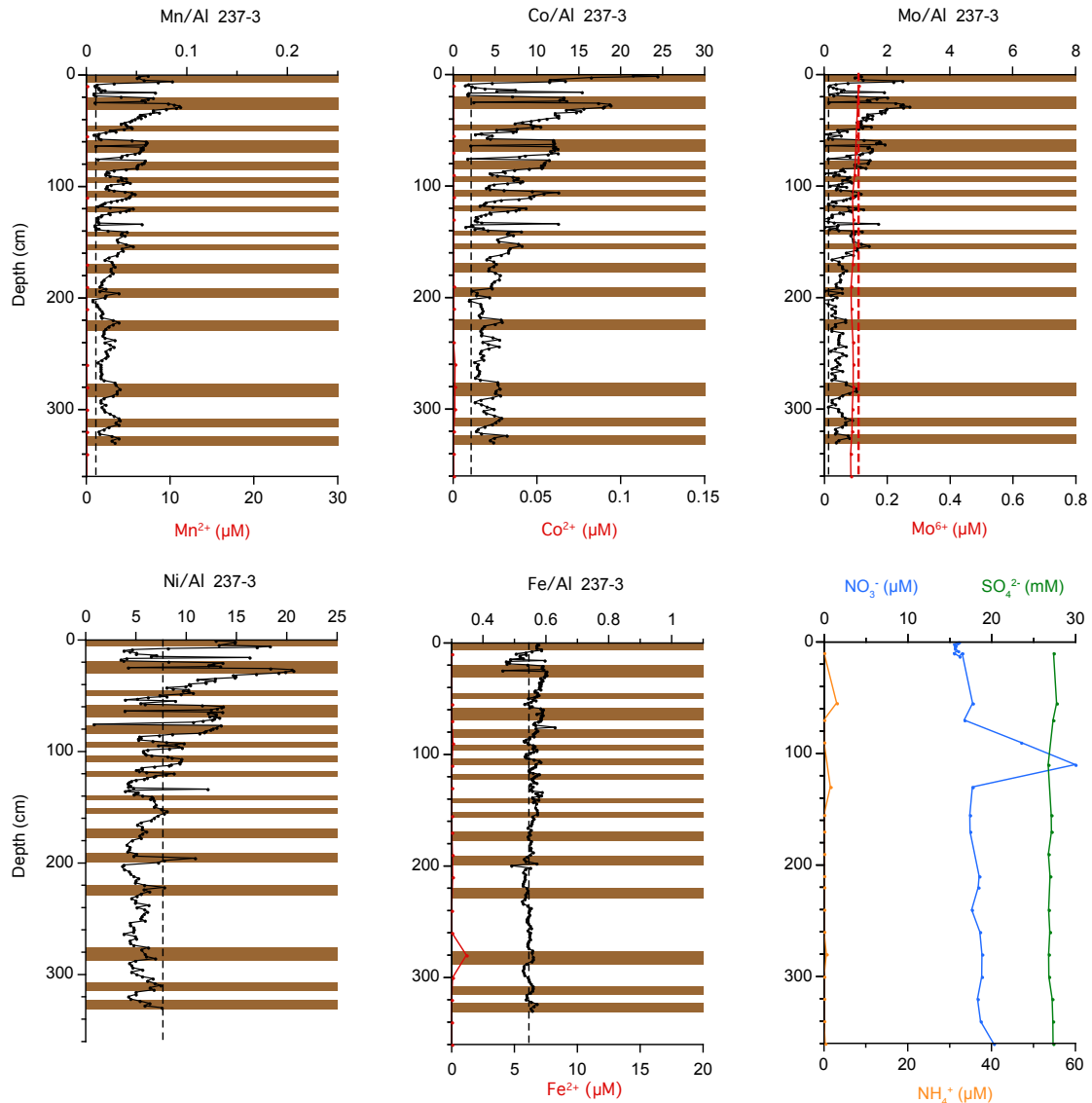


Abb. 29: Sedimentary Mn/Al, Fe/Al, Co/Al, Mo/Al, and Ni/Al values (black) and pore water Mn<sup>2+</sup>, Co<sup>2+</sup>, Mo<sup>6+</sup> (all red), NO<sub>3</sub><sup>-</sup> (blue), SO<sub>4</sub><sup>2-</sup> (green) and NH<sub>4</sub><sup>+</sup> (orange) concentrations in core 237-3. For additional information see Abb. 23

The sediment and pore water characteristics of core 343-1 from the Mendeleev Ridge were already described by März et al. (2011). The authors found similar Mn-trace metal relationships in the solid phase of the sediment core, and a similar diagenetic recycling of Mn as in core 248-6 (Abb. 30).

They used Co/Mo instead of  $\text{Co}_{\text{XS}}/\text{Mo}_{\text{XS}}$ , but their Co/Mo value is also higher in samples located in the Mn reduction zone, which is related to diagenetic loss of Mn. Compared to the other cores dissolved Co is very low, despite the availability of significant sedimentary Co enrichments. In this core, Co does not seem to be reduced during dissolution of sedimentary Mn phases.

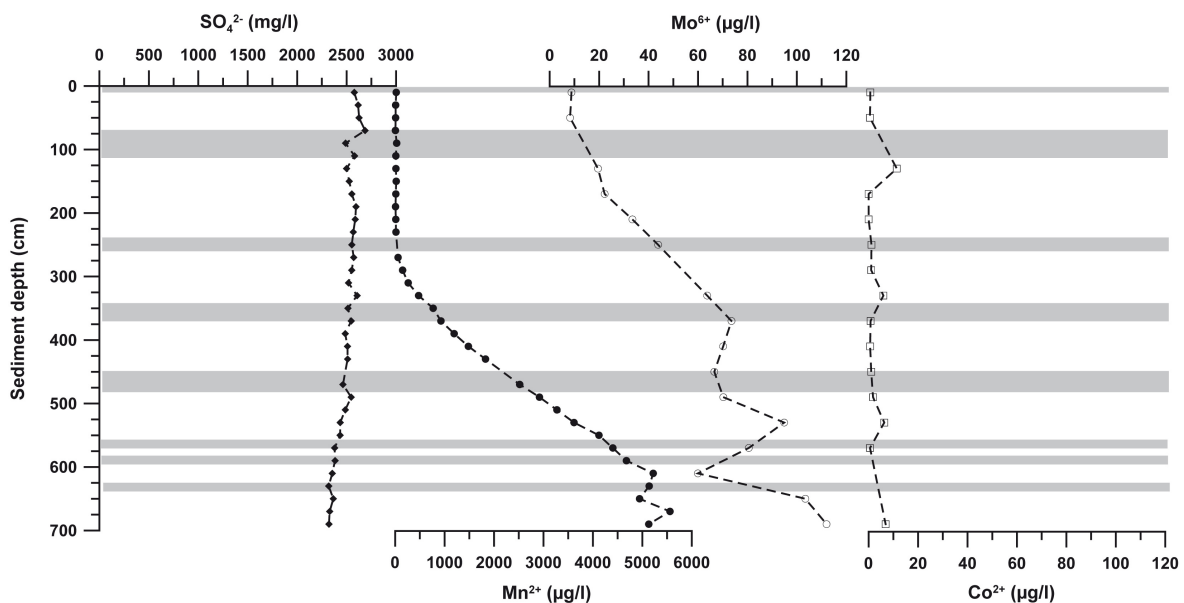


Abb. 30: Pore water  $\text{SO}_4^{2-}$ ,  $\text{Mn}^{2+}$ ,  $\text{Mo}^{6+}$ , and  $\text{Co}^{2+}$  concentrations in core 343-1 (from März et al., 2011). Gray bars represent dark brown sediment layers.

In summary, the observations described above demonstrate the occurrence of different diagenetic regimes in different parts of the central Arctic Ocean:

1) Core 237-3 from the Canada Basin does not show any signs of current diagenesis. 2) Core 248-6 from the Lomonosov Ridge is diagenetically influenced by Mn reduction and associated Co and Mo cycling, which in part affects a dark brown sediment layer at ~460 cm depth. In core 220-7 from the Lomonosov Ridge close to the North Pole, pore water data indicate Mn, Co, and Mo remobilization as well, but possible effects on specific dark brown layers could not be quantified.

3) Cores 206-3 from the Gakkel Ridge and 343-1 from the Mendeleev Ridge are clearly influenced by Mn reduction. However, in core 206-3 this is only associated with Co reduction, and in core 343-1 only with Mo reduction.

The data also show that Co and Mo are not remobilized in the same way during the dissolution of Mn layers in different parts of the Arctic Ocean. In cores 248-6 and 343-1, pore water data indicate that Mn is removed from the pore water in one specific sediment layer, while Mo seems to precipitate in the overlying sediment as well (Abb. 23, 30). In core 220-7, on the other hand, both Mn and Mo seem to precipitate in the same sediment layer (Abb. 28). In all cores Mn diagenesis is evidently controlled by the  $\text{NO}_3^-$  penetration depth. The absence of diagenetic overprint of core 237-3 might be related to its distal position in the Canada Basin and the deeper water depth compared to the other cores (Tab. 5).

Based on these geochemical pore water and sediment data, we can conclude that, despite some discrepancies in Co and Mo remobilization into the pore waters,  $\text{Co}_{\text{xs}}/\text{Mo}_{\text{xs}}$  values can indeed be indicative for diagenetic overprint of Mn-rich sediment layers in most of the studied sediment cores from the Arctic Ocean.

### 5.3.6 Sedimentary Fe enrichments

Our data show that Fe diagenesis is negligible in all studied cores. Therefore the question arises whether Fe enrichment patterns could be used as diagenetically stable tracers for elevated metal inputs into the Arctic Ocean, as already proposed by März et al. (2012). Iron isotopic signatures could additionally provide information about different sources of metals to the Arctic Ocean (including coastal erosion, river input, hydrothermal input). These hypotheses will be explored in the following section.

#### 5.3.6.1 Iron budget

To assess the potential origin of the Fe enrichments in the studied sediments, we constructed an iron budget for the Arctic Ocean (Tab. 8). Based on the approach of Macdonald and Gobeil (2012), we used the inputs and outputs of water and sediment, literature values for the concentrations of the different parameters in Tab. 8, and our own sediment data.

Tab. 8: Parameters and references for the Fe budget. <sup>a</sup>Wagemann et al., 1977; Gaillardet et al., 1999. <sup>b</sup>Reeder et al. 1972. <sup>c</sup>Nolting et al., 1996; Rachold et al., 1996; Gordeev et al., 2004; Hölemann et al., 2005. <sup>d</sup>Martin et al., 1993; Hölemann et al., 1995; 1999; 2005; Pokrovsky et al., 2010. <sup>e</sup>Average b and d. <sup>f</sup>3% of the global estimate from Duce and Tindale, 1991, and Zhuang et al., 1995. <sup>g</sup>Aguilar-Islas et al., 2007; Kuma et al., 2013. <sup>h</sup>Klunder et al., 2012. <sup>i</sup>Turekian and Wedepohl, 1961. <sup>j</sup>See chapter 3.7.1. <sup>k</sup>Strekopytov 2003. <sup>l</sup>Data from cores 206-3, 220-7, 237-3, and 248-6.

		Dissolved µg/l	Particulate µg/g	Dissolved kt/a	Particulate kt/a	Total kt/a
<i>Inputs</i>						
Mackenzie	total		36,075 <sup>a</sup>		4,473	
	lithogenic		28,860		3,579	3,579
	non-lithogenic	20 <sup>b</sup>	7,215	7	895	901
Siberian rivers	total		48,864 <sup>c</sup>		5,033	
	lithogenic		39,092		4,026	4,026
	non-lithogenic	169 <sup>d</sup>	9,773	502	1,007	1,508
Groundwater	non-lithogenic	94 <sup>e</sup>		28		28
Atmospheric	total				870 <sup>f</sup>	
	lithogenic				696	2,560
	non-lithogenic	0.2 <sup>f</sup>		1	174	175
Pacific inflow	non-lithogenic	0.14 <sup>g</sup>		4		4
Atlantic inflow	non-lithogenic	0.039 <sup>h</sup>		4		4
Coastal erosion	lithogenic		37,760 <sup>i</sup>		16,237	16,237
	non-lithogenic		9,440 <sup>i</sup>		4,059	4,059
Hydrothermal	non-lithogenic					100 <sup>j</sup>
<b>Total</b>	lithogenic					24,538
	non-lithogenic					6,779
	total					<b>31,317</b>
<i>Outputs</i>						
Atlantic outflow	non-lithogenic	0.039 <sup>h</sup>		-4		-4
CAA outflow	non-lithogenic	0.039 <sup>h</sup>		-1		-1
Ice export	lithogenic		37,760 <sup>i</sup>		-325	-325
	non-lithogenic		9,440 <sup>i</sup>		-81	-81
Sediment export	lithogenic		37,760 <sup>i</sup>		-1,850	-1,850
	non-lithogenic		9,440 <sup>i</sup>		-463	-463
Shelf sediments	lithogenic		47,761 <sup>k</sup>		-22,113	-22,113
	non-lithogenic		11,427 <sup>k</sup>		-5,291	-5,291
Basin sediments	lithogenic		29,000 <sup>l</sup>		-4,118	-4,118
	non-lithogenic		11,848 <sup>l</sup>		-1,682	-1,682
<b>Total</b>	lithogenic					-28,406
	non-lithogenic					-7,522
	total					<b>-35,929</b>

Particulate matter was partitioned into lithogenic ( $Fe_{Lith}$ ) and non-lithogenic ( $Fe_{NL}$ ) fractions (see definition above in chapter 5.3.2). To determine  $Fe_{Lith}$  and  $Fe_{NL}$ , we used data for shelf sediments from Strekopytov (2003). For simplification,

we calculated the average  $Fe_{xs}$  in these cores, which we regard as  $Fe_{NL}$  (11,427 mg/kg). Subtracting this value from the total Fe results in an average  $Fe_{Lith}$  of 47,761 mg/kg. The ratio of  $Fe_{Lith}/Fe_{NL}$  is 80/20, therefore 80% of a parameter in Tab. 8 accounts for the lithogenic component, and 20% for the non-lithogenic component.

Inputs and outputs of water and sediment per year from Macdonald and Gobeil (2012) were used to calculate the different Fe amounts per year for the parameters in Tab. 8.

Iron concentrations of dissolved river water are from Reeder et al. (1972), Martin et al. (1993), Hölemann et al. (1995; 1999; 2005), and Pokrovsky et al. (2010), whereas particulate matter concentrations are from Wagemann et al. (1977), Nolting et al. (1996), Rachold et al. (1996), Gaillardet et al. (1999), Gordeev et al. (2004), and Hölemann et al. (2005). To our knowledge, direct measurements of atmospheric Fe input to the Arctic Ocean are missing. We used 3% of the global estimate from Duce and Tindale (1991) and Zhuang et al. (1995), because the area of the Arctic Ocean is ~3% of the world's oceans (Jakobsson et al., 2003). Pacific inflow data are from Aguilar-Islas et al. (2007) and Kuma et al. (2013), and Atlantic inflow data are from Klunder et al. (2012). For coastal erosion, the mean composition of shale from Turekian and Wedepohl (1961) was used.

Hydrothermal activity in the Arctic Ocean has been observed at the ultraslow spreading Gakkel Ridge (e.g., Edmonds et al., 2003). However, we can only estimate the amount of hydrothermal Fe, because there are no direct measurements of material fluxes. For the Pacific and Atlantic outflow, we used the same concentrations as for the inflows. Particulate matter from ice and sediment export is thought to have the same concentration as material from coastal erosion. Data from Strekopytov (2003) are used for Arctic shelf sediments, and our own data for basin and submarine ridge sediments.

The input/output ratios of lithogenic, non-lithogenic, and total Fe in Tab. 8 are 0.86, 0.90, and 0.87, respectively. According to these numbers, 10-15% of the Fe inventory is exported from the Arctic Ocean. Because the output term includes deposition into shelf and basin sediments, it is likely that these 10-15% are accumulated in the sediments, rather than being exported completely from the Arctic Ocean.



The Fe accumulation rate in core 248-6 ( $ar_{Fe248}$ ) is  $7.7 \cdot 10^{-5} \text{ g cm}^{-2} \text{ a}^{-1}$ . Taking the input values from our budget, more than 100% of the Fe enrichment in the core can be explained by the external sources (Tab. 6). This is in accordance with the pore water data (Abb. 23), which do not indicate any Fe addition from deeper sediment layers. In two other cores (206-3 and 220-7) the external sources explain much more than 100% of the Fe enrichment as well (Tab. 6). So we assume that the input parameters used by Macdonald and Gobeil (2012) are only applicable to calculate the present Fe budget of the Arctic Ocean, and that the Fe input could have been lower in the past. In the next step, we will evaluate the Fe isotopic signature of several sediment cores to be able to distinguish between different lithogenic and non-lithogenic Fe sources to the Arctic Ocean basins, and their variation over time.

### 5.3.6.2 Iron isotope ratios and the Arctic Fe shuttle

We determined  $\delta^{56}\text{Fe}$  values in 26 samples from eight different coring sites across the central Arctic Ocean, including seven surface sediment samples, nine samples from brown layers, three samples from gray layers, and seven background sediment samples (Abb. 21, Tab. 5). Overall, the  $\delta^{56}\text{Fe}$  values in all studied samples range from -0.22 to +0.27‰ (Abb. 31, Tab. 5).

Most of the samples have  $\delta^{56}\text{Fe}$  values between 0 and 0.1‰ and dark brown sediment layers show only slightly lower values (0.045 on average) than olive brown layers (0.056 on average). These variations are within the standard deviation of the measurements and imply that different environmental conditions during glacial and interglacial periods have only a minor influence on the isotopic fractionation in central Arctic Ocean sediments. Distinct variations are seen in the gray layers of cores 206-3 and 248-6, yielding higher  $\delta^{56}\text{Fe}$  values ranging from 0.17 to 0.27‰. These gray layers have very low Fe and Mn contents (Abb. 23, 27) and very high ratios of  $\text{Fe}_{\text{Lith}}/\text{Fe}_{\text{NL}}$  (from 27 to 125; Tab. 5), implying that the Fe pool is dominated by terrigenous, non-reactive Fe.

## 5. Diagenetic regimes in Arctic Ocean sediments

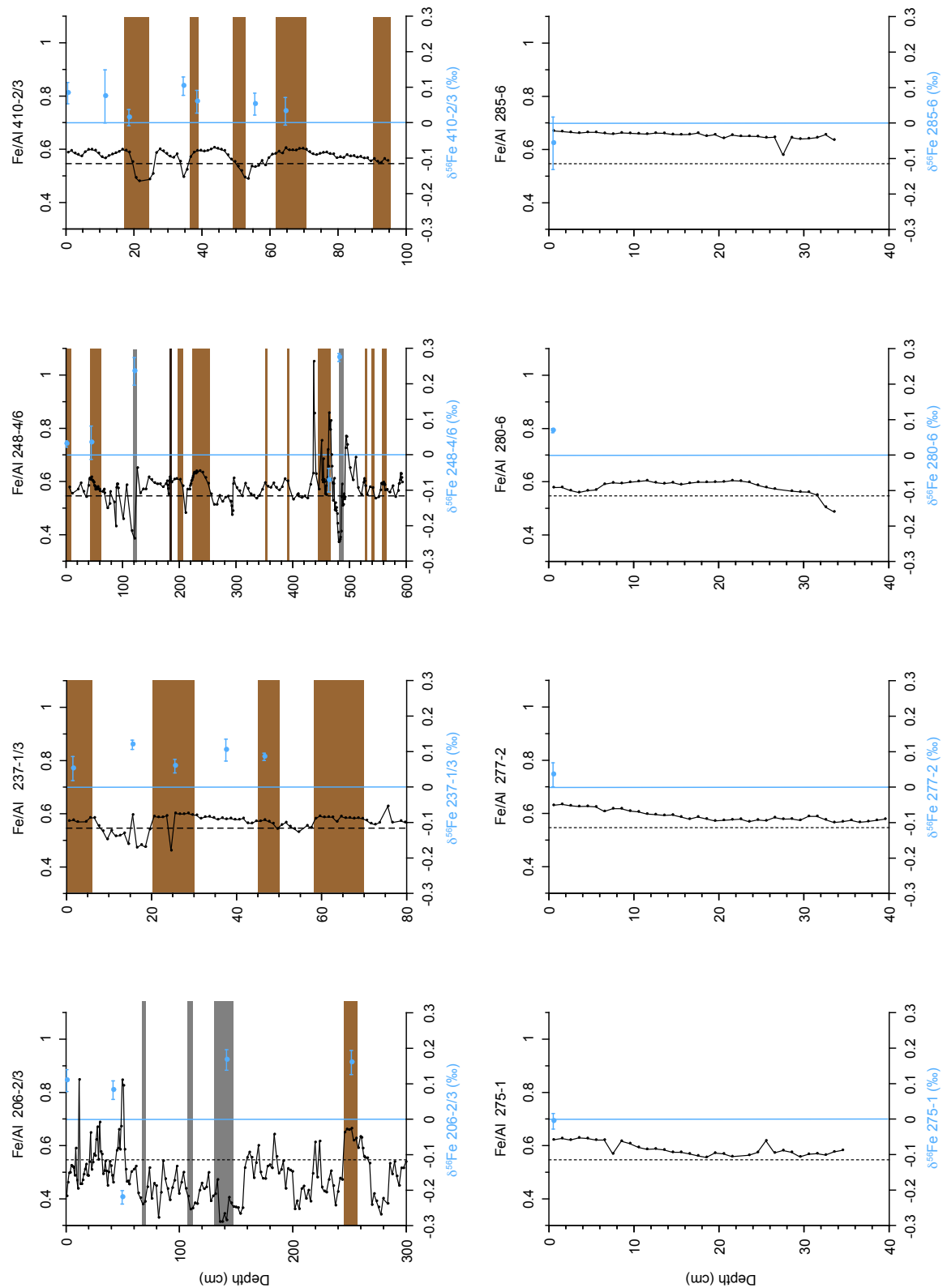


Abb. 31: Fe/Al (black) and  $\delta^{56}\text{Fe}$  values (blue) of sediment cores 206, 237, 248, 410 (gravity corer and multicorer), 275, 277, 280, and 285 (multicorer). See also Tab. 5. Dashed black line represents average shale (Wedepohl 1971, 1991), blue line represents  $\delta^{56}\text{Fe} = 0$ , gray bars represent gray sediment layers, brown bars represent dark brown sediment layers.

Lower  $\delta^{56}\text{Fe}$  values (-0.22 and -0.072) are found in two Fe- and Mn-rich sediment layers in cores 206-3 and 248-6 with low  $\text{Fe}_{\text{Lith}}/\text{Fe}_{\text{NL}}$  (between 0.6 and 0.8), which indicates the dominance of redox-reactive iron. Sediment cores 237-3 and 410-3 show less pronounced variations in Fe/Al and  $\delta^{56}\text{Fe}$  values than cores 206-3 and 248-6.

All samples show a clear negative relationship between their Fe/Al and  $\delta^{56}\text{Fe}$  values (Abb. 32, data in Tab. 5). The Fe pool in Fe-poor samples (with low Fe/Al compared to average shale and generally higher  $\text{Fe}_{\text{Lith}}/\text{Fe}_{\text{NL}}$ ) is isotopically relatively heavy, indicating an earlier loss of isotopically light Fe due to weathering before deposition (e.g., Fantle and DePaolo, 2004). In contrast, samples with high Fe/Al and all surface samples have lower  $\delta^{56}\text{Fe}$  values, indicating addition of an isotopically light Fe fraction to the sediment (Bergquist and Boyle 2006; Fehr et al., 2008; Severmann et al., 2008). Samples with lower  $\delta^{56}\text{Fe}$  values have generally also higher Mn/Al values, which indicates a close association of Fe with Mn. Recently it could be shown that Fe may be released from labile Fe-Mn oxides already during Mn reduction and that this Fe has low  $\delta^{56}\text{Fe}$  values, leaving the residual Fe with a higher isotopic signature (Schuth et al., 2015).

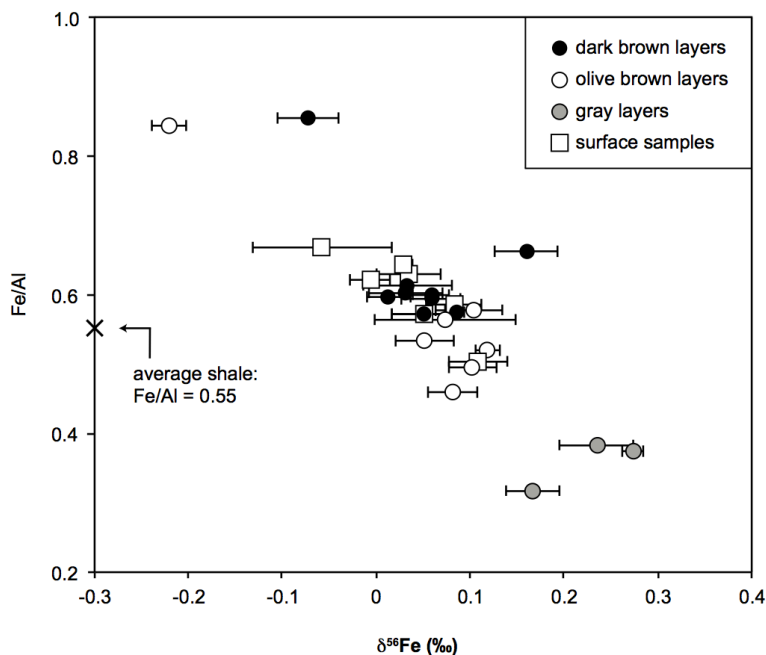


Abb. 32: Fe/Al relative to  $\delta^{56}\text{Fe}$  values. Residual Fe in the gray layers is isotopically heavier, indicating the lithogenic background. Fe-rich samples and surface samples are isotopically lighter, indicating a mobile Fe fraction.

The same negative Fe/Al to  $\delta^{56}\text{Fe}$  relationship was found e.g. in recent sediments from the Black Sea (sub)oxic shelf and euxinic basin (Severmann et al., 2008; Eckert et al., 2013) and this pattern was attributed to the diagenetic loss of reactive, isotopically light iron from suboxic shelf sediments via dissimilatory iron reduction (DIR), followed by shuttling of the remobilized Fe pool across the basin, and its deposition in the euxinic deep water setting as isotopically light Fe sulphides.

In contrast to the Black Sea, the constant pore water  $\text{SO}_4^{2-}$  concentrations and very low sedimentary S contents (close to the detection limit; not shown) in the studied Arctic Ocean sediments strongly argue against euxinic conditions and significant syngenetic or diagenetic pyrite formation. Evidence for this diagenetically driven shelf-to-basin Fe shuttle has also been found along other continental margins that are affected by upwelling of nutrient-rich waters and oxygen minimum zones (e.g., Homoky et al., 2012; Scholz et al., 2014), but the Arctic Ocean shelves and margins are not affected by oxygen-depleted water masses (Jakobsson et al., 2007; Stein 2008). Therefore, other biogeochemical and/or depositional processes must be invoked to explain the basin-wide negative Fe/Al to  $\delta^{56}\text{Fe}$  relationship across all studied sediment cores.

We will first focus on the gray layers in cores 206-3 and 248-6 (Abb. 31) that are isotopically heavier than all other samples and have the lowest Fe/Al (Abb. 32, Tab. 5). These geochemical patterns either represent the residual Fe fraction after dissolution and loss of more labile Fe minerals with lower  $\delta^{56}\text{Fe}$  values (e.g., during continental weathering; Fantle and DePaolo, 2004), or document a different sediment provenance. These gray layers are depleted in Fe, but enriched in the elements Si and Zr (not shown) that are usually associated with coarse-grained/high-density detrital minerals (e.g., Calvert and Pedersen, 2007; März et al., 2011). Therefore, the gray layers were most likely deposited under glacial conditions by two possible events (see chapter 5.3.1). During iceberg discharge events from the Barents-Kara ice sheet, these icebergs would carry the specific isotopic signature from the Barents-Kara hinterland. Unfortunately,  $\delta^{56}\text{Fe}$  source rock data are so far missing for the Arctic, but bulk granitoids, which represent a major fraction of continental crustal rock material, have positive  $\delta^{56}\text{Fe}$  values from

~0.1 to 0.4‰ (Poitrasson and Freydier, 2005). During the outburst of ice-dammed lakes, large amounts of material were quickly deposited in the Arctic basins, shielding the underlying sediment from the oxic water column. These gray layers have higher organic matter contents than the surrounding sediments (Löwemark et al., 2014), and therefore should provide fuel for diagenetic processes, including DIR. During this process, isotopically light Fe would have been liberated to the pore waters and diffused out of this layer, leaving the residual sediment with a more positive signature, and therefore a higher  $\delta^{56}\text{Fe}$  (e.g., Crosby et al., 2005; 2007; Johnson et al., 2008). The gray layers have very low Mo contents (partly below quantification limit), resulting in high  $\text{Co}_{\text{xs}}/\text{Mo}_{\text{xs}}$  values indicative for diagenetic loss of Mn and possibly associated Fe (see chapter 5.3.3). However, we can only infer that this diagenetic process occurred in the past, as the present pore water profiles show no sign of significant Fe reduction in the gray layers (Abb. 23, 27). We therefore define the gray layers with the lowest Fe/Al and highest  $\delta^{56}\text{Fe}$  values as the lithogenic background for our sediment cores that has been largely deprived of its reactive, isotopically light Fe fraction. With increasing addition of Fe to the sediment (resulting in higher Fe/Al), the  $\delta^{56}\text{Fe}$  values decrease. This shows that the additional Fe had a light isotopic signature that strongly suggests diagenetic mobilization by DIR or abiotic reduction by  $\text{HS}^-$  (Berner, 1984; Beard et al., 1999; Haese et al., 2000; Brantley et al., 2004), either from underlying sediment layers by diagenesis (see mechanism described above) or from the continental shelf (via a shuttle transport mechanism). We will focus our discussion on the tentative shelf-to-basin shuttling of isotopically light Fe. As stated above, such an Fe shuttle in the well-oxygenated Arctic Ocean must have been different from Fe shuttling in oxygen minimum zones or anoxic zones as present in the Black Sea.

There have been a number of hypotheses on the transport of different iron species from Arctic shelves to the deep basins, including hypopycnal distribution of organically complexed riverine Fe in the fresh surface layer, resuspension of Fe particles on the shelf by currents, and transport of Fe particles by seasonal sea ice (e.g., Nakayama et al., 2011; Thuroczy et al., 2011; März et al., 2012; Klunder et al., 2012). To explain the light iron isotope signature, any of these sources must

provide and distribute Fe species that have undergone isotopic fractionation during DIR, and this process occurs in the organic-rich Arctic shelf sediments that often display non-lithogenic Fe (oxyhydr)oxide enrichments at the sediment surface (Turner and Harriss, 1970; Nolting et al., 1996; Hölemann et al., 1999; Streckopytov, 2003). Remobilization of these non-lithogenic, isotopically light Fe (oxyhydr)oxides across the Arctic basins, in particular during deglacial and interglacial periods (März et al., 2012), could explain the high Fe/Al and low  $\delta^{56}\text{Fe}$  values of the studied brown layers (Abb. 31, 32).

Another explanation for the negative  $\delta^{56}\text{Fe}$  values is an input of isotopically light Fe from the water column, probably via hydrothermal fluids, continental runoff, oceanic crust alteration and shelf pore fluids (Beard et al., 2003; Bergquist and Boyle 2006; Severmann et al., 2006). Core 206-3 is located at the ultra-low spreading Gakkel Ridge (Edmonds et al., 2003) and might have received periodic input of hydrothermal Fe. Additional studies are required to further discriminate between specific transport pathways or different Fe sources to the sediment.

## 5.4 Conclusions

The dark brown color of specific sediment layers from the central Arctic Ocean is related either to enhanced Mn (oxyhydr)oxide content, Fe (oxyhydr)oxide content, or a combination of both. These layers are associated with enhanced Mo, Co, and Ni contents due to scavenging from the water column. Pore water measurements reveal different diagenetic regimes in Arctic Ocean sediment cores, ranging from strong reduction and diagenetic overprint of Mn, Co, and Mo to the absence of these processes in deeper sediment layers. Pore water flux calculations show that the sedimentary enrichments of Mn, Co, and Mo can result from a significant post-depositional contribution from the current pore water flux. Ratios of  $\text{Co}_{\text{xs}}/\text{Mo}_{\text{xs}}$  of the dark brown layers are helpful to identify sediment layers with diagenetic addition from the pore water or diagenetic dissolution in the Mn reduction zone. We emphasize a combined study of sediment and corresponding pore water geochemistry to identify a possible diagenetic overprint before using dark brown sediment layers in the Arctic Ocean for core correlation. Only dark

brown layers above the topmost Mn reduction zone can reliably be used as a stratigraphic tool in Quaternary sediments.

Sedimentary Fe enrichments are primarily derived from external input. The lithogenic Fe fraction accounts for 80% of the total Fe, only 20% are non-lithogenic. Gray layers define the lithogenic background with low Fe/Al, high  $Fe_{Lith}/Fe_{NL}$ , and positive  $\delta^{56}Fe$  values. With increasing Fe/Al the  $\delta^{56}Fe$  value decreases. This indicates the presence of a diagenetic Fe fraction enriched in the light Fe isotope. Pore water Fe data prove that remobilization from deeper layers within the sediment can be excluded. Therefore the presence of lighter Fe isotopes is likely a result of Fe transport from the shelf to the basin due to dissimilatory Fe reduction on the shelves. The absence of large variations in  $\delta^{56}Fe$  values between dark brown and lighter layers indicates that the different environmental conditions during glacial and interglacial times have a minor influence on the Fe isotopic fractionation in the studied Arctic Ocean sediments. Thus, sedimentary iron isotopes in combination with pore water data and modeling are a potential tool for the identification of different diagenetic remobilization processes and, together with sedimentary Mn, Co, and Mo data, different transport processes.

## 5.5 Acknowledgements

The authors would like to thank the master, crew, and shipboard scientists onboard R/V *Polarstern* during the ARK-XXII/3 and ARK-XXVI/3 expeditions, and E. Gründken, C. Lehnert and M. Schulz for substantial analytical assistance. This study was supported by the German Research Foundation (DFG grant BR 775/27-1) within the IODP SPP, which is gratefully acknowledged.

## 6. Manganese-rich brown layers in Arctic Ocean sediments: Composition, formation mechanisms, and diagenetic overprint

März, C.<sup>a</sup>, Stratmann, A.<sup>a</sup>, Matthiessen, J.<sup>b</sup>, Meinhardt, A.-K.<sup>a</sup>, Eckert, S.<sup>a</sup>,  
Schnetger, B.<sup>a</sup>, Vogt, C.<sup>c</sup>, Stein, R.<sup>b</sup>, Brumsack, H.-J.<sup>a</sup>

<sup>a</sup> Microbiogeochemistry, Institute for Chemistry and Biology of the Marine Environment (ICBM), Carl-von-Ossietzky-Universität Oldenburg, Carl-von-Ossietzky-Strasse 9-11, 26129 Oldenburg, Germany

<sup>b</sup> Marine Geology and Paleontology, Alfred Wegener Institute for Polar and Marine Research (AWI), 27568 Bremerhaven, Germany

<sup>c</sup> Crystallography/ZEKAM, Department of Geosciences, Universität Bremen, 28334 Bremen, Germany

Dieses Kapitel wurde publiziert in: *Geochimica et Cosmochimica Acta* 75 (23), 7668-7687 (2011).

### Abstract

We present inorganic geochemical analyses of pore waters and sediments of two Late Quaternary sediment cores from the western Arctic Ocean (southern Mendeleev Ridge, RV Polarstern Expedition ARK-XXIII/3), focussing on the composition and origin of distinct, brown-colored, Mn-rich sediment layers. Carbonate enrichments occur in association with these layers as peaks in Ca/Al, Mg/Al, Sr/Al and Sr/Mg, suggesting enhanced input of both ice-rafted and biogenic carbonate. For the first time, we show that the Mn-rich layers are also consistently enriched in the scavenged trace metals Co, Cu, Mo and Ni. Distinct bioturbation patterns, specifically well-defined brown burrows into the underlying sediments, suggest these metal enrichments formed close to the sediment–water interface. The geochemical signature of these metal- and carbonate-rich layers most probably documents formation under warmer climate conditions with an intensified continental hydrological cycle and only seasonal sea ice cover. Both



rivers and sea ice delivered trace metals to the Arctic Ocean, while enhanced seasonal productivity exported reactive organic matter to the sea floor. The coeval deposition of organic matter, Mn (oxyhydr)oxides and trace metals triggered intense diagenetic Mn cycling at the sediment–water interface. These processes resulted in the formation of Mn and trace metal enrichments, and the degradation of labile organic matter. With the onset of cooler conditions, reduced riverine runoff and/or a solid sea ice cover terminated the input of riverine trace metal and fresh organic matter, resulting in deposition of grayish-yellowish, metal-poor sediments. Oxygen depletion of Arctic bottom waters under these cooler conditions is not supported by our data, and did not cause the sedimentary Mn distribution. While the original composition and texture of the brown layers resulted from specific climatic conditions and corresponding diagenetic processes, pore water data show that diagenetic Mn redistribution is still affecting the organic-poor deeper sediments. Given persistent steady state conditions, purely authigenic Mn-rich brown layers may form, while others may be partly or completely dissolved. The degree of diagenetic Mn redistribution largely depends on the depositional environment, the Mn and organic matter availability, and apparently affected the Co/Mo ratios of Mn-rich layers. Thus, brown Arctic layers are not necessarily synchronous features, and should not be correlated across the Arctic Ocean without additional age control.

## 7. Silica diagenesis and benthic fluxes in the Arctic Ocean

März, C.<sup>1</sup>, Meinhardt, A.-K.<sup>2</sup>, Schnetger, B.<sup>2</sup>, Brumsack, H.-J.<sup>2</sup>

<sup>1</sup> School of Civil Engineering and Geosciences, Newcastle University, NE1 7RU  
Newcastle upon Tyne, United Kingdom

<sup>2</sup> Institut für Chemie und Biologie des Meeres (ICBM), Carl von Ossietzky  
Universität Oldenburg, 26111 Oldenburg, Germany

Dieses Kapitel wurde publiziert in: *Marine Chemistry* 171, 1-9 (2015).

### Abstract

Early diagenetic processes play an important role in the environmental cycling of silicic acid ( $\text{H}_4\text{SiO}_4$ ), one of the most important macronutrients in the ocean. Here, we present the first compilation of silicic acid concentrations in sediment pore water sampled in various parts of the Central Arctic Ocean. Based on these data, we calculate benthic fluxes of silicic acid from the sediments to Arctic bottom waters and interpret the pore water profiles in terms of silica dissolution–precipitation reactions deeper within the sediments. Silicic acid concentrations are very low in Arctic pore waters to sediment depths of ~8 m, with maxima ranging from 30  $\mu\text{mol/L}$  on the Mendeleev Ridge to 300  $\mu\text{mol/L}$  on the Alpha Ridge. These values are 1–2 orders of magnitude lower than silicic acid pore water concentrations in Atlantic, Indian, and Pacific Ocean sediments, reflecting the low biosilica productivity in the oligotrophic, seasonally ice-covered Arctic Ocean. Low silicic acid pore water concentrations translate into equally low benthic silicic acid fluxes, ranging between 1 and 15  $\text{mmol m}^{-2} \text{a}^{-1}$  ( $1 * 10^9$  to  $1.5 * 10^{10}$   $\mu\text{mol km}^{-2} \text{a}^{-1}$ ) at most study sites. With increasing sediment depth, asymptotic patterns typically observed in marine sediments occur at only five of twelve study sites. Deviations from this asymptotic shape at the other sites most likely reflect specific sediment intervals with elevated rates of biosilica dissolution (potentially from underlying

Eocene-Cretaceous strata) in association with iron oxide dissolution, or with the consumption of silicic acid by neo-formation of authigenic clay minerals.

## 8. Zusammenfassung und Ausblick

In dieser Arbeit wurde eine umfassende anorganisch-geochemische Charakterisierung von Sedimenten des Arktischen Ozeans durchgeführt, um diagnostische Parameter zu identifizieren, die Aussagen über Materialeintrag, Strömungssysteme inkl. Tiefenwasserzirkulation, diagenetische Milieus und die Variabilität dieser Parameter auf Glazial-/Interglazialzeitskalen ermöglichen sowie der Frage nachzugehen, ob dunkelbraune Sedimentlagen als stratigraphisches Werkzeug zur Altersdatierung benutzt werden können.

### **Geochemische Zusammensetzung der Sedimente**

In den oberflächennahen Sedimenten (max. 40 cm) des Mendeleev-Rückens sind dunkelbraune Sedimentlagen durch erhöhte Gehalte an Mn, Fe, As, Co, Cu, Mo und Ni gekennzeichnet. Simultane Muster der Anreicherungen von Mn, Co, Mo und Ni zeigen, dass diese Spurenmetalle hauptsächlich an Mn-Phasen adsorbiert sind, während Fe, As und Cu ein anderes Muster aufweisen, das darauf hindeutet, dass As und Cu vorwiegend an Fe-Phasen gebunden sind. Die dunkelbraune Sedimentfarbe, welche zuvor ausschließlich auf erhöhte Mn-Gehalte zurückgeführt wurde, wird auch durch erhöhte Fe-Gehalte beeinflusst. Dies haben Berechnungen von Überschussgehalten gegenüber dem lokalen Hintergrund gezeigt. Die dunkelbraunen Lagen dokumentieren erhöhten Materialeintrag durch Küstenerosion und Flusseintrag und sind in den hier untersuchten Oberflächensedimenten primärer Natur. Signaturen von Dolomit wurden in den Ca/Al, Mg/Al und TIC Profilen sichtbar und dokumentieren den Eintrag vom Arktischen Archipel. Si/Al und K/Al Profile sind diagnostisch für eine basaltische Komponente, vermutlich vom sibirischen Hinterland. Die Parameter  $Ca_{bio}$  und  $Sr_{XS}$  können als Anzeiger für erhöhten Eintrag einer biogenen Komponente verwendet werden.

## **Tiefenwasserzirkulation und Provenanz**

Die Untersuchung der Tiefenwasserzirkulation mit Hilfe von Nd-Isotopenverhältnissen wurde im Arktischen Ozean bisher hauptsächlich an vereinzelt Sedimentkernen durchgeführt. In dieser Arbeit wurde eine größere räumliche Auflösung gewählt, um auch kleinere Änderungen zu erfassen. Die Ergebnisse der Oberflächensedimente bestätigen aktuelle Studien und zeigen eine homogene Verteilung der Nd-Isotopensignatur mit einem deutlichen Einfluss von Wassermassen aus dem Nordatlantik und starker Durchmischung des Tiefenwassers. Die Ergebnisse der Proben aus dem letzten glazialen Maximum (LGM) zeigen weniger einheitliche Nd-Isotopensignaturen. Es dominieren lokale Einflüsse, wie die Bildung von „brines“ in den Schelfgebieten der Kara- und Laptevsee. Weiterhin ist der Einstrom von Tiefenwasser aus dem Makarow-Becken in das Amundsen-Becken über ein inneres Becken des Lomonosov-Rückens deutlich erkennbar. Die Untersuchung der Nd- und Sr-Isotopensignatur der lithogenen Sedimentkomponente ergab ein Mischsignal unterschiedlicher Quellen. Die untersuchten Sedimente weisen keine eindeutige Signatur eines bestimmten Umgebungsgesteins auf. Proben des arktischen Beckens sind jedoch stärker durch Sedimenteintrag von arktischer Seite beeinflusst und Proben des eurasischen Beckens durch eurasische Quellen. Während des LGM haben die Proben ein ähnliches Verteilungsmuster der Isotopensignaturen, weisen aber eine größere Streuung auf. Ursache sind die spezifischen Umweltbedingungen während des LGM: eine größere Eisbedeckung und ein verringerter Meeresspiegel ließen die Küstenlinie näher an den Arktischen Ozean reichen und verkürzten somit die Sediment-Transportwege.

## **Nutzung von dunkelbraunen Lagen als Altersmarker**

Untersuchungen von Sedimentkernen bis maximal 6 m Tiefe ergaben, dass die dunkelbraune Farbe der Sedimentlagen durch variable Anreicherungen von Mn- und Fe-Phasen hervorgerufen wird. Damit einher gehen erhöhte Gehalte an Spurenmetallen wie Co, Mo und Ni, die durch „scavenging“ aus der Wassersäule entfernt wurden. In den untersuchten Sedimentkernen herrschen unterschiedliche

diagenetische Milieus. Einige Bereiche sind durch stark reduzierende Bedingungen geprägt (Mn- Reduktion, Co- und Mo-Freisetzung), die zu diagenetischer Überprägung der dunkelbraunen Lagen führen. In anderen Bereichen sind diese Prozesse abwesend, sodass keine diagenetische Veränderung der Sedimentlagen auftritt. Die Tiefe der Mn-Reduktionszone wird dabei durch die  $\text{NO}_3^-$ -Eindringtiefe bestimmt. Metallanreicherungen im Sediment können zu einem signifikanten Anteil aus dem diffusiven Porenwasserstrom gebildet werden. Dies führt dazu, dass die Lagen nicht ohne Kenntnis der Diagenesebedingungen als primärer Indikator für wechselnde Glazial- und Interglazialzyklen verwendet werden können. Um diagenetisch überprägte Sedimentlagen zu erkennen, sind Verhältnisse der Überschussgehalte von Co und Mo ein diagnostischer Parameter, wenn Porenwasseruntersuchungen fehlen. Die Mn-Anreicherungen sind zum größten Teil nicht-lithogen, also nicht in die Mineralmatrix eingebunden, und deshalb redoxaktiv. Synchron zu Mn ist auch Fe in diesen Lagen angereichert. Anhand der Verhältnisse stabiler Fe-Isotope konnten verschiedene Transportwege entschlüsselt werden, was durch alleinige Betrachtung von Fe/Al Verhältnissen nicht möglich gewesen wäre. Dabei wurde festgestellt, dass die Fe-Lagen hauptsächlich aus lithogenem Material bestehen und primärer Natur sind. Die Fe-Isotopenmessungen ergaben höhere  $\delta^{56}\text{Fe}$  Werte im lithogenen Hintergrundgestein, welches niedrige Fe/Al Verhältnisse aufweist. Die  $\delta^{56}\text{Fe}$  Werte werden mit zunehmender Fe-Anreicherung im Sediment niedriger. Die Werte untermauern daher die Annahme, dass isotopisch leichteres Fe in den Schelfregionen mikrobiell reduziert, mobilisiert und Richtung Tiefsee exportiert wird. Diesem Mechanismus unterliegen vermutlich auch die Mn-Anreicherungen, jedoch können für Mn keine Isotopenverhältnisse bestimmt werden, da nur ein stabiles Mn-Isotop existiert. Zusammenfassend kann man die Aussage treffen, dass die dunkelbraunen Sedimentlagen nur dann stratigraphisch genutzt werden sollten, wenn begleitende diagenetische Untersuchungen gemacht werden.

## **Ausblick**

Die geochemischen Untersuchungen von Sedimentkernen des Arktischen Ozeans haben gezeigt, dass die bearbeiteten Fragestellungen wichtig sind, wenn man die Sedimentfärbung als stratigraphisches Werkzeug nutzen will. Aufgrund der großräumigen Verteilung der Kernlokationen können die Ergebnisse bei der Planung zukünftiger Expeditionen sinnvoll genutzt werden. Von Interesse wären hierbei längere Sedimentkerne, in denen gelöstes Fe im Porenwasser erfasst werden müsste. An diesen Kernen könnte der potentielle diagenetische Einfluss auf sedimentäre Fe-Phasen untersucht werden um herauszufinden, ob Fe ein zu Mn vergleichbares Verhalten aufweist oder deutlich weniger mobil ist.

In den untersuchten Sedimentkernen wurden verschiedene diagenetische Milieus diagnostiziert. Detaillierte Untersuchungen zu den Ursachen dieser Unterschiede könnten behilflich sein, Probenahme-Lokationen danach auszuwählen, ob die sedimentären Mn- und Fe-Phasen diagenetisch beeinflusst wurden.

Die Nutzung von Nd-Isotopensignaturen zur Untersuchung der Paläo-Tiefenwasserzirkulation ist ein vielversprechendes Werkzeug. Hierbei erwies sich die große räumliche Abdeckung als sinnvoll. Diese sollte für die Erfassung weiterer Zeitscheiben in den Sedimentkernen beibehalten werden. Mit Hilfe der Daten konnten lokale Einflüsse erkannt werden. Ob diese Einflüsse auch in weiteren Glazial-/Interglazialzyklen auftraten, kann in zukünftigen Studien untersucht werden.

Die Messung von Verteilungsmustern der seltenen Erdelemente (REE) an der lithogenen Sedimentfraktion könnte detailliertere Aussagen über Sedimentquellen ermöglichen, da z.B. Granite andere REE-Signaturen als Basalte aufweisen.

## 9. Literatur

- Aagaard, K., Swift, J.H., Carmack, E.C., 1985. Thermohaline Circulation in the Arctic Mediterranean Seas. *Journal of Geophysical Research-Oceans* 90 (C3), 4833-4846.
- Adler, R.E., Polyak, L., Ortiz, J.D., Kaufman, D.S., Channell, J.E.T., Xuan, C., Grottoli, A.G., Sellén, E., Crawford, K.A., 2009. Sediment record from the western Arctic Ocean with an improved Late Quaternary age resolution: HOTRAX core HLY0503-8JPC, Mendeleev Ridge. *Global and Planetary Change* 68, 18–29.
- Aguilar-Islas, A.M., Hurst, M.P., Buck, K.N., Sohst, B., Smith, G.J., Lohan, M.C., Bruland, K.W., 2007. Micro- and macronutrients in the southeastern Bering Sea: Insight into iron-replete and iron-depleted regimes. *Progress in Oceanography* 73 (2), 99-126.
- Akinin, V.V., Andronikov, A.V., Mukasa, S.B., Miller, E.L., 2013. Cretaceous lower crust of the continental margins of the northern pacific: Petrological and geochronological data on lower to middle crustal xenoliths. *Petrology* 21 (1), 28-65.
- Alexanderson, H., Backman, J., Cronin, T.M., Funder, S., Ingólfsson, Ó., Jakobsson, M., Landvik, J.Y., Löwemark, L., Mangerud, J., März, C., Möller, P., O'Regan, M., Spielhagen, R.F., 2014. An Arctic perspective on dating Mid-Late Pleistocene environmental history. *Quaternary Science Reviews* 92, 9-31.
- Aller, R.C., 1994. The sedimentary Mn cycle in Long Island Sound: Its role as intermediate oxidant and the influence of bioturbation, O<sub>2</sub>, and C<sub>org</sub> flux on diagenetic reaction balances. *Journal of Marine Research* 52 (2), 259-295.
- Anbar, A.D., Rouxel, O., 2007. Metal stable isotopes in paleoceanography. *Annual Review of Earth and Planetary Sciences* 35, 717-746.
- Andersson, P., 2012. Neodymium measured on water bottle samples during POLARSTERN cruise ARK-XXII/2 (SPACE). doi:10.1594/PANGAEA.789039.
- Andersson, P.S., Porcelli, D., Frank, M., Björk, G., Dahlqvist, R., Gustafsson, Ö., 2008. Neodymium isotopes in seawater from the Barents Sea and Fram Strait Arctic-Atlantic gateways. *Geochimica et Cosmochimica Acta* 72 (12), 2854-2867.



- Andronikov, A.V., Mukasa, S.B., 2010.  $^{40}\text{Ar}/^{39}\text{Ar}$  eruption ages and geochemical characteristics of Late Tertiary to Quaternary intraplate and arc-related lavas in interior Alaska. *Lithos* 115 (1-4), 1-14.
- Anisimov, O.A., Vaughan, D.G., Callaghan, T.V., Furgal, C., Marchant, H., Prowse, T.D., Vilhjálmsson, H., Walsh, J.E., 2007. Polar Regions (Arctic and Antarctic). *Climate Change 2007: Impacts, Adaptation and Vulnerability*. In: Parry, M.L., Canziani, O.F., Palutikof, J.P., van der Linden, P.J., Hanson, C.E. (Eds.), *Contribution of Working Group II to the Fourth Assessment Report of the Intergovernmental Panel on Climate Change*. Cambridge University Press, Cambridge, pp. 653–685.
- Babu, C.P., Brumsack, H.-J., Schnetger, B., 1999. Distribution of organic carbon in surface sediments along the eastern Arabian Sea: a revisit. *Marine Geology* 162 (1), 91–103.
- Backman, J., Jakobsson, M., Løvlie, R., Polyak, L., Febo, L.A., 2004. Is the central Arctic Ocean a sediment starved basin? *Quaternary Science Reviews* 23 (11-13), 1435-1454.
- Backman, J., Moran, K., McInroy, D.B., Mayer, L.A., and the Expedition 302 Scientists, 2006. Sites M0001-M0004. *Proceedings of the Integrated Ocean Drilling Program 302*.
- Beard, B.L., Johnson, C.M., Cox, L., Sun, H., Neelson, K.H., Aguilar, C., 1999. Iron isotope biosignatures. *Science* 285 (5435), 1889-1892.
- Beard, B.L., Johnson, C.M., Von Damm, K.L., Poulson, R.L., 2003. Iron isotope constraints on Fe cycling and mass balance in oxygenated Earth oceans. *Geology* 31 (7), 629-632.
- Belshaw, N.S., Zhu, X.K., Guo, Y., O'Nions, R.K., 2000. High precision measurement of iron isotopes by plasma source mass spectrometry. *International Journal of Mass Spectrometry* 197, 191-195.
- Belzile, N., Tessier, A., 1990. Interactions between arsenic and iron oxyhydroxides in lacustrine sediments. *Geochimica et Cosmochimica Acta* 54, 103–109.
- Benesch, R., Mangelsdorf, P., 1972. Eine Methode zur colorimetrischen Bestimmung von Ammoniak in Meerwasser. *Helgoland Marine Research* 23 (3), 365-375.

- Bergquist, B.A., Boyle, E.A., 2006. Iron isotopes in the Amazon River system: Weathering and transport signatures. *Earth and Planetary Science Letters* 248 (1-2), 54-68.
- Berner, R.A., 1984. Sedimentary pyrite formation - An update. *Geochimica et Cosmochimica Acta* 48 (4), 605-615.
- Bertine, K.K., Turekian, K.K., 1973. Molybdenum in Marine Deposits. *Geochimica et Cosmochimica Acta* 37 (6), 1415-1434.
- Bigeleisen, J., Mayer, M.G., 1947. Calculation of Equilibrium Constants for Isotopic Exchange Reactions. *Journal of Chemical Physics* 15 (5), 261-267.
- Bischof, J., Clark, D.L., Vincent, J.-S., 1996. Origin of ice-rafted debris: Pleistocene paleoceanography in the western Arctic Ocean. *Paleoceanography* 11 (6), 743–756.
- Bischof, J.F., Darby, D.A., 1997. Mid- to Late Pleistocene ice drift in the western Arctic Ocean: evidence for a different circulation in the past. *Science* 277, 74-78.
- Björk, G., Jakobsson, M., Rudes, B., Swift, J.H., Anderson, L., Darby, D.A., Backman, J., Coakley, B., Winsor, P., Polyak, L., Edwards, M., 2007. Bathymetry and deep-water exchange across the central Lomonosov Ridge at 88-89 degrees N. *Deep-Sea Research Part I-Oceanographic Research Papers* 54 (8), 1197-1208.
- Boudreau, B.P., 1997. *Diagenetic Models and Their Implementation. Modelling Transport and Reactions in Aquatic Sediments.* Springer Verlag Berlin Heidelberg.
- Brantley, S.L., Liermann, L.J., Gwynn, R.L., Anbar, A., Icopini, G.A., Barling, J., 2004. Fe isotopic fractionation during mineral dissolution with and without bacteria. *Geochimica et Cosmochimica Acta* 68 (15), 3189-3204.
- Brennan, C.E., Meissner, K.J., Eby, M., Hillaire-Marcel, C., Weaver, A.J., 2013. Impact of sea ice variability on the oxygen isotope content of seawater under glacial and interglacial conditions. *Paleoceanography* 28 (3), 388-400.
- Broecker, W.S., Peng, T., 1982. *Tracers in the Sea.*
- Brumsack, H.-J., 1989. Geochemistry of recent TOC-rich sediments from the Gulf of California and the Black Sea. *Geologische Rundschau* 78 (3), 851–882.

- Brumsack, H.-J., 2006. The trace metal content of recent organic carbon-rich sediments: Implications for Cretaceous black shale formation. *Palaeogeography Palaeoclimatology Palaeoecology* 232 (2-4), 344-361.
- Burdige, D.J., 1993. The biogeochemistry of manganese and iron reduction in marine sediments. *Earth-Science Reviews* 35, 249–284.
- Calvert, S.E., Pedersen, T.F., 1993. Geochemistry of Recent Oxidic and Anoxic Marine-Sediments - Implications for the Geological Record. *Marine Geology* 113 (1-2), 67-88.
- Calvert, S.E., Pedersen, T.F., 2007. Elemental Proxies for Paleoclimatic and Paleoceanographic Variability in Marine Sediments: Interpretation and Application. In: *Developments in Marine Geology, Vol. 1, Proxies in Late Cenozoic Paleoceanography*, pp. 567-644.
- Canfield, D.E., Thamdrup, B., 2009. Towards a consistent classification scheme for geochemical environments, or, why we wish the term 'suboxic' would go away. *Geobiology* 7 (4), 385-392.
- Chester, R., Hughes, M.J., 1967. A chemical technique for the separation of ferromanganese minerals, carbonate minerals and adsorbed trace elements from pelagic sediments. *Chemical Geology* 2, 249-262.
- Clark, D.L., Whitman, R.R., Morgan, K.A., Mackey, S.D., 1980. Stratigraphy and glacial-marine sediments of the Amerasian Basin, central Arctic Ocean. *Geological Society of America Special Papers* 181 (57 pp.).
- Cleroux, C., Cortijo, E., Anand, P., Labeyrie, L., Bassinot, F., Caillon, N., Duplessy, J.C., 2008. Mg/Ca and Sr/Ca ratios in planktonic foraminifera: Proxies for upper water column temperature reconstruction. *Paleoceanography* 23 (3).
- Cronin, T.M., Dwyer, G.S., Farmer, J., Bauch, H.A., Spielhagen, R.F., Jakobsson, M., Nilsson, J., Briggs, W.M., Stepanova, A., 2012. Deep Arctic Ocean warming during the last glacial cycle. *Nature Geoscience* 5 (9), 631-634.
- Crosby, H.A., Johnson, C.M., Roden, E.E., Beard, B.L., 2005. Coupled Fe(II)-Fe(III) electron and atom exchange as a mechanism for Fe isotope fractionation during dissimilatory iron oxide reduction. *Environmental Science & Technology* 39 (17), 6698-6704.

- Crosby, H.A., Roden, E.E., Johnson, C.M., Beard, B.L., 2007. The mechanisms of iron isotope fractionation produced during dissimilatory Fe(III) reduction by *Shewanella putrefaciens* and *Geobacter sulfurreducens*. *Geobiology* 5 (2), 169-189.
- Crowe, S.A., O'Neill, A.H., Kulczycki, E., Weisener, C.G., Roberts, J.A., Fowle, D.A., 2007. Reductive dissolution of trace metals from sediments. *Geomicrobiology Journal* 24, 157–165.
- Dahlqvist, R., Andersson, P.S., Porcelli, D., 2007. Nd isotopes in Bering Strait and Chukchi Sea waters. *Goldschmidt Conference Abstracts*.
- Damm, E. (1999): Manganese, iron, and nutrients in pore water profiles from the Ob and Yenisei estuaries (Kara Sea). In: Matthiessen, J.; Stepanets, O.V.; Stein, R.; Fütterer, D.K. and Galimov, E.M. (eds.), *The Kara Sea Expedition of RV Akademik Boris Petrov 1997: First Results of a Joint Russian-German Pilot Study*, Reports on Polar Research, Alfred Wegener Institute for Polar and Marine Research, Bremerhaven, 300, 127-130, hdl:10013/epic.10303.d001
- Darby, D.A., 2003. Sources of sediment found in sea ice from the western Arctic Ocean, new insights into processes of entrainment and drift patterns. *Journal of Geophysical Research* 108 (C8), 3257.
- Darby, D.A., Bischof, J.F., Jones, G.A., 1997. Radiocarbon chronology of depositional regimes in the western Arctic Ocean. *Deep-Sea Research II* 44 (8), 1745–1757.
- Darby, D.A., Polyak, L., Bauch, H.A., 2006. Past glacial and interglacial conditions in the Arctic Ocean and marginal seas - a review. *Progress in Oceanography* 71 (2-4), 129-144.
- Dauphas, N., Pourmand, A., Teng, F.Z., 2009. Routine isotopic analysis of iron by HR-MC-ICPMS: How precise and how accurate? *Chemical Geology* 267 (3-4), 175-184.
- Dellwig, O., Bosselmann, K., Kölsch, S., Hentscher, M., Hinrichs, J., Böttcher, M.E., Reuter, R., Brumsack, H.-J., 2007. Sources and fate of manganese in a tidal basin of the German Wadden Sea. *Journal of Sea Research* 57 (1), 1–18.
- DePaolo, D.J., Wasserburg, G.J., 1976. Nd Isotopic Variations and Petrogenetic Models. *Geophysical Research Letters* 3 (5), 249-252.

- Devitre, R., Belzile, N., Tessier, A., 1991. Speciation and adsorption of arsenic on diagenetic iron oxyhydroxides. *Limnology and Oceanography* 36 (7), 1480–1485.
- Driscoll, N.W., Haug, G.H., 1998. A short circuit in thermohaline circulation: A cause for northern hemisphere glaciation? *Science* 282 (5388), 436-438.
- Duce, R.A., Tindale, N.W., 1991. Atmospheric Transport of Iron and Its Deposition in the Ocean. *Limnology and Oceanography* 36 (8), 1715-1726.
- Dupuy, C., Michard, A., Dostal, J., Dautel, D., Baragar, W.R.A., 1992. Proterozoic flood basalts from the Coppermine River area, Northwest Territories: isotope and trace element geochemistry. *Canadian Journal of Earth Sciences* 29 (9), 1937-1943.
- Eckert, S., Brumsack, H.-J., Severmann, S., Schnetger, B., März, C., Fröllje, H., 2013. Establishment of euxinic conditions in the Holocene Black Sea. *Geology* 41 (4), 431-434.
- Edmonds, H.N., Michael, P.J., Baker, E.T., Connelly, D.P., Snow, J.E., Langmuir, C.H., Dick, H.J.B., Muhe, R., German, C.R., Graham, D.W., 2003. Discovery of abundant hydrothermal venting on the ultraslow-spreading Gakkel ridge in the Arctic. *Nature* 421 (6920), 252-256.
- Eisenhauer, A., Meyer, H., Rachold, V., Tütken, T., Wiegand, B., Hansen, B.T., Spielhagen, R.F., Lindemann, F., Kassens, H., 1999. Grain size separation and sediment mixing in Arctic Ocean sediments: evidence from the strontium isotope systematic. *Chemical Geology* 158 (3-4), 173-188.
- Emerson, S., Jahnke, R., Bender, M., Froelich, P., Klinkhammer, G., Bowser, C., Setlock, G., 1980. Early Diagenesis in Sediments from the Eastern Equatorial Pacific, 1. Pore Water Nutrient and Carbonate Results. *Earth and Planetary Science Letters* 49 (1), 57-80.
- Estrada, S., Höhndorf, A., Henjes-Kunst, F., 2001. Cretaceous/Tertiary Volcanism in North Greenland: the Kap Washington Group. *Polarforschung* 69, 17-23.
- Expedition 302 Scientists, 2006. Moisture and density measured on Hole 302-M0004C. doi:10.1594/PANGAEA.326708.

- Fagel, N., Not, C., Gueibe, J., Mattielli, N., Bazhenova, E., 2014. Late Quaternary evolution of sediment provenances in the Central Arctic Ocean: mineral assemblage, trace element composition and Nd and Pb isotope fingerprints of detrital fraction from the Northern Mendeleev Ridge. *Quaternary Science Reviews* 92, 140-154.
- Fantle, M.S., DePaolo, D.J., 2004. Iron isotopic fractionation during continental weathering. *Earth and Planetary Science Letters* 228 (3-4), 547-562.
- Fehr, M.A., Andersson, P.S., Hålenius, U., Mörth, C.M., 2008. Iron isotope variations in Holocene sediments of the Gotland Deep, Baltic Sea. *Geochimica et Cosmochimica Acta* 72 (3), 807-826.
- Froelich, P.N., Klinkhammer, G.P., Bender, M.L., Luedtke, N.A., Heath, G.R., Cullen, D., Dauphin, P., Hammond, D., Hartman, B., Maynard, V., 1979. Early Oxidation of Organic-Matter in Pelagic Sediments of the Eastern Equatorial Atlantic - Suboxic Diagenesis. *Geochimica et Cosmochimica Acta* 43 (7), 1075-1090.
- Gaillardet, J., Dupre, B., Allegre, C.J., 1999. Geochemistry of large river suspended sediments: Silicate weathering or recycling tracer? *Geochimica et Cosmochimica Acta* 63 (23-24), 4037-4051.
- Gendron, A., Silverberg, N., Sundby, B., Lebel, J., 1986. Early diagenesis of cadmium and cobalt in sediments of the Laurentian Trough. *Geochimica et Cosmochimica Acta* 50 (5), 741-747.
- GeoRem database reference values for BCR-2: [http://georem.mpch-mainz.gwdg.de/single\\_values\\_detail.asp?itemmeas=d56Fe&refmatid=USGS%20BCR-2](http://georem.mpch-mainz.gwdg.de/single_values_detail.asp?itemmeas=d56Fe&refmatid=USGS%20BCR-2) (zuletzt geprüft am 23. Juli 2015)
- Gobeil, C., Macdonald, R.W., Sundby, B., 1997. Diagenetic separation of cadmium and manganese in suboxic continental margin sediments. *Geochimica et Cosmochimica Acta* 61 (21), 4647-4654.
- Gobeil, C., Sundby, B., Macdonald, R.W., Smith, J.N., 2001. Recent change in organic carbon flux to the Arctic Ocean deep basins: evidence from acid volatile sulfide, manganese and rhenium discord in sediments. *Geophysical Research Letters* 28, 1743–1746.

- Goldberg, E.D., 1954. Marine Geochemistry 1. Chemical Scavengers of the Sea. *Journal of Geology* 62 (3), 249-265.
- Goldstein, S.L., Onions, R.K., Hamilton, P.J., 1984. A Sm-Nd Isotopic Study of Atmospheric Dusts and Particulates from Major River Systems. *Earth and Planetary Science Letters* 70 (2), 221-236.
- Gordeev, V.V., Martin, J.M., Sidorov, I.S., Sidorova, M.V., 1996. A reassessment of the Eurasian river input of water, sediment, major elements, and nutrients to the Arctic Ocean. *American Journal of Science* 296 (6), 664-691.
- Gordeev, V.V., Rachold, V., Vlasova, I.E., 2004. Geochemical behaviour of major and trace elements in suspended particulate material of the Irtysh river, the main tributary of the Ob river, Siberia. *Applied Geochemistry* 19 (4), 593-610.
- Gordeev, V.V., Beeskow, B., Rachold, V., 2007. Geochemistry of the Ob and Yenisey estuaries: a comparative study. *Berichte zur Polar- und Meeresforschung* 557, 1–235.
- Grygar, T., Polyak, L., Schneeweiss, O., 2007. Nature of Fe-precipitates in sediments from the Mendeleev Ridge, Arctic Ocean. *Geophysical Research Abstracts* 9 (SRef-ID: 1607-7962/ gra/EGU2007-A-02001).
- Haese, R.R., Schramm, J., van der Loeff, M.M.R., Schulz, H.D., 2000. A comparative study of iron and manganese diagenesis in continental slope and deep sea basin sediments off Uruguay (SW Atlantic). *International Journal of Earth Sciences* 88 (4), 619-629.
- Haley, B.A., Frank, M., Spielhagen, R.F., Eisenhauer, A., 2008a. Influence of brine formation on Arctic Ocean circulation over the past 15 million years. *Nature Geoscience* 1 (1), 68-72.
- Haley, B.A., Frank, M., Spielhagen, R.F., Fietzke, J., 2008b. Radiogenic isotope record of Arctic Ocean circulation and weathering inputs of the past 15 million years. *Paleoceanography* 23 (1).
- Haley, B.A., Polyak, L., 2013. Pre-modern Arctic Ocean circulation from surface sediment neodymium isotopes. *Geophysical Research Letters* 40 (5), 893-897.
- Hanslik, D., Löwemark, L., Jakobsson, M., 2013. Biogenic and detrital-rich intervals in central Arctic Ocean cores identified using X-ray fluorescence scanning. *Polar Research* 32, 18386.

- Hillaire-Marcel, C., de Vernal, A., Polyak, L., Darby, D., 2004. Size-dependent isotopic composition of planktic foraminifers from Chukchi Sea vs. NW Atlantic sediments - implications for the Holocene paleoceanography of the western Arctic. *Quaternary Science Reviews* 23 (3-4), 245-260.
- Hinrichs, J., Schnetger, B., Schale, H., Brumsack, H.-J., 2001. A high resolution study of NE Atlantic sediments at station Bengal: geochemistry and early diagenesis of Heinrich layers. *Marine Geology* 177 (1–2), 79–92.
- Hodell, D.A., Channell, J.E.T., Curtis, J.H., Romero, O.E., Röhl, U., 2008. Onset of “Hudson Strait” Heinrich events in the eastern North Atlantic at the end of the middle Pleistocene transition (~640 ka)? *Paleoceanography* 23 (4), PA4218.
- Hölemann, J.A., Schirmacher, M., Prange, A., 1995. Transport and distribution of trace elements in the Laptev Sea: first results of the TRANSDRIFT expeditions. *Reports on Polar and Marine Research* 176 (297-302).
- Hölemann, J.A., Schirmacher, M., Kassens, H., Prange, A., 1999. Geochemistry of surficial and ice-rafted sediments from the Laptev Sea (Siberia). *Estuarine Coastal and Shelf Science* 49, 45–59.
- Hölemann, J.A., Schirmacher, M., Prange, A., 2005. Seasonal variability of trace metals in the Lena River and the southeastern Laptev Sea: Impact of the spring freshet. *Global and Planetary Change* 48 (1-3), 112-125.
- Holmes, R.M., McClelland, J.W., Peterson, B.J., Shiklomanov, I.A., Shiklomanov, A.I., Zhulidov, A.V., Gordeev, V.V., Bobrovitskaya, N.N., 2002. A circumpolar perspective on fluvial sediment flux to the Arctic Ocean. *Global Biogeochemical Cycles* 16 (4).
- Homoky, W.B., Severmann, S., McManus, J., Berelson, W.M., Riedel, T.E., Statham, P.J., Mills, R.A., 2012. Dissolved oxygen and suspended particles regulate the benthic flux of iron from continental margins. *Marine Chemistry* 134, 59-70.
- Huerta-Diaz, M.A., Morse, J.W., 1992. Pyritization of trace metals in anoxic marine sediments. *Geochimica et Cosmochimica Acta* 56, 2681–2702.
- Hulth, S. et al., 1996: (Tables 1, 3) Pore water chemistry of Arctic surface sediments. doi:10.1594/PANGAEA.78615, In Supplement to: Hulth, S., Hall, P., Blackburn, T.H., Landén, A., 1996: Arctic sediments (Svalbard): pore water and solid phase distributions of C, N, P and Si. *Polar Biology*, 16(6), 447-462.



- Hulth, S., Aller, R.C., Gilbert, F., 1999. Coupled anoxic nitrification/manganese reduction in marine sediments. *Geochimica et Cosmochimica Acta* 63 (1), 49-66.
- Jacobsen, S.B., Wasserburg, G.J., 1980. Sm-Nd Isotopic Evolution of Chondrites. *Earth and Planetary Science Letters* 50 (1), 139-155.
- Jakobsson, M., 2002. Hypsometry and volume of the Arctic Ocean and its constituent seas. *Geochemistry Geophysics Geosystems* 3.
- Jakobsson, M., Løvlie, R., Al-Hanbali, H., Arnold, E., Backman, J., Mörth, M., 2000. Manganese and color cycles in Arctic Ocean sediments constrain Pleistocene chronology. *Geology* 28 (1), 23-26.
- Jakobsson, M., Løvlie, R., Arnold, E.M., Backman, J., Polyak, L., Knutsen, J.O., Musatov, E., 2001. Pleistocene stratigraphy and paleoenvironmental variation from Lomonosov Ridge sediments, central Arctic Ocean. *Global and Planetary Change* 31 (1-4), 1-22.
- Jakobsson, M., Grantz, A., Kristoffersen, Y., Macnab, R., 2003. Physiographic provinces of the Arctic Ocean seafloor. *Geological Society of America Bulletin* 115 (12), 1443-1455.
- Jakobsson, M., Backman, J., Rudels, B., Nycander, J., Frank, M., Mayer, L., Jokát, W., Sangiorgi, F., O'Regan, M., Brinkhuis, H., King, J., Moran, K., 2007. The early Miocene onset of a ventilated circulation regime in the Arctic Ocean. *Nature* 447 (7147), 986-990.
- Jakobsson, M., Macnab, R., Mayer, L., Anderson, R., Edwards, M., Hatzky, J., Schenke, H.W., Johnson, P., 2008. An improved bathymetric portrayal of the Arctic Ocean: implications for ocean modeling and geological, geophysical and oceanographic analyses. *Geophysical Research Letters* 35, L07602.
- Jakobsson, M., Andreassen, K., Bjarnadottir, L.R., Dove, D., Dowdeswell, J.A., England, J.H., Funder, S., Hogan, K., Ingólfsson, Ó., Jennings, A., Larsen, N.K., Kirchner, N., Landvik, J.Y., Mayer, L., Mikkelsen, N., Möller, P., Niessen, F., Nilsson, J., O'Regan, M., Polyak, L., Norgaard-Pedersen, N., Stein, R., 2014. Arctic Ocean glacial history. *Quaternary Science Reviews* 92, 40-67.

- Jang, K., Han, Y., Huh, Y., Nam, S.-I., Stein, R., Mackensen, A., Matthiessen, J., 2013. Glacial fresh-water discharge events recorded by authigenic neodymium isotopes in sediments from the Mendeleev Ridge, western Arctic Ocean. *Earth and Planetary Science Letters* 369–370, 148–157.
- Johansson, Å., Gee, D.G., 1999. The late Palaeoproterozoic Eskolabreen granitoids of southern Ny Friesland, Svalbard Caledonides - geochemistry, age, and origin. *Gff* 121, 113-126.
- Johansson, Å., Gee, D.G., Björklund, L., Witt-Nilsson, P., 1995. Isotope Studies of Granitoids from the Bangenhuk Formation, Ny-Friesland Caledonides, Svalbard. *Geological Magazine* 132 (3), 303-320.
- Johnson, C.M., Beard, B.L., Roden, E.E., 2008. The iron isotope fingerprints of redox and biogeochemical cycling in the modern and ancient Earth. *Annual Review of Earth and Planetary Sciences* 36, 457-493.
- Jokat, W. (Ed.), 2009. The Expedition ARK-XXIII/3 of RV Polarstern in 2008. *Berichte zur Polar- und Meeresforschung*, 597, pp. 1–159.
- Kalsbeek, F., Frei, R., 2006. The Mesoproterozoic Midsommerso dolerites and associated high-silica intrusions, North Greenland: crustal melting, contamination and hydrothermal alteration. *Contributions to Mineralogy and Petrology* 152 (1), 89-110.
- Kalsbeek, F., Jepsen, H.F., 1983. The Midsommers-Phi Dolerites and Associated Intrusions in the Proterozoic Platform of Eastern North Greenland - a Study of the Interaction between Intrusive Basic Magma and Sialic Crust. *Journal of Petrology* 24 (4), 605-634.
- Kalsbeek, F., Jepsen, H.F., 1984. The Late Proterozoic Zig-Zag Dal Basalt Formation of Eastern North Greenland. *Journal of Petrology* 25 (3), 644-664.
- Katsev, S., Sundby, B., Mucci, A., 2006. Modeling vertical excursions of the redox boundary in sediments: Application to deep basins of the Arctic Ocean. *Limnology and Oceanography* 51 (4), 1581-1593.
- Kiczka, M., Wiederhold, J.G., Frommer, J., Voegelin, A., Kraemer, S.M., Bourdon, B., Kretzschmar, R., 2011. Iron speciation and isotope fractionation during silicate weathering and soil formation in an alpine glacier forefield chronosequence. *Geochimica et Cosmochimica Acta* 75 (19), 5559-5573.

- Klinkhammer, G.P., 1980. Early diagenesis in sediments from the eastern Equatorial Pacific. 2. Pore water metal results. *Earth and Planetary Science Letters* 49, 81–101.
- Klunder, M.B., Bauch, D., Laan, P., de Baar, H.J.W., van Heuven, S., Ober, S., 2012. Dissolved iron in the Arctic shelf seas and surface waters of the central Arctic Ocean: Impact of Arctic river water and ice-melt. *Journal of Geophysical Research-Oceans* 117.
- Knauer, G.A., Martin, J.H., Gordon, R.M., 1982. Cobalt in north-east Pacific Waters. *Nature* 297 (5861), 49-51.
- Knies, J., Müller, C., Nowaczyk, N., Vogt, C., Stein, R., 2000. A multiproxy approach to reconstruct the environmental changes along the Eurasian continental margin over the last 150 kyr. *Marine Geology* 163, 317–344.
- Kuma, K., Takata, H., Kitayama, S., Omata, A., 2013. Water Column Iron Dynamics in the North Pacific Ocean, Bering Sea and Western Arctic Ocean. *Bunseki Kagaku* 62 (12), 1057-1069.
- Lambeck, K., Esat, T.M., Potter, E.K., 2002. Links between climate and sea levels for the past three million years. *Nature* 419 (6903), 199-206.
- Landvik, J.Y., Bondevik, S., Elverhøi, A., Fjeldskaar, W., Mangerud, J., Salvigsen, O., Siegert, M.J., Svendsen, J.I., Vorren, T.O., 1998. The last glacial maximum of Svalbard and the Barents Sea area: Ice sheet extent and configuration. *Quaternary Science Reviews* 17 (1-3), 43-75.
- Ledneva, G.V., Pease, V.L., Sokolov, S.D., 2011. Permo-Triassic hypabyssal mafic intrusions and associated tholeiitic basalts of the Kolyuchinskaya Bay, Chukotka (NE Russia): Links to the Siberian LIP. *Journal of Asian Earth Sciences* 40 (3), 737-745.
- Lettmann, K.A., Riedinger, N., Ramlau, R., Knab, N., Böttcher, M.E., Khalili, A., Wolff, J.O., Jørgensen, B.B., 2012. Estimation of biogeochemical rates from concentration profiles: A novel inverse method. *Estuarine Coastal and Shelf Science* 100, 26-37.
- Li, Y.H., Bischoff, J., Mathieu, G., 1969. The Migration of Manganese in the Arctic Basin Sediment. *Earth and Planetary Science Letters* 7 (3), 265-270.

- Li, Y.H., Gregory, S., 1974. Diffusion of Ions in Sea-Water and in Deep-Sea Sediments. *Geochimica et Cosmochimica Acta* 38 (5), 703-714.
- Lightfoot, P.C., Hawkesworth, C.J., Hergt, J., Naldrett, A.J., Gorbachev, N.S., Fedorenko, V.A., Doherty, W., 1993. Remobilization of the continental lithosphere by a mantle plume: major-, trace-element, and Sr-, Nd-, and Pb-isotope evidence from picritic and tholeiitic lavas of the Noril'sk District, Siberian Trap, Russia. *Contributions to Mineralogy and Petrology* 114 (2), 171-188.
- Löwemark, L., Jakobsson, M., Mörth, M., Backmann, J., 2008. Arctic Ocean manganese contents and sediment colour cycles. *Polar Research* 27, 105–113.
- Löwemark, L., O'Regan, M., Hanebuth, T.J.J., 2012. Late Quaternary spatial and temporal variability in Arctic deep-sea bioturbation and its relation to Mn cycles. *Palaeogeography, Palaeoclimatology, Palaeoecology* 365–366, 192–208.
- Löwemark, L., März, C., O'Regan, M., Gyllencreutz, R., 2014. Arctic Ocean Mn-stratigraphy: genesis, synthesis and inter-basin correlation. *Quaternary Science Reviews* 92, 97-111.
- Lovley, D.R., Phillips, E.J.P., 1988. Novel Mode of Microbial Energy Metabolism: Organic Carbon Oxidation Coupled to Dissimilatory Reduction of Iron or Manganese. *Applied and Environmental Microbiology* 54 (6), 1472-1480.
- Maccali, J., Hillaire-Marcel, C., Carignan, J., Reisberg, L.C., 2013. Geochemical signatures of sediments documenting Arctic sea-ice and water mass export through Fram Strait since the Last Glacial Maximum. *Quaternary Science Reviews* 64, 136-151.
- Macdonald, R.W., Bowers, J.M., 1996. Contaminants in the arctic marine environment: Priorities for protection. *Ices Journal of Marine Science* 53 (3), 537-563.
- Macdonald, R.W., Gobeil, C., 2012. Manganese Sources and Sinks in the Arctic Ocean with Reference to Periodic Enrichments in Basin Sediments. *Aquatic Geochemistry* 18 (6), 565-591.
- Magen, C., Mucci, A., Sundby, B., 2011. Reduction Rates of Sedimentary Mn and Fe Oxides: An Incubation Experiment with Arctic Ocean Sediments. *Aquatic Geochemistry* 17 (4-5), 629-643.

- März, C., Schnetger, B., Brumsack, H.-J., 2010. Paleoenvironmental implications of Cenozoic sediments from the central Arctic Ocean (IODP Expedition 302) using inorganic geochemistry. *Paleoceanography* 25, PA3206.
- März, C., Stratmann, A., Matthiessen, J., Meinhardt, A.-K., Eckert, S., Schnetger, B., Vogt, C., Stein, R., Brumsack, H.-J., 2011. Manganese-rich brown layers in Arctic Ocean sediments: Composition, formation mechanisms, and diagenetic overprint. *Geochimica et Cosmochimica Acta* 75 (23), 7668-7687.
- März, C., Poulton, S.W., Brumsack, H.-J., Wagner, T., 2012. Climate-controlled variability of iron deposition in the Central Arctic Ocean (southern Mendeleev Ridge) over the last 130,000 years. *Chemical Geology* 330, 116-126.
- März, C., Meinhardt, A.-K., Schnetger, B., Brumsack, H.-J., 2015. Silica diagenesis and benthic fluxes in the Arctic Ocean. *Marine Chemistry* 171, 1-9.
- Mansfeldt, T., Schuth, S., Hausler, W., Wagner, F.E., Kaufhold, S., Overesch, M., 2012. Iron oxide mineralogy and stable iron isotope composition in a Gleysol with petrogleyic properties. *Journal of Soils and Sediments* 12 (1), 97-114.
- Martin, E.E., Haley, B.A., 2000. Fossil fish teeth as proxies for seawater Sr and Nd isotopes. *Geochimica et Cosmochimica Acta* 64 (5), 835-847.
- Martin, J.M., Guan, D.M., Elbaz-Poulichet, F., Thomas, A.J., Gordeev, V.V., 1993. Preliminary assessment of the distributions of some trace elements (As, Cd, Cu, Fe, Ni, Pb and Zn) in a pristine aquatic environment - the Lena River estuary (Russia). *Marine Chemistry* 43 (1-4), 185-199.
- Martinez, N.C., Murray, R.W., Dickens, G.R., Kölling, M., 2009. Discrimination of sources of terrigenous sediment deposited in the central Arctic Ocean through the Cenozoic. *Paleoceanography* 24, PA1210.
- Matthiessen, J., 2011. Documentation of sediment core PS78/248-6. doi:10.1594/PANGAEA.771320
- McCulloch, M.T., Wasserburg, G.J., 1978. Sm-Nd and Rb-Sr Chronology of Continental Crust Formation. *Science* 200 (4345), 1003-1011.
- Meinhardt, A.-K. (2009) Anorganische Geochemie von Oberflächensedimenten auf einem Ost-West-Transekt über den Mendeleev-Rücken (81° N, Ostsibirische See, Arktischer Ozean). Diplomarbeit, Carl von Ossietzky Universität Oldenburg.

- Meinhardt, A.-K., März, C., Schuth, S., Lettmann, K., Schnetger, B., Wolff, J.-O., Brumsack, H.-J., submitted. Diagenetic regimes in Arctic Ocean sediments: Implications for sediment geochemistry and core correlation. *Geochimica et Cosmochimica Acta*.
- Meinhardt, A.-K., März, C., Stein, R., Brumsack, H.-J., 2014. Regional variations in sediment geochemistry on a transect across the Mendeleev Ridge (Arctic Ocean). *Chemical Geology* 369, 1-11.
- Middag, R., de Baar, H.J.W., Laan, P., Klunder, M.B., 2011. Fluvial and hydrothermal input of manganese into the Arctic Ocean. *Geochimica et Cosmochimica Acta* 75 (9), 2393-2408.
- Milliman, J.D., Meade, R.H., 1983. World-Wide Delivery of River Sediment to the Oceans. *Journal of Geology* 91 (1), 1-21.
- Millot, R., Gaillardet, J., Dupre, B., Allegre, C.J., 2003. Northern latitude chemical weathering rates: Clues from the Mackenzie River Basin, Canada. *Geochimica et Cosmochimica Acta* 67 (7), 1305-1329.
- Morford, J.L., Emerson, S., 1999. The geochemistry of redox sensitive trace metals in sediments. *Geochimica et Cosmochimica Acta* 63 (11-12), 1735-1750.
- Mühe, R., Bohrmann, H., Garbe-Schönberg, D., Kassens, H., 1997. E-MORB glasses from the Gakkel Ridge (Arctic Ocean) at 87°N: evidence for the Earth's most northerly volcanic activity. *Earth and Planetary Science Letters* 152 (1-4), 1-9.
- Müller, B., Granina, L., Schaller, T., Ulrich, A., Wehrli, B., 2002. P, As, Sb, Mo, and other elements in sedimentary Fe/Mn layers of Lake Baikal. *Environmental Science & Technology* 36, 411–420.
- Murray, J., Irvine, R., 1895. On the Manganese Oxides and Manganese Nodules in Marine Deposits. *Transactions of the Royal Society of Edinburgh* 37 (4), 721-742.
- Murray, J.W., 1975. The interaction of metal ions at the manganese dioxide-solution interface. *Geochimica et Cosmochimica Acta* 39 (4), 505-519.
- Murray, J.W., Dillard, J.G., 1979. The oxidation of cobalt(II) adsorbed on manganese dioxide. *Geochimica et Cosmochimica Acta* 43 (5), 781-787.

- Nakayama, Y., Fujita, S., Kuma, K., Shimada, K., 2011. Iron and humic-type fluorescent dissolved organic matter in the Chukchi Sea and Canada Basin of the western Arctic Ocean. *Journal of Geophysical Research-Oceans* 116.
- Nam, S.-I., 2009. Results of coarse fraction analysis. In: Jokat, W. (Ed.), *The Expedition ARK- XXIII/3 of RV Polarstern in 2008. Reports on Polar and Marine Research*, 597, pp. 53–58.
- Nansen, F., 1906. Northern waters: Captain Roald Amundsen's oceanographic observations in the Arctic Seas in 1901. *Videnskab-Selskabets Skrifter* 1. *Mathematisk-Naturv. Klasse 3*, 145 pp.
- Nolting, R.F., vanDalen, M., Helder, W., 1996. Distribution of trace and major elements in sediment and pore waters of the Lena Delta and Laptev Sea. *Marine Chemistry* 53 (3-4), 285-299.
- Oeser, M., Weyer, S., Horn, I., Schuth, S., 2014. High-Precision Fe and Mg Isotope Ratios of Silicate Reference Glasses Determined In Situ by Femtosecond LA-MC-ICP-MS and by Solution Nebulisation MC-ICP-MS. *Geostandards and Geoanalytical Research* 38 (3), 311-328.
- Oswald, W.W., Anderson, P.M., Brown, T.A., Brubaker, L.B., Hu, F.S., Lozhkin, A.V., Tinner, W., Kaltenrieder, P., 2005. Effects of sample mass and macrofossil type on radiocarbon dating of arctic and boreal lake sediments. *Holocene* 15 (5), 758-767.
- Palmer, M.R., Elderfield, H., 1986. Rare earth elements and neodymium isotopes in ferromanganese oxide coatings of Cenozoic foraminifera from the Atlantic-Ocean. *Geochimica et Cosmochimica Acta* 50 (3), 409-417.
- Patchett, P.J., Embry, A.F., Ross, G.M., Beauchamp, B., Harrison, J.C., Mayr, U., Isachsen, C.E., Rosenberg, E.J., Spence, G.O., 2004. Sedimentary cover of the Canadian shield through Mesozoic time reflected by Nd isotopic and geochemical results for the Sverdrup Basin, Arctic Canada. *Journal of Geology* 112 (1), 39-57.
- Phillips, R.L., Grantz, A., 2001. Regional variations in provenance and abundance of ice-rafted clasts in Arctic Ocean sediments: implications for the configuration of late Quaternary oceanic and atmospheric circulation in the Arctic. *Marine Geology* 172, 91–115.

- Piepgras, D.J., Wasserburg, G.J., 1987. Rare earth element transport in the western North Atlantic inferred from Nd isotopic observations. *Geochimica et Cosmochimica Acta* 51 (5), 1257-1271.
- Pin, C., Zalduendi, J.F.S., 1997. Sequential separation of light rare-earth elements, thorium and uranium by miniaturized extraction chromatography: Application to isotopic analyses of silicate rocks. *Analytica Chimica Acta* 339 (1-2), 79-89.
- Poitrasson, F., Freydier, R., 2005. Heavy iron isotope composition of granites determined by high resolution MC-ICP-MS. *Chemical Geology* 222 (1-2), 132-147.
- Pokrovsky, O.S., Viers, J., Shirokova, L.S., Shevchenko, V.P., Filipov, A.S., Dupre, B., 2010. Dissolved, suspended, and colloidal fluxes of organic carbon, major and trace elements in the Severnaya Dvina River and its tributary. *Chemical Geology* 273 (1-2), 136-149.
- Polyak, L., Curry, W.B., Darby, D.A., Bischof, J., Cronin, T.M., 2004. Contrasting glacial/interglacial regimes in the western Arctic Ocean as exemplified by a sedimentary record from the Mendeleev Ridge. *Palaeogeography Palaeoclimatology Palaeoecology* 203 (1-2), 73-93.
- Polyak, L., Stanovoy, V., Lubinski, D.J., 2003. Stable isotopes in benthic foraminiferal calcite from a river-influenced Arctic marine environment, Kara and Pechora Seas. *Paleoceanography* 18 (1), 1003.
- Polyak, L., Bischof, J., Ortiz, J.D., Darby, D.A., Channell, J.E.T., Xuan, C., Kaufmann, D.S., Løvlie, R., Schneider, D.A., Eberl, D.D., Adler, R., Council, E.A., 2009. Late Quaternary stratigraphy and sedimentation patterns in the western Arctic Oceans. *Global and Planetary Change* 68, 5–17.
- Polyak, L., Alley, R.B., Andrews, J.T., Brigham-Grette, J., Cronin, T.M., Darby, D.A., Dyke, A.S., Fitzpatrick, J.J., Funder, S., Holland, M., Jennings, A.E., Miller, G.H., O'Regan, M., Saville, J., Serreze, M., St. John, K., White, J.W.C., Wolff, E., 2010. History of sea ice in the Arctic. *Quaternary Science Reviews* 29 (15–16), 1757–1778.
- Porcelli, D., Andersson, P.S., Baskaran, M., Frank, M., Björk, G., Semiletov, I., 2009. The distribution of neodymium isotopes in Arctic Ocean basins. *Geochimica et Cosmochimica Acta* 73 (9), 2645-2659.



- Rachold, V., Alabyan, A., Hubberten, H.W., Korotaev, V.N., Zaitsev, A.A., 1996. Sediment transport to the Laptev Sea - Hydrology and geochemistry of the Lena River. *Polar Research* 15 (2), 183-196.
- Rachold, V., Grigoriev, M.N., Are, F.E., Solomon, S., Reimnitz, E., Kassens, H., Antonow, M., 2000. Coastal erosion vs riverine sediment discharge in the Arctic Shelf seas. *International Journal of Earth Sciences* 89 (3), 450-460.
- Raczek, I., Jochum, K.P., Hofmann, A.W., 2003. Neodymium and strontium isotope data for USGS reference materials BCR-1, BCR-2, BHVO-1, BHVO-2, AGV-1, AGV-2F GSP-1, GSP-2 and eight MPI-DING reference glasses. *Geostandards Newsletter-the Journal of Geostandards and Geoanalysis* 27 (2), 173-179.
- Reeder, S.W., Hitchon, B., Levinson, A.A., 1972. Hydrogeochemistry of the surface waters of the Mackenzie River drainage basin, Canada-1. Factors controlling inorganic composition. *Geochimica et Cosmochimica Acta* 36 (8), 825-865.
- Renard, M., 1986. Pelagic carbonate chemostratigraphy (Sr, Mg,  $^{18}\text{O}$ ,  $^{13}\text{C}$ ). *Marine Micropaleontology* 10, 117–164.
- Rickaby, R.E.M., Schrag, D.P., Zondervan, I., Riebesell, U., 2002. Growth rate dependence of Sr incorporation during calcification of *Emiliana huxleyi*. *Global Biogeochemical Cycles* 16 (1).
- Rudels, B., Anderson, L., Eriksson, P., Fahrbach, E., Jakobsson, M., Jones, E.P., Melling, H., Prinsenberg, S., Schauer, U., Yao, T., 2012. Observations in the Ocean. In: Lemke, P., Jacobi, H.-W. (Eds.), *Arctic Climate Change: The ACSYS Decade and Beyond*. Atmospheric and Oceanographic Sciences Library 43.
- Sakshaug, E., 2004. Primary and secondary production in the Arctic seas. In: Stein, R., Macdonald, R.W. (Eds.), *The Organic Carbon Cycle in the Arctic Ocean*. Springer Verlag, Heidelberg, pp. 57–82.
- Schauer, U., 2012. The expedition of the research vessel "Polarstern" to the Arctic in 2011 (ARK-XXVI/3 - TransArc). *Reports on Polar and Marine Research* 649.
- Schnetger, B., Lehnert, C., 2014. Determination of nitrate plus nitrite in small volume marine water samples using vanadium(III)chloride as a reduction agent. *Marine Chemistry* 160, 91-98.

- Scholz, F., Severmann, S., McManus, J., Hensen, C., 2014. Beyond the Black Sea paradigm: The sedimentary fingerprint of an open-marine iron shuttle. *Geochimica et Cosmochimica Acta* 127, 368-380.
- Schoster, F., 2005. Terrigenous sediment supply and paleoenvironment in the Arctic Ocean during the late Quaternary: reconstructions from major and trace elements. *Reports on Polar and Marine Research* 498.
- Schoster, F., Behrends, M., Müller, C., Stein, R., Wahsner, M., 2000. Modern river discharge and pathways of supplied material in the Eurasian Arctic Ocean: evidence from mineral assemblages and major and minor element distribution. *International Journal of Earth Science* 89, 486–495.
- Schuth, S., Hurraß, J., Münker, C., Mansfeldt, T., 2015. Redox-dependent fractionation of iron isotopes in suspensions of a groundwater-influenced soil. *Chemical Geology* 392, 74-86.
- Schulz, H.D., 2006. Quantification of Early Diagenesis: Dissolved Constituents in Marine Pore Water, in: Schulz, H.D., Zabel, M. (Eds.), *Marine Geochemistry*, Springer Verlag Berlin Heidelberg.
- Seeberg-Elverfeldt, J., Schlüter, M., Feseker, T., Kölling, M., 2005. Rhizon sampling of porewaters near the sediment-water interface of aquatic systems. *Limnology and Oceanography-Methods* 3, 361-371.
- Sellén, E., Jakobsson, M., Frank, M., Kubik, P.W., 2009. Pleistocene variations of beryllium isotopes in central Arctic Ocean sediment cores. *Global and Planetary Change* 68, 38–47.
- Severmann, S., Johnson, C.M., Beard, B.L., McManus, J., 2006. The effect of early diagenesis on the Fe isotope compositions of porewaters and authigenic minerals in continental margin sediments. *Geochimica et Cosmochimica Acta* 70 (8), 2006-2022.
- Severmann, S., Lyons, T.W., Anbar, A., McManus, J., Gordon, G., 2008. Modern iron isotope perspective on the benthic iron shuttle and the redox evolution of ancient oceans. *Geology* 36 (6), 487-490.
- Sharma, M., Basu, A.R., Nesterenko, G.V., 1992. Temporal Sr-, Nd- and Pb-isotopic variations in the Siberian flood basalts: Implications for the plume-source characteristics. *Earth and Planetary Science Letters* 113 (3), 365-381.

- Shaw, T.J., Gieskes, J.M., Jahnke, R.A., 1990. Early diagenesis in differing depositional environments: The response of transition metals in pore water. *Geochimica et Cosmochimica Acta* 54 (5), 1233-1246.
- Shimmield, G.B., Price, N.B., 1986. The Behavior of Molybdenum and Manganese during Early Sediment Diagenesis - Offshore Baja-California, Mexico. *Marine Chemistry* 19 (3), 261-280.
- Spielhagen, R.F., Bonani, G., Eisenhauer, A., Frank, M., Frederichs, T., Kassens, H., Kubik, P.W., Mangini, A., Nørgaard-Pedersen, N., Nowaczyk, N.R., Schäper, S., Stein, R., Thiede, J., Tiedemann, R., Wahsner, M., 1997. Arctic Ocean evidence for Late Quaternary initiation of northern Eurasian ice sheets. *Geology* 25, 783–786.
- Spielhagen, R.F., Baumann, K.H., Erlenkeuser, H., Nowaczyk, N.R., Nørgaard-Pedersen, N., Vogt, C., Weiel, D., 2004. Arctic Ocean deep-sea record of northern Eurasian ice sheet history. *Quaternary Science Reviews* 23 (11-13), 1455-1483.
- Stein, R., 2008. Arctic Ocean Sediments: Processes, Proxies, and Paleoenvironment. *Developments in Marine Geology* 2, Elsevier, 592 pp.
- Stein, R., Nam, S.-I., Schubert, C., Vogt, C., Fütterer, D., Heinemeier, J., 1994. The last deglaciation event in the eastern central Arctic Ocean. *Science* 264, 692–696.
- Stein, R., Usbeck, R., Polozek, K., 2004. Physical properties of sediment core PS51/058-3. doi:10.1594/PANGAEA.205436
- Stein, R., Matthiessen, J., Niessen, F., 2010a. Re-coring at Ice Island T3 site of key core FL- 224 (Nautilus Basin, Amerasian Arctic): sediment characteristics and stratigraphic framework. *Polarforschung* 79 (2), 81–96.
- Stein, R., Matthiessen, J., Niessen, F., Krylov, A., Nam, S.-I., Bazhenova, E., 2010b. Towards a better (litho-) stratigraphy and reconstruction of Quaternary paleoenvironment in the Amerasian Basin (Arctic Ocean). *Polarforschung* 79 (2), 97–121.
- Stokes, C.R., Clark, C.D., Darby, D.A., Hodgson, D.A., 2005. Late pleistocene ice export events into the Arctic Ocean from the M'Clure Strait Ice Stream, Canadian Arctic Archipelago. *Global and Planetary Change* 49 (3-4), 139-162.

- Stordal, M.C., Wasserburg, G.J., 1986. Neodymium isotopic study of Baffin Bay water: sources of REE from very old terranes. *Earth and Planetary Science Letters* 77 (3-4), 259-272.
- Strekopytov, S.V., 2003. Geochemistry of diagenesis of sediments in the Barents Sea: Forms of iron and sulfur. *Lithology and Mineral Resources* 38 (1), 1-11.
- Sundby, B., Lecroart, P., Anschutz, P., Katsev, S., Mucci, A., 2015. When deep diagenesis in Arctic Ocean sediments compromises manganese-based geochronology. *Marine Geology* 366, 62-68.
- Svendsen, J.I., Alexanderson, H., Astakhov, V.I., Demidov, I., Dowdeswell, J.A., Funder, S., Gataullin, V., Henriksen, M., Hjort, C., Houmark-Nielsen, M., Hubberten, H.W., Ingólfsson, Ó., Jakobsson, M., Kjær, K.H., Larsen, E., Lokrantz, H., Lunkka, J.P., Lyså, A., Mangerud, J., Matiouchkov, A., Murray, A., Möller, P., Niessen, F., Nikolskaya, O., Polyak, L., Saarnisto, M., Siegert, C., Siegert, M.J., Spielhagen, R.F., Stein, R., 2004. Late quaternary ice sheet history of northern Eurasia. *Quaternary Science Reviews* 23 (11-13), 1229-1271.
- Tachikawa, K., Athias, V., Jeandel, C., 2003. Neodymium budget in the modern ocean and paleo-oceanographic implications. *Journal of Geophysical Research-Oceans* 108 (C8).
- Takei, H., Yokoyama, T., Makishima, A., Nakamura, E., 2001. Formation and suppression of AlF<sub>3</sub> during HF digestion of rock samples in Teflon bomb for precise trace element analyses by ICP-MS and ID-TIMS. *Proceedings of the Japan Academy Series B-Physical and Biological Sciences* 77 (1), 13-17.
- Tanaka, T., Togashi, S., Kamioka, H., Amakawa, H., Kagami, H., Hamamoto, T., Yuhara, M., Orihashi, Y., Yoneda, S., Shimizu, H., Kunimaru, T., Takahashi, K., Yanagi, T., Nakano, T., Fujimaki, H., Shinjo, R., Asahara, Y., Tanimizu, M., Dragusanu, C., 2000. JNdi-1: a neodymium isotopic reference in consistency with LaJolla neodymium. *Chemical Geology* 168 (3-4), 279-281.
- Thirlwall, M.F., 1991. Long-term reproducibility of multicollector Sr and Nd isotope ratio analysis. *Chemical Geology* 94 (2), 85-104.

- Thorarinsson, S.B., Holm, P.M., Duprat, H., Tegner, C., 2011. Silicic magmatism associated with Late Cretaceous rifting in the Arctic Basin-petrogenesis of the Kap Kane sequence, the Kap Washington Group volcanics, North Greenland. *Lithos* 125 (1-2), 65-85.
- Thuroczy, C.E., Gerringa, L.J.A., Klunder, M., Laan, P., Le Guitton, M., de Baar, H.J.W., 2011. Distinct trends in the speciation of iron between the shallow shelf seas and the deep basins of the Arctic Ocean. *Journal of Geophysical Research-Oceans* 116.
- Tikhomirov, P.L., Akinin, V.V., Ispolatov, V.O., Alexander, P., Cherepanova, I.Y., Zagoskin, V.V., 2006. The Okhotsk–Chukotka volcanic belt: age of its northern part according to new Ar–Ar and U–Pb geochronological data. *Stratigraphy and Geological Correlation* 14 (5), 524–537.
- Tovar-Sánchez, A., Duarte, C.M., Alonso, J.C., Lacorte, S., Tauler, R., Galbán-Malagón, C., 2010. Impacts of metals and nutrients released from melting multiyear Arctic sea ice. *Journal of Geophysical Research-Oceans* 115.
- Tribovillard, N., Algeo, T.J., Lyons, T., Riboulleau, A., 2006. Trace metals as paleoredox and paleoproductivity proxies: An update. *Chemical Geology* 232 (1-2), 12-32.
- Tütken, T., Eisenhauer, A., Wiegand, B., Hansen, B.T., 2002. Glacial-interglacial cycles in Sr and Nd isotopic composition of Arctic marine sediments triggered by the Svalbard/Barents Sea ice sheet. *Marine Geology* 182 (3-4), 351-372.
- Turekian, K.K., Wedepohl, K.H., 1961. Distribution of the Elements in Some Major Units of the Earth's Crust. *Geological Society of America Bulletin* 72 (2), 175-192.
- Turner, R.R., Harriss, R.C., 1970. The distribution of non-detrital iron and manganese in two cores from the Kara Sea. *Deep-Sea Research* 17 (3), 633-636.
- Upton, B.G.J., Ramo, O.T., Heaman, L.M., Blichert-Toft, J., Kalsbeek, F., Barry, T.L., Jepsen, H.F., 2005. The Mesoproterozoic Zig-Zag Dal basalts and associated intrusions of eastern North Greenland: mantle plume-lithosphere interaction. *Contributions to Mineralogy and Petrology* 149 (1), 40-56.

- Van der Weijden, C.H., 2002. Pitfalls of normalization of marine geochemical data using a common divisor. *Marine Geology* 184, 167–187.
- Vance, D., Burton, K., 1999. Neodymium isotopes in planktonic foraminifera: a record of the response of continental weathering and ocean circulation rates to climate change. *Earth and Planetary Science Letters* 173 (4), 365-379.
- Viscosi-Shirley, C., Mammone, K., Pisiias, N., Dymond, J., 2003. Clay mineralogy and multi-element chemistry of surface sediments on the Siberian–Arctic shelf: implications for sediment provenance and grain size sorting. *Continental Shelf Research* 23, 1175–1200.
- Vogt, C., 1997. Regional and temporal variations of mineral assemblages in Arctic Ocean sediments as climatic indicator during glacial/interglacial changes. *Reports on Polar and Marine Research* 251.
- Vogt, C., 2009. Data report: semiquantitative determination of detrital input to ACEX sites based on bulk sample X-ray diffraction data. In: Backmann, J., Moran, K., McInroy, D.B., Mayer, L.A., the Expedition 302 Scientists (Eds.), *Proceedings of the Integrated Ocean Drilling Program, 302*. Integrated Ocean Drilling Program Management International, Inc., Edinburgh.
- Wagemann, R., Brunskill, G.J., Graham, B.W., 1977. Composition and Reactivity of Some River Sediments from the Mackenzie Valley, N.W.T., Canada. *Environmental Geology* 1 (6), 349-358.
- Weber, J.N., 1964. Trace element composition of dolostones and dolomites and its bearing of the dolomite problem. *Geochimica et Cosmochimica Acta* 28, 1817-1868.
- Wedepohl, K.H., 1971. Environmental influences on the chemical composition of shales and clays, in Ahrens, L.H., Press, F., Runcorn, S.K. and Urey, H.C. (eds), *Physics and Chemistry of the Earth*, vol. 8. Pergamon Press, Oxford, p. 307-333.
- Wedepohl, K.H., 1991. The Composition of the Upper Earth's Crust and the Natural Cycles of Selected Metals. *Metals in Natural Raw Materials. Natural Resources*, in Merian, E. (ed), *Metals and their Compounds in the Natural Environment*, VCH-Verlag, Weinheim, p. 1-17.

- Weyer, S., Schwieters, J., 2003. High precision Fe isotope measurements with high mass resolution MC-ICPMS. *International Journal of Mass Spectrometry* 226 (3), 355-368.
- Wilson, M., 1989. *Igneous petrogenesis*. Unwin Hyman, London.
- Winter, B.L., Johnson, C.M., Clark, D.L., 1997. Strontium, neodymium, and lead isotope variations of authigenic and silicate sediment components from the Late Cenozoic Arctic Ocean: Implications for sediment provenance and the source of trace metals in seawater. *Geochimica et Cosmochimica Acta* 61 (19), 4181-4200.
- Wooden, J.L., Czamanske, G.K., Fedorenko, V.A., Arndt, N.T., Chauvel, C., Bouse, R.M., King, B.S.W., Knight, R.J., Siems, D.F., 1993. Isotopic and Trace-Element Constraints on Mantle and Crustal Contributions to Siberian Continental Flood Basalts, Norilsk Area, Siberia. *Geochimica et Cosmochimica Acta* 57 (15), 3677-3704.
- Zhuang, G.S., Yi, Z., Wallace, G.T., 1995. Iron(II) in rainwater, snow, and surface seawater from a coastal environment. *Marine Chemistry* 50 (1-4), 41-50.
- Zimmermann, B., Porcelli, D., Frank, M., Andersson, P.S., Baskaran, M., Lee, D.C., Halliday, A.N., 2009. Hafnium isotopes in Arctic Ocean water. *Geochimica et Cosmochimica Acta* 73 (11), 3218-3233.

## 10. Appendix

A1: Berechnungen zu Sedimentakkumulation und Porenwasserfluss zu Kapitel 5.

### 1. Calculation of the sediment accumulation rate for Mn at station 248:

$$ar_{\text{Mn248}} = \text{Mn}_{\text{xs0-480}} \cdot \rho_d \cdot sr$$

$ar_{\text{Mn248}}$  = Mn accumulation rate in core 248

$\text{Mn}_{\text{xs0-480}}$  = mean Mn excess content from 0-480 cm depth = 4134 mg/kg

$\rho_d$  = sediment dry bulk density =  $1.15 \text{ g}\cdot\text{cm}^{-3}$  (own values have not been determined, we refer to published data from Lomonosov Ridge sediments by Expedition 302 Scientists, 2006)

$sr$  = mean linear sedimentation rate =  $480 \text{ cm} / 135000 \text{ a} = 0.0036 \text{ cm}\cdot\text{a}^{-1}$  (see chapter 3.1)

$$ar_{\text{Mn248}} = 4134 \text{ mg}\cdot\text{kg}^{-1} \cdot 1.15 \text{ g}\cdot\text{cm}^{-3} \cdot 0.0036 \text{ cm}\cdot\text{a}^{-1} = 1.69 \cdot 10^{-5} \text{ g}\cdot\text{cm}^{-2}\cdot\text{a}^{-1}$$

### 2. Calculation of the diffusive pore water $\text{Mn}^{2+}$ flux at station 248:

$$J_{\text{sed}} = -\Phi \cdot D_{\text{sed}} \cdot dC/dx$$

$J_{\text{sed}}$  = diffusive pore water flux

$\Phi$  = sediment porosity = 0.6 (own values have not been determined, we averaged published data from Stein et al., 2004)

$D_{\text{sed}}$  = sea water diffusion coefficient  $D_{\text{sw}}/\text{tortuosity } \theta^2 = 3.02 \cdot 10^{-10} \text{ m}^2\cdot\text{s}^{-1} / 2.02 = 1.5 \cdot 10^{-10} \text{ m}^2\cdot\text{s}^{-1}$  ( $D_{\text{sw}}$  at 0 °C and  $\theta^2$ : Schulz, 2006)

$dC/dx$  = concentration gradient =  $(46.4 - 15.4 \text{ } \mu\text{mol}\cdot\text{l}^{-1}) / (485 - 470 \text{ cm}) = 0.21 \text{ mol}\cdot\text{m}^{-4}$

$$J_{\text{sed}} = -0.6 \cdot 1.5 \cdot 10^{-10} \text{ m}^2\cdot\text{s}^{-1} \cdot 0.21 \text{ mol}\cdot\text{m}^{-4} = -0.59 \cdot 10^{-3} \text{ mol}\cdot\text{m}^{-2}\cdot\text{a}^{-1}$$

### 3. Calculation of the advective pore water $\text{Mn}^{2+}$ flux at station 248:

$$J_{\text{ad}} = \Phi \cdot sr \cdot C$$

$C$  = pore water  $\text{Mn}^{2+}$  concentration directly below the Mn rich sediment layer =  $15.4 \text{ } \mu\text{mol}\cdot\text{l}^{-1}$

$$J_{\text{ad}} = 0.6 \cdot 0.0036 \text{ cm}\cdot\text{a}^{-1} \cdot 15.4 \text{ } \mu\text{mol}\cdot\text{l}^{-1} = 3.29 \cdot 10^{-7} \text{ mol}\cdot\text{m}^{-2}\cdot\text{a}^{-1}$$

The advective pore water flux is 3 orders of magnitude lower than the diffusive pore water flux and can therefore be neglected.



**4. Calculation of the sedimentary  $Mn_{xs}$  that can be derived from the diffusive pore water flux in the Mn rich sediment layer from 445 to 470 cm in a representative time:**

$$Mn_{xs} = (t \cdot |J_{sed}| \cdot M_{Mn} \cdot area) / m_{sed445-470}$$

$t$  = approximate age of the sediment layer from 445 to 470 cm = 120,000 a

$M_{Mn}$  = molar mass of Mn = 54.94 g·mol<sup>-1</sup>

area = 1 m<sup>2</sup>

$m_{sed445-470}$  = mass of the total sediment in the interval from 445 to 470 cm = volume of the interval ·  $\rho_d$  = (25 cm · 100 cm · 100 cm) · 1.15 g·cm<sup>-3</sup>  
= 288 kg

$$Mn_{xs} = (120,000 \text{ a} \cdot 0.59 \cdot 10^{-3} \text{ mol} \cdot \text{m}^{-2} \cdot \text{a}^{-1} \cdot 54.94 \text{ g} \cdot \text{mol}^{-1} \cdot 1 \text{ m}^2) / 288 \text{ kg} = 13.5 \text{ g} \cdot \text{kg}^{-1}$$

This amount of sedimentary  $Mn_{xs}$  can be generated by the current pore water flux in 120,000 years. The mean  $Mn_{xs}$  of the sediment interval from 445 to 470 cm is only 9.1 g·kg<sup>-1</sup>, implying that the influence of the pore water flux on this layer started significantly after its deposition.

**5. Calculation of the required time to build up the complete sedimentary  $Mn_{xs}$  in the layer from 445 to 470 cm depth in core 248:**

$$t = m_{Mn445-470} / |J_{sed}|$$

$t$  = time needed to build up the solid phase Mn layer via precipitation from the current pore water flux under steady state conditions

$m_{Mn445-470}$  = mass of  $Mn_{xs}$  in the sediment interval from 445 to 470 cm

$$m_{Mn445-470} = m_{sed445-470} \cdot Mn_{xs445-470}$$

$Mn_{xs445-470}$  = mean Mn excess content of the sediment interval from 445 to 470 cm = 9.1 g·kg<sup>-1</sup>

With the molar mass of Mn (54.94 g·mol<sup>-1</sup>) and the given area of 1 m<sup>2</sup> it follows:

$$t = (288 \text{ kg} \cdot 9.1 \text{ g} \cdot \text{kg}^{-1}) / (0.59 \cdot 10^{-3} \text{ mol} \cdot \text{m}^{-2} \cdot \text{a}^{-1} \cdot 54.94 \text{ g} \cdot \text{mol}^{-1} \cdot 1 \text{ m}^2) = 80,510 \text{ a}$$

**6. Calculation of the sedimentary  $Mn_{xs}$  that can be derived from the diffusive pore water flux in the Mn rich sediment layer from 445 to 470 cm in 12,000 years (onset of the Holocene):**

$$Mn_{xs} = (12,000 \text{ a} \cdot 0.59 \cdot 10^{-3} \text{ mol} \cdot \text{m}^{-2} \cdot \text{a}^{-1} \cdot 54.94 \text{ g} \cdot \text{mol}^{-1} \cdot 1 \text{ m}^2) / 288 \text{ kg} = 1.35 \text{ g} \cdot \text{kg}^{-1}$$

This amount is 15% of the total  $Mn_{xs}$  inventory between 445 and 470 cm.

## Danksagung

Prof. Dr. Hans-Jürgen Brumsack danke ich herzlich für die Aufnahme in seiner Arbeitsgruppe und die Möglichkeit, über arktische Sedimente zu promovieren. Seine fortwährende Unterstützung, Diskussionsbereitschaft und fachliche Kompetenz haben entscheidend zum Gelingen dieser Arbeit beigetragen.

Ich danke Dr. Katharina Pahnke für die Übernahme des Zweitgutachtens und die angenehme und produktive Kooperation zur Nd- und Sr-Isotopie.

Durch die Vermittlung analytischen Wissens von Dr. Bernhard Schnetger stehen die erhobenen Daten auf einem sicheren Fundament. Ich danke ihm für den stets kritischen Gedankenaustausch und dafür, dass er mir eine analytische Arbeitsweise beigebracht hat sowie Dinge zu hinterfragen.

Ein besonderer Dank gilt Dr. Christian März, der mich mit Expertise und Tatkraft während der gesamten Zeit unterstützt und stets mit Enthusiasmus motiviert hat, sowohl vor Ort als auch über den kleinen Teich hinweg.

Danken möchte ich allen Mitarbeitern der Marinen Isotopengeochemie, die mich zeitweise wie eine der ihren aufgenommen haben, besonders Dr. Philipp Böning für die Messung und Martina Schulz für die Unterstützung im Labor.

Den Mitarbeitern des Instituts für Mineralogie der Leibniz Universität Hannover danke ich für die Gastfreundschaft und Unterstützung während meines Ausflugs zu den Fe-Isotopen, vor allem Dr. Stephan Schuth, Prof. Dr. Stefan Weyer und Alexandra Tangen.

Ein großer Dank gilt Dr. Karsten Lettmann für die Vereinfachung komplexer Sachverhalte und die Modellierung.

Den Kooperationspartnern des Alfred Wegener Instituts Bremerhaven danke ich ganz herzlich, hier im Speziellen Prof. Dr. Ruediger Stein sowie Dr. Jens Matthiessen.

Den vielen Helfern im Labor danke ich für die Mithilfe bei der Bewältigung der vielen Proben: Eleonore Gründken und Carola Lehnert sowie Janis Ahrens, Alexandra Arbandt, Sanja Asendorf, Alexander Buß, Simone Hanekamp, Eva Kienle, Marlene Klenke, René Neuholz, Ronja Paffrath, Dorothee Schumacher und Karl Thieme.

An die Besatzung und Wissenschaftler der Polarsternexpeditionen ARK-XXIII/3 und ARK-XXVI/3 ein großes Dankeschön für die Hilfe bei der Gewinnung der Proben.

Die „geochemische Familie“ war ein essentieller Bestandteil meiner Zeit am ICBM. Ich danke euch für die soziale Komponente neben der Arbeit.

Ein herzliches Dankeschön an meine Familie für die bedingungslose Unterstützung und an meine Freunde für die Bereicherung meines Lebens.

Der Deutschen Forschungsgemeinschaft danke ich für die finanzielle Unterstützung.

## Lebenslauf

Name Ann-Katrin Meinhardt

Geburtsdatum 27.07.1985

Geburtsort Cuxhaven

### Schulbildung

1991 – 1995 Franzenburger Schule Franzenburg

1995 – 1997 Orientierungsstufe der Geschwister-Scholl-Schule  
Altenwalde

1997 – 2004 Lichtenberg Gymnasium Cuxhaven (Abitur)

### Akademischer Werdegang

10/2004 – 09/2009 Chemiestudium an der Carl von Ossietzky Universität  
Oldenburg, Abschluss: Diplom  
Diplomarbeit: „Anorganische Geochemie von Oberflächen-  
sedimenten auf einem Ost-West-Transekt über den  
Mendeleev-Rücken (81° N, Ostsibirische See, Arktischer  
Ozean)“

seit 03/2010 Promotionsstudium an der Carl von Ossietzky Universität  
Oldenburg

Thema: „Anorganisch-geochemische Untersuchung  
quartärer Sedimente des Arktischen Ozeans“

seit 04/2012 Promotionsstudium „Environmental Sciences and  
Biodiversity“ der Graduiertenschule Naturwissenschaft und  
Technik der Fakultät V der Carl von Ossietzky Universität  
Oldenburg

## Erklärung

Hiermit versichere ich, dass ich die vorliegende Arbeit unter Berücksichtigung der Leitlinien guter wissenschaftlicher Praxis an der Carl von Ossietzky Universität Oldenburg selbstständig angefertigt und keine anderen als die angegebenen Quellen und Hilfsmittel verwendet habe. Zusätzlich erkläre ich, dass diese Dissertation weder in ihrer Gesamtheit noch in Teilen einer anderen wissenschaftlichen Hochschule zur Begutachtung in einem Promotionsvorhaben vorliegt oder vorgelegen hat und dass im Zusammenhang mit dem Promotionsvorhaben keine kommerziellen Vermittlungs- oder Beratungsdienste in Anspruch genommen worden sind.

Oldenburg, im Juli 2015

Ann-Katrin Meinhardt